

Supported ZIF and Mixed Matrix Membranes for Pervaporation and Permeation

Von der Naturwissenschaftlichen Fakultät der
Gottfried Wilhelm Leibniz Universität Hannover

zur Erlangung des Grades

Doktorin der Naturwissenschaften (Dr. rer. nat.)

genehmigte Dissertation

von

M. Sc. Lisa Maria Diestel

geboren am 11.04.1987 in Fürstenfeldbruck

2015

Referee: Prof. Dr. rer. nat. Jürgen Caro

Co-referee: Prof. Dr. rer. nat. Detlef Bahnemann

Day doctorate conferred: 14.07.2015

Preface

The results presented in this thesis were achieved while I was a member of the scientific research group of Prof. Dr. Jürgen Caro at the Gottfried Wilhelm Leibniz University of Hannover, Institute of physical chemistry and electrochemistry from Nov. 2011 until Apr. 2015.

During this period, I took part in the German Research Foundation (Deutsche Forschungsgemeinschaft - DFG) program SPP 1362 “Porous Metal-Organic Frameworks”, organized by Prof. Dr. Stefan Kaskel.

This thesis includes five publications that were written by me as first or cooperative author. Furthermore, I am first or co-author, respectively, of four additional papers which are not included in this thesis, but listed in chapter 5. The following part will clarify the contributions of each author to the published articles.

The first article (chapter 2.2) presented in this thesis was written by me with the kind support from my co-workers. My contribution was to prepare the ZIF-8 membrane and the ZIF-8 powder. Additionally, I characterized the ZIF-8 powder and the membrane by powder XRD and performed the SEM pictures. Furthermore, I tested the membrane for the pervaporation of an equimolar n-hexane/benzene and mesitylene/benzene mixture and proved the liquid adsorption by liquid adsorption studies. Frank Steinbach showed me how to produce clear SEM pictures. Dr. Helge Bux contributed to the publication by helpful suggestions. M. Sc. Dennis Wachsmuth built up the pervaporation apparatus during his master thesis. And finally, Prof. Dr. Jürgen Caro supported the work by valuable discussions and corrections.

The second publication (chapter 2.3) was written by Dr. Daniil Kolokolov. My contribution to this paper was to perform the macroscopic measurements of the diffusivity of benzene in ZIF-8 by membrane pervaporation studies and to calculate the Maxwell-Stefan diffusivity using the measured parameters.

The third article (chapter 3.2) was also written by me as the first author with kind support from my co-authors. My contribution was to synthesize the neat ZIF-8 membrane, to perform the permeation measurements and to prepare the powder XRDs and SEM pictures of the membranes. Dr. Xinlei Liu prepared the PMPS

membrane and the mixed matrix membrane. Prof. Dr. Yanshuo Li, Prof. Dr. Weishen Yang and Prof. Dr. Jürgen Caro supported the paper by helpful criticism and corrections.

The fourth article (chapter 3.3) was also written by me with kind support from my colleagues. My contribution was to synthesize the membranes, to perform the SEM pictures of the neat ZIF membranes and to characterize all membranes by XRD. Furthermore, I carried out the permeation experiments. M. Sc. Nanyi Wang showed me how to synthesize the neat ZIF-90 membranes and the ZIF-90 nanoparticles. M. Sc. Alexander Schulz and Frank Steinbach prepared the mixed matrix membranes for the SEM and TEM characterization and Frank Steinbach produced the SEM and TEM pictures of the mixed matrix membranes. Prof. Dr. Jürgen Caro contributed to the paper by valuable comments and corrections.

The fifth publication (chapter 3.4) is a paper written by me as the first author and supported by my colleagues and co-authors. My contribution was to synthesize the membranes, to characterize the neat ZIF membranes and mixed matrix membranes by SEM and to carry out the permeation measurements. Bärbel Schwiedland and Prof. Dr. Ulrich Giese helped me with the DSC measurements and by their discussions. I would like to thank Frank Steinbach for the clear TEM, and SAED characterizations of the mixed matrix membranes and Prof. Dr. Jürgen Caro for the discussions and the corrections.

Acknowledgement

First of all, I wish to thank Prof. Dr. Jürgen Caro for his excellent and helpful support during my PhD time. He gave me the opportunity to envelope my research topic and he encouraged me on this way continually. Thus, I could gain insight into two important membrane fields: the metal-organic framework membranes and the new class of mixed matrix membranes.

Furthermore, I would like to thank my co-referees Prof. Dr. Detlef Bahnemann and Prof. Dr. Josef-Christian Buhl for their reviews.

I am grateful to Appl. Prof. Dr. Armin Feldhoff and Frank Steinbach for supporting me in the SEM and TEM measurements. Special thanks also to my cooperation partners Dr. Helge Bux, Prof. Dr. Dieter Freude, M. Sc. Sebastian Friebe, Prof. Dr. Ulrich Giese, Dr. Daniil Kolokolov, Prof. Dr. Yanshuo Li, Dr. Xinlei Liu, Dr. Yi Liu, Dipl.-Nano. Sc. Alexander Mundstock, M. Sc. Alexander Schulz, Bärbel Schwiedland, Prof. Dr. Alexander Stepanov, M. Sc. Dennis Wachsmuth, M. Sc. Nanyi Wang, and Prof. Dr. Weishen Yang.

Furthermore, I would like to thank Kerstin Battermann, Wilfried Becker, Yvonne Gabbey-Uebe, Kerstin Janze, Markus Köhler, Jan Kuckuck, Peter Mühr, and Marita Schlüter for their organizational and technical assistance during the past years.

I wish to express my thanks to all colleagues for the pleasant working atmosphere, in particular to Dipl.-Chem. Patrick Adel, Dr. Nadja Bigall, M. Sc. Michael Bittner, Dr. Dirk Dorfs, M. Sc. Wei Fang, M. Sc. Axel Freytag, M. Sc. Benjamin Geppert, M. Sc. Dominik Hinrichs, M. Sc. Franziska Lübkemann, M. Sc. Jan Miethe, M. Sc. Tarek Mohamed, M. Sc. Suraj Naskar, M. Sc. Kaveh Partovi, M. Sc. Olga Ravkina, Dr. Sara Sanchez Paradinas, Dr. Yanying Wei, M. Sc. Andreas Wolf, and M. Sc. Jian Xue.

Finally, I want to thank my friends, my family – especially Andreas and Franz – and Torben for their patience and loving support.

Abstract

The following thesis discusses the development of cost-intensive and rarely reproducible Metal-Organic Framework membranes (MOF membranes) towards cheaper and more easily reproducible Mixed Matrix Membranes (MMMs). For the studies the prototypical MOFs ZIF-8 and ZIF-90 (Zeolitic Imidazolate Framework) were used. This thesis includes five articles published in internationally renowned journals, which are rearranged in a logical order.

First of all, the – for the gas separation already successful tested – ZIF-8 membrane was used for the pervaporative separation of alkanes from aromatic compounds. It was found that benzene was able to permeate through the dense ZIF-8 membrane layer despite of its small pore size. The reason for this adsorption is the significant framework flexibility of ZIF-8. To prove this unexpected finding an additional ^2H NMR (nuclear magnetic resonance) study was performed which established the movement patterns of a benzene molecule within the ZIF-8 cage and its self-diffusion coefficient. Since the manufacture of ZIF membranes is very time- and cost-intensive, as well as not scalable, a new type of membrane was examined – the MMM. This composite membrane is able to combine the excellent separation performance of MOF membranes with the flexibility and easy handling of polymer membranes. Within this thesis ZIF-8 and ZIF-90 nanoparticle MMMs with rubbery or glassy polymer matrices were produced und tested for gas permeation in comparison with the neat ZIF and polymer membrane. The MMM with polymethylphenylsiloxane (PMPS) as rubbery polymer matrix showed the same separation results as the neat PMPS membrane, but combined with a noticeably higher gas permeability. This behavior results from an increased free volume of the PMPS polymer after introduction of ZIF-8 nanoparticles. By contrast, the MMMs with glassy Matrimid as polymer matrix often showed improved separation results but lower gas permeabilities than expected. An additional study allowed to explain this phenomenon with a hindrance of the ZIF framework flexibility due to the surrounding polymer. This effect was reproducible by using other glassy polymers like 2,2'-bis(3,4-carboxyphenyl) hexafluoropropane dianhydride-diamino-mesitylene (6-FDA-DAM).

Keywords: Permeation, Pervaporation, MOF membranes, Mixed Matrix Membranes

Zusammenfassung

Die vorliegende Dissertation beinhaltet die Entwicklung von metallorganischen Membranen (MOF Membran) hin zu leichter herstellbaren Mixed Matrix Membranen (MMM). Für die Untersuchungen wurden die prototypischen MOFs ZIF-8 und ZIF-90 (ZIF = zeolith-artige Imidazolat-Gerüststrukturen) verwendet. Die Arbeit schließt insgesamt fünf in internationalen Fachzeitschriften veröffentlichte Publikationen ein, die in logischer Reihenfolge aufgeführt sind.

Die in der Gastrennung bereits erfolgreich getestete ZIF-8 Membran wurde in dieser Arbeit zunächst zur pervaporativen Trennung von Alkanen und Aromaten genutzt, wobei zu beobachten war, dass Benzol durch die engporige ZIF Membran permeierte. Aufbauend auf diesem erwarteten Ergebnis wurde eine ^2H NMR (nuclear magnetic resonance)-Studie zur Charakterisierung und Quantifizierung der Benzoladsorption am ZIF-8 durchgeführt. Hierbei konnte das Bewegungsmuster eines Benzolmoleküls in einer ZIF-8 Gerüststruktur und dessen Selbstdiffusionskoeffizient ermittelt werden. Da die Herstellung einer ZIF Membran sehr kosten- und zeitintensiv und zudem die Membran praktisch nicht hochskalierbar ist, wurden nachfolgend MMMs eingehender untersucht. Wie sich herausstellte, kann dieser Membrantyp unter bestimmten Umständen sowohl die guten Separationseigenschaften der ZIFs als auch die Flexibilität und gute Bearbeitbarkeit der Polymere aufweisen. Hierzu wurden ZIF-8 und ZIF-90 Nanopartikel-MMMs mit gummi- und glasartigen Polymeren hergestellt und in der Gastrennung mit den reinen ZIF und den reinen Polymermembranen verglichen. Es ergab sich, dass die MMM mit dem gummiartigen Polymethylphenylsiloxan (PMPS) ähnliche Trenneigenschaften aufwies wie die reine PMPS-Membran, wobei die Gaspermeabilität deutlich erhöht war. Dieses Resultat ist darauf zurückzuführen, dass die ZIF-8 Nanopartikel die Struktur des PMPS stören und Hohlräume erzeugen. Bei den MMMs mit dem glasartigen Matrimid konnten dagegen häufig deutlich verbesserte Separationen mit leicht verringerten Permeabilitäten festgestellt werden. Eine aufbauende Studie konnte zeigen, dass diese Ergebnisse durch eine behinderte ZIF Gitterflexibilität entstehen und auch bei anderen glasartigen Polymeren wie 2,2'-bis(3,4-carboxyphenyl)hexafluorpropandianhydrid-diaminomesitylen (6-FDA-DAM) auftreten.

Schlagwörter: Permeation, Pervaporation, MOF Membranen, Mixed Matrix Membranen

Contents

Preface	I
Acknowledgement	III
Abstract	V
Zusammenfassung	VII
Contents	1
1 Introduction	3
1.1 Motivation.....	3
1.2 Metal organic framework membranes	6
1.2.1 MOFs and their structure	6
1.2.2 MOF nomenclature and classification	7
1.2.3 MOF subgroup: ZIFs	8
1.2.4 Chemical and physical stability properties of ZIFs	10
1.2.5 Mass transfer in ZIFs	10
1.2.5.1 Sorption on ZIFs	12
1.2.5.2 Diffusion in ZIFs.....	15
1.2.6 Gas separation with ZIF membranes	17
1.3 Mixed Matrix Membranes (MMMs).....	18
1.3.1 The advantages of MMMs	18
1.3.2 MMM Classification	19
1.3.2.1 MMMs with rubbery and glassy polymer	19
1.3.2.2 MMMs with inorganic fillers	20
1.3.2.3 MMMs with inorganic-organic fillers.....	21
1.3.3 Limitations of the MMM synthesis.....	21
1.3.3.1 Particle size, sedimentation, and agglomeration	21
1.3.3.2 Interface morphologies	22

1.3.4	Mass transport and permeability	24
2	Pervaporative separation of benzene containing mixtures on ZIF-8 membranes.....	38
2.1	Summary	38
2.2	Pervaporation studies of n-hexane, benzene, mesitylene and their mixtures on zeolitic imidazolate framework-8 membranes.....	39
2.3	Rotational and translational motion of benzene in ZIF-8 studied by ² H NMR: Estimation of microscopic self-diffusivity and its comparison with macroscopic measurements	46
3	Mixed matrix membranes as alternative for MOF and polymeric membranes.....	54
3.1	Summary	54
3.2	Comparative permeation studies on three supported membranes: Pure ZIF-8, pure polymethylphenylsiloxane, and mixed matrix membranes	56
3.3	Matrimid-based mixed matrix membranes: Interpretation and Correlation of experimental findings for zeolitic imidazolate frameworks as filler in H ₂ /CO ₂ Separation	63
3.4	MOF based MMMs with enhanced selectivity due to hindered linker distortion	74
4	Conclusions.....	81
5	Appendix.....	84

1 Introduction

1.1 Motivation

The separation of gases and liquids by membranes plays an increasingly important role in the reduction of industrial process costs.[1, 2] Accordingly, membranes are already applied in reverse osmosis (e.g., sea water desalination), nanofiltration (e.g., water removal to concentrate sugar), ultrafiltration (e.g., oil/water emulsions separation), and microfiltration (e.g., wastewater treatment). Further industrial applications with increasing demand are gas separations (e.g., natural gas refining) and pervaporations (e.g., alcohol extraction from organic solvents).[3, 4] The membrane technology offers a number of benefits over other separation technologies. In contrast to conventional gas separations that require much energy due to a gas-to-liquid phase change in the gas mixture (for example cryogenic distillation of air or condensation to remove condensable organic vapor from gas mixtures), this step is not necessary in membrane technology. Another advantage is that gas separation membrane units are smaller than other types of plants and that membrane systems are less complex mechanically.[5] Currently, gas selective membranes are most widely used in industry for [6]:

- Hydrogen separation
- Separation of nitrogen from air
- Carbon dioxide and water removal from natural gas
- Organic vapor removal from air and nitrogen streams

For the liquid separation (pervaporation) the membrane technology offers an additional advantage. Many commonly used organic solvents form azeotropes that cannot be easily separated by conventional methods. Thus, pervaporation is a widely accepted technology for

- The removal of water from organic mixtures
- The separation of volatile organic components from gas streams.

Considerable efforts have also been devoted to develop membranes that separate aromatic hydrocarbons - like benzene - from aliphatic ones and olefin from paraffin.[7]

The most widely used membranes are non-porous polymeric membranes. They are very attractive as membranes because they can be processed into hollow fibers with large surface areas. The relatively low manufacturing costs make them interesting for large-scale industrial applications.[8] Unfortunately, the efficiency of a membrane separation process is determined by the membrane's separation properties - its permeability and selectivity with respect to different gas or liquid mixtures. For most gas selective membranes the following rule applies: as selectivity increases, permeability decreases and vice versa. This upper-bound limit for the performance of polymeric membranes was predicted by Robeson.[9, 10] Significantly higher diffusivity selectivities than for polymeric materials were expected for molecular sieves like zeolites and for metal organic frameworks (MOFs).[11] The accurate size and shape discrimination resulting from their narrow pore distributions ensures superior selectivities. Additionally, MOF membranes can also be modified to achieve enhanced solubility-based separations.[12-20]

For the pervaporation thin and defect-free polymeric hollow fibers with sufficient chemical, mechanical, and thermal stability are in use. However, the chemical stability of the organic polymer limits the application.[1] Thus, zeolite membranes have been developed that are much more stable and show high fluxes and selectivities. But unfortunately, the quick launching of inorganic membranes is still seriously hindered by the extremely high costs for the membrane production, the brittleness and the lack of technology to produce defect-free membranes. A slight improvement has been achieved by using MOFs as sieving material. The critical and energy-intensive calcination step, necessary for most zeolite productions, can be avoided in the template-free MOF production.

Nevertheless, a new approach was needed to get cost-efficient, selective and permeable membranes which are less fragile and easy to reproduce. Thus, the research has focused on composite membranes like mixed matrix membranes (MMMs). MMMs are defined as the incorporation of a solid dispersed phase (here MOFs) into a continuous polymer matrix. MMMs have the potential to achieve

higher gas selectivity, higher gas permeability or both in relation to the neat polymeric membrane which results from the embedded porous particles. At the same time, the fragility of the MOF membranes can be reduced by using a flexible polymer as continuous matrix.[21-23] Using polymer, however, makes the new membranes susceptible to inorganic liquids.

Thus, the aim of this work was to examine at first existing MOF membranes for the pervaporative separation of aliphatic organic liquids from aromatic liquids. And, as MOF membranes are difficult to reproduce and to handle, MMMs with MOFs were developed and tested for applications in gas separation. Additionally, we developed a model to explain the enhanced selectivity results of MMMs in comparison to the neat MOF and the neat polymer membrane.

1.2 Metal organic framework membranes

1.2.1 MOFs and their structure

Metal organic frameworks (MOFs) are highly crystalline materials (see Fig. 1) with an ultrahigh porosity of about 90 % free volume. Consequently, these materials have large internal surface areas, extending beyond 6000 m²/g. With this property, MOFs are ideal as gas storage media, high-capacity adsorbents and separation media. Additionally, MOFs exhibit a high degree of variability for both the organic and the metal building unit. Thus, a further application for MOFs is the catalysis.[24]

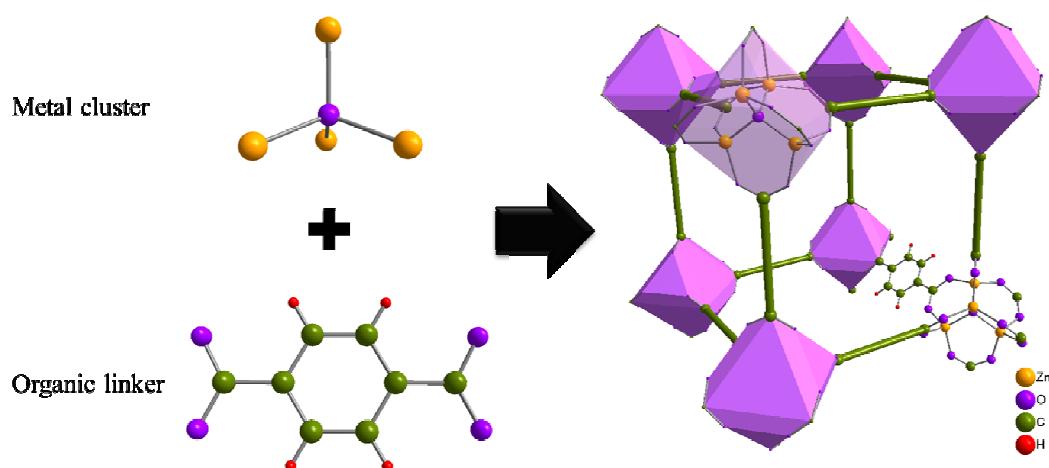


Fig. 1: Basic construction principle of MOFs: The metal clusters or centers are coordinatively bonded with multiple bonding organic linkers thus building an ordered, porous framework. Above the simple cubic MOF-5 with $(Zn_4O)^{6+}$ metal cluster units and 1,4-benzenedicarboxylate linker molecules is shown.

Due to their structural and chemical flexibility, the area of MOFs has become one of the fastest growing fields in chemistry. The MOF research can be classified by the following five categories: (1) advances in cluster chemistry, (2) linker preparation and post-synthetic modification, (3) improvements in structure determination and development of programs for the evaluation of sorption

properties, (4) interdisciplinary research, and (5) research for applications.[25] The term “MOF” dates back to publications by Yaghi and his coworkers in 1995. In this work, the synthesis and characterization of the $\text{Co(II)(BTC')}_2(\text{PYR})_2(\text{PYR})_{0.67}$ - with $\text{BTC}' = 1,3,5\text{-benzenetricarboxylate}$ and $\text{PYR} = \text{pyridine}$ – were described. According to Yaghi and coworkers these frameworks show a selective and reversible uptake of aromatic molecules.[26] Already 30 years ago, in 1959, Kinoshita and coworkers found the first polymeric metal-organic structure $(\text{Cu(I)(AND)}_2(\text{NO}_3))_n$ with $\text{AND} = \text{adiponitrile}$. Unfortunately, they never performed any adsorption studies on this new material.[27]

1.2.2 MOF nomenclature and classification

Similar to the zeolites, MOFs are often denoted by three letters plus a number. These letters are often abbreviations for the origin university or for certain structural properties – for example, MIL stands for “Material of Institute Lavoisier” and UiO for “University of Oslo” whereas ZIF stands for “zeolitic imidazolate framework”, BIF for “zeolitic boron imidazolate framework” and MOF for “metal organic framework”. Thus, it happens that one and the same structure has different names: ZIF-8, for example, is also called MAF-4 (metal azolate framework-4) and CPO-27 (coordination polymer of Oslo-27) is the same structure as MOF-74.[28, 29]

Until now, there are different approaches to classify MOFs. Kitagawa and his coworkers, for example, subdivided the MOFs into different generations. The first MOF generation includes all types of frameworks that are instable after removing solvent molecules. The second generation includes MOFs with a rigid and stable network during sorption processes, and MOFs with a stable but flexible network during sorption processes form the third generation of MOFs.[30] Férey and his coworkers, in contrast, classified MOFs into groups with different connectivity dimensions of the inorganic building unit.[31] However, in most cases the structures are divided into sub-groups, depending on their structural similarity to other materials or special building units. ZMOFs (zeolite-like metal organic frameworks), for example, are MOFs that have a zeolite-like structure. In this

subgroup we can find the ZIFs (zeolitic imidazolate frameworks). These are zeolite-like MOFs with imidazolate linkers.

1.2.3 MOF subgroup: ZIFs

In general, ZIFs consist of tetrahedrally-coordinated transition metal ions (Zn^{2+} , Co^{2+} , Cu^{2+} , Fe^{2+}) and imidazolate ligands.[32] Since the metal-imidazolate-metal angle is similar to the 145° Si-O-Si angle in zeolites, ZIFs resemble the zeolite networks.[33] A large variety of ZIFs has been synthesized in the past decade and most of them exhibit high chemical stability and permanent porosity. ZIF-8 ($\text{Zn}(\text{mim})_2$, mim = 2-methylimidazolate) and ZIF-90 ($\text{Zn}(\text{ica})_2$, ica = Imidazolate-2-carboxaldehyd), for example, are zeotype to the sodalite structure. This means that ZIF-8 and ZIF-90 built a cubic sodalite structure (space group $I\bar{4}3m$) with β -cages, which consist of six four-membered and eight six-membered rings. The cages are connected by the four- and six-membered rings (see Fig. 2). The corners of the β -cages consist of tetrahedrally coordinated zinc ions and the edges are formed by the imidazolate linkers.[34]

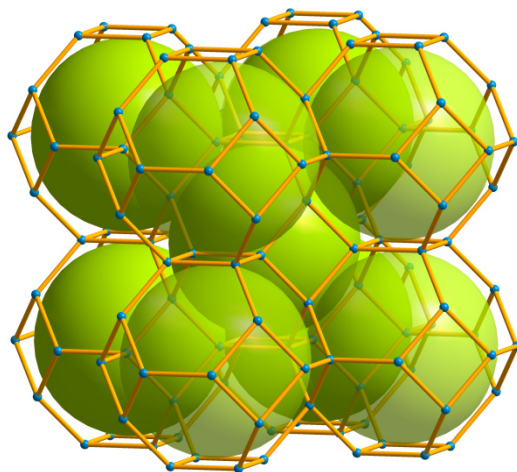


Fig. 2: Cubic ZIF-8 structure built up with tetrahedrally coordinated Zn^{2+} ions (blue balls) and 2-methylimidazolate linker molecules (yellow sticks) forming a sodalite network.

ZIF-8 and ZIF-90 consist of different imidazolate linkers. Hence, both frameworks have different unit cells and pore sizes. The cubic unit cell of ZIF-8, for example, has a length of 16.99 Å. The largest cavity diameter is 11.4 Å and the largest pore diameter of the rigid framework is 3.4 Å (see Fig. 3a). Besides, the Langmuir surface area amounts to 1810 m² g⁻¹, the BET surface area is 1813 m² g⁻¹ and the density of the ZIF-8 framework is 0.93 g cm⁻³. [33] ZIF-90, in contrast, has a cell length of 17.27 Å, a maximum cavity diameter of 11.0 Å and a maximum pore diameter of 3.5 Å in the rigid framework (see Fig. 3b). The Langmuir surface area amounts to 1320 m² g⁻¹, the BET surface is 1270 m² g⁻¹ and the density of the ZIF-90 framework is 0.99 g cm⁻³. [34]

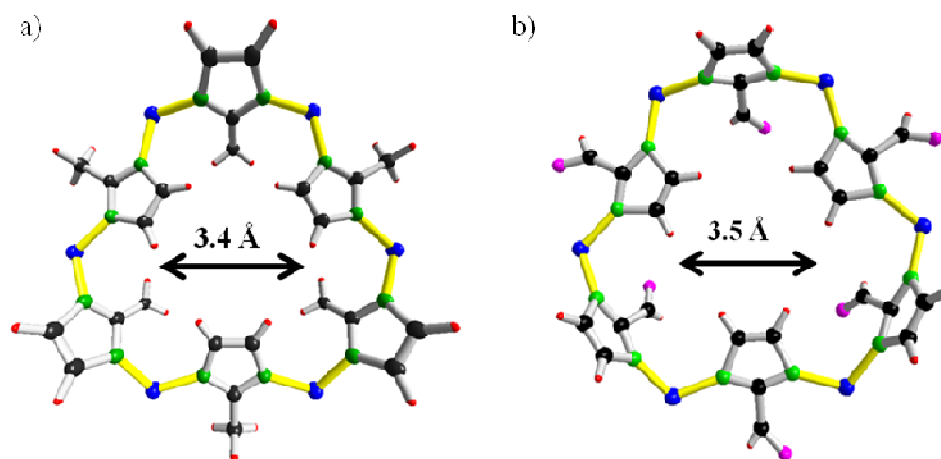


Fig. 3: (a) ZIF-8 pore: The zinc (blue balls) and the nitrogen atoms (green balls) form a ring structure (yellow bindings) in which the 2-methyl-imidazolate linkers (black balls = carbon atoms, red balls = hydrogen atoms) extend. Accordingly, the pore aperture is 3.4 Å in the rigid ZIF-8 framework. (b) ZIF-90 pore: The zinc (blue balls) and the nitrogen atoms (green balls) form a ring structure (yellow bindings) in which the 2-carboxaldehyd-imidazolate linkers (black balls = carbon atoms, red balls = hydrogen atoms, pink balls = oxygen atoms) extend. Accordingly, the pore aperture is 3.5 Å in the rigid ZIF-90 framework.

1.2.4 Chemical and physical stability properties of ZIFs

Most ZIFs have an exceptional chemical stability in refluxing organic solvents, water, and aqueous alkaline solutions; an outstanding finding for MOFs. Additionally, ZIF-8 can be heated up to 550 °C in N₂. [33, 35, 36] The thermogravimetric analysis of ZIF-90 shows very similar results. Up to a temperature of 300 °C, the framework loses solvent molecules, whereas in the subsequent region (300 - 500 °C) no further mass loss is observed. At 500 °C, the framework starts to decompose. Consequently, many ZIFs are good candidates for separation and storage applications at medium temperature ranges of up to 500 °C. Unfortunately, ZIFs exhibit only low physical stability. Coudert and coworkers were able to show that the very high porosity of the empty ZIF-8 causes a low resistance to shear and pressure-induced shear softening. Thus, the ZIF-8 framework could be damaged at 0.4 GPa. [37] Furthermore, ZIF frameworks show no rigid frameworks at room temperature. There are some recent reports for the neat ZIF-8 and the neat ZIF-90 frameworks that demonstrate an adsorption of bulky molecules such as benzene or xylenes [38-40], despite of their pore openings of 3.4 Å and 3.5 Å respectively, as found by Rietveld XRD analysis. [32, 33] Hence, it seems to be possible that adsorbed molecules can open the pores (also called “gate”) under certain conditions. Furthermore, gas sorption studies on different ZIF powders show hysteresis that arises from threshold pressures inducing the “gate opening”. [41-48]

1.2.5 Mass transfer in ZIFs

Generally, a mass transfer through a membrane is possible if a driving force is applied. In our case, the mass transfer takes place due to a constant pressure difference Δp between the feed side and the permeate side of the membrane. [49] The feed gas is the applied gas mixture that crosses the membrane. A part of the gas mixture cannot pass the membrane and hence form the retentate. The other gas molecules will permeate through the membrane and make up the permeate which is transported through the pipes by an inert sweep gas (see Fig. 4).

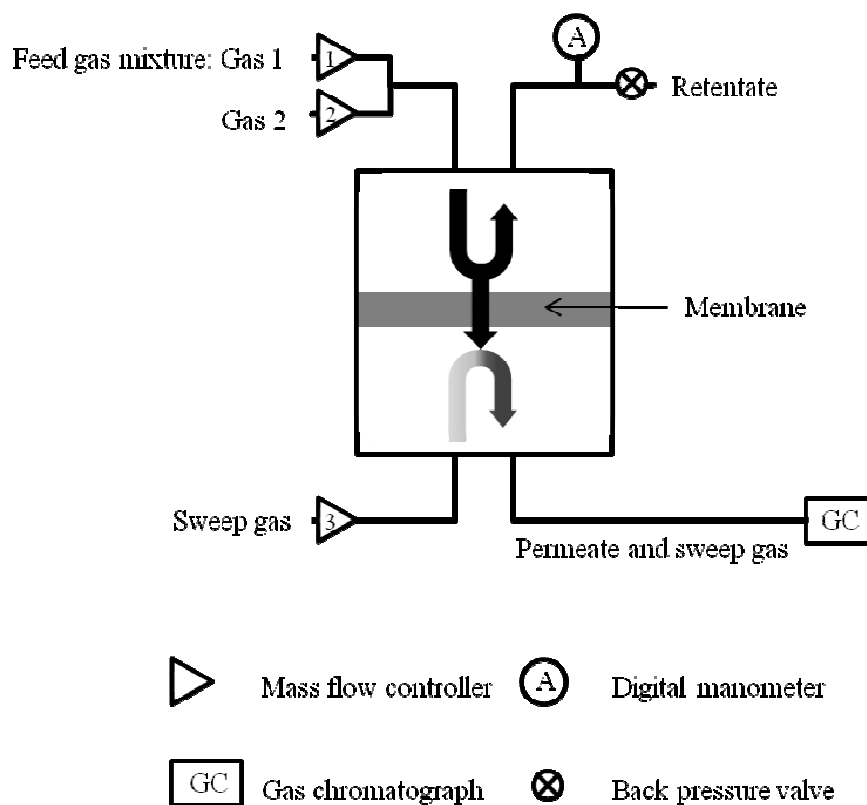


Fig. 4: Schematical illustration of the permeation apparatus. The mixed feed gas (gas 1 and gas 2) crosses a membrane. A part of the gas mixture does not permeate through the membrane and leaves the apparatus as retentate. The other part of the gas mixture permeates through the membrane and is transported via sweep gas into a gas chromatograph. To apply a pressure difference across the membrane the back pressure valve can be closed. The digital manometer indicates the pressure on the feed side of the membrane.

The ZIF membranes have been prepared on stabilizing macroporous alpha-alumina supports, which may influence the mass transfer. But their effects on the separation process are negligible compared to the influence of the microporous ZIF layer.[50] Thus, the following chapter will only focus on the mass transfer through ZIFs.

1.2.5.1 Sorption on ZIFs

The sorption of a gas on or inside a ZIF is an equilibrium process during which the molecules interact with the surface by chemisorption or physisorption. Chemisorption means a covalent bonding between the adsorbate and the adsorbent with an adsorption enthalpy of about 200 to 400 kJ/mol. The chemisorption is usually exothermic and the adsorbed molecules often decompose during this process. Between the gaseous species and the ZIF surface, physisorption normally takes place. Compared to chemisorption physisorption is a much weaker sorption. The gaseous species are only bonded by Van der Waals interactions with an adsorption enthalpy of about 20 to 40 kJ/mol. This weak interaction often results in breaking the bonds between the adsorptive agent and the adsorbate which means that the gaseous species stay unchanged.[51] The energetic effect of the sorption process can be described by the following parameters, the adsorption enthalpy $\Delta_{ad}H$ and the adsorption entropy $\Delta_{ad}S$ (see equation (1)). $\Delta_{ad}S$ is normally negative since the adsorption process increases the order of the system. Thus, the adsorption enthalpy has to be more negative than $T\Delta_{ad}S$ (exothermic process) so that the reaction occurs spontaneously ($\Delta_{ad}G < 0$):

$$\Delta_{ad}G = \Delta_{ad}H - T\Delta_{ad}S \quad (1)$$

$\Delta_{ad}H$ can be measured calorimetrically and is determined by :

$$\left(\frac{\partial \ln\left(\frac{p_i}{p}\right)}{\partial T} \right)_{k_i} = - \frac{\Delta_{ad}H}{RT^2} \quad (2)$$

wherein $\frac{p_i}{p}$ is the normalized partial pressure of the gas i , the temperature is denoted by T , k_i is the constant adsorbate concentration and R represents the ideal gas constant.[2, 51]

The sorption process is often illustrated by the coverage ratio θ as a function of the partial pressure p_i at a constant temperature T . The coverage ratio is thereby defined as:

$$\theta = \frac{V}{V_{mono}} \quad (3)$$

with V as the volume of the whole adsorbate and V_{mono} as the volume of the adsorbate that forms a monolayer on the substrate. The resulting curves are called isotherms. According to IUPAC, the isotherms are subdivided into six groups (see Fig. 5) [52, 53]:

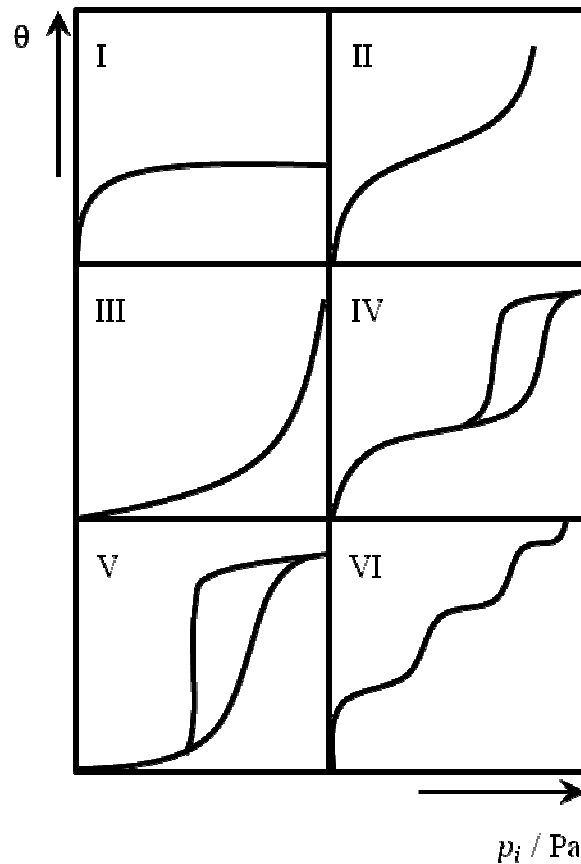


Fig. 5: Types of adsorption isotherms according to the IUPAC definition (I-VI) as a function of the coverage ratio θ in dependence of the partial pressure p_i .

Pure microporous materials often show type I isotherms, which means a steep increase of the adsorbed concentration at low pressures, until the micropores are completely filled and the coverage ratio remains constant. To describe a type I isotherm the Langmuir model is mostly used.[2]

The Langmuir model is a very simple theoretical model, which assumes that:

- The adsorbed molecules form only a monolayer
- The surface is uniform on the molecular level, which means that all adsorption bindings are equal and

- The adsorbed molecules don't have any interaction between each other

Thus, the dynamic equilibrium of the gas molecules i and the binding sites M on the surface can be described by $i(g) + M(\text{surface}) \rightleftharpoons iM(\text{surface})$. In the reaction shown, the adsorption takes place with a velocity k_{ad} and the desorption with a velocity k_{de} . The variation of the coverage ratio with respect to time during the adsorption can now be described by k_{ad} and the partial pressure p_i , the number of all binding sites N and the ratio of the not covered binding sites $(1 - \theta)$:

$$\frac{d\theta}{dt} = k_{ad}p_iN(1 - \theta) \quad (4)$$

The variation of the coverage ratio with respect to time by desorption accordingly is:

$$\frac{d\theta}{dt} = k_{de}N\theta \quad (5)$$

Using equation (4) and (5), the coverage ratio θ in the Langmuir model is given by:

$$\theta = \frac{\frac{k_{ad}p_i}{k_{de}}}{1 + \frac{k_{ad}p_i}{k_{de}}} = \frac{K_i p_i}{1 + K_i p_i} \quad (6)$$

This basic equation (6) can be modified to describe the coverage ratio of i in a multi-component isotherm of two gas species i and j :

$$\theta_i = \frac{K_i p_i}{1 + K_i p_i + K_j p_j} \quad (7)$$

Although the Langmuir isotherm fits very well to the experimental data, the surface area obtained does not describe the true inner surface areas of ZIFs, because the filling of the micropores does not necessarily lead to a large monolayer. [51] For a better fitting the multilayer model of Stephen Brunauer, Paul Emmett and Edward Teller (BET model) is often used.

The BET isotherm characterizes the coverage ratio of a gas species i (θ_i) as a function of the equilibrium pressure p , the saturation pressure p^* of the species i above the adsorbate-multilayer and a constant c :

$$\theta_i = \frac{c \frac{p}{p^*}}{\left(1 - \frac{p}{p^*}\right) \cdot \left\{1 - (1-c) \cdot \frac{p}{p^*}\right\}} \quad (8)$$

The proportionality constant c depends on the desorption enthalpy $\Delta_{de}H$ and the evaporation enthalpy Δ_vH as well as on the ideal gas constant R and the temperature T :

$$c = e^{\left(\frac{\Delta_{de}H - \Delta_vH}{RT}\right)} \quad (9)$$

The BET model requires:

- An energetically homogenous surface
- The possibility of forming undefined numbers of adsorbate layers
- No lateral interactions between the adsorbed molecules.

Accordingly, the BET model is only able to indicate the values of the inner surface for microporous materials, but it is not able to quantify the real values.[2, 51]

1.2.5.1 Diffusion in through ZIFs

The gas permeation through ZIF membranes is caused by a pressure difference Δp_i applied across the membrane. During the steady-state the upper/feed and the bottom/permeate membrane sites thus show a concentration gradient $\nabla c_i = c_{i,B} - c_{i,U}$ (concentration of the upper site $c_{i,U}$ and the bottom site $c_{i,B}$).

The mass transfer through a ZIF membrane can be quantitatively described by Fick's empirically found first law, which defines the diffusivity (D_i):

$$J_i = -D_i \frac{\partial c_i}{\partial z} = -D_i \nabla c_i \quad (10)$$

where J_i is the flux of a component i and ∇c_i means the concentration gradient in the z direction. If the concentration varies in all three directions, then Fick's second law applies:

$$\frac{\partial c_i}{\partial t} = \nabla(D_i \nabla c_i) \quad (11)$$

which when expanded is

$$\frac{\partial c_i}{\partial t} = D_i \left(\frac{\partial^2 c_i}{\partial x^2} + \frac{\partial^2 c_i}{\partial y^2} + \frac{\partial^2 c_i}{\partial z^2} \right) \quad (12)$$

It should be noted that the diffusivity D_i is not a constant, but can show a strong concentration dependence. Generally, Fick's first law can also be used for multicomponent diffusion systems.[54] In that case, the flux J_i of a component i in a system with $n - 1$ other components is described by

$$J_i = - \sum_{j=1}^{n-1} D_{ij} \nabla c_j \quad (13)$$

with the mixture diffusivity D_{ij} which may significantly differ from the diffusivity D_i if the components influence each other in a multicomponent system. In Eq. (13) one component (component n) has to be a solvent.

Fick's first law implies that the driving force for the diffusion is the concentration gradient. This is, however, only a macroscopic observation. The actual driving force is the difference in the chemical potential μ_i . If the diffusion is considered as a flow driven by a chemical potential gradient in the z direction $\frac{d\mu_i}{dz}$, a counteracting force can be defined – the frictional force with a friction coefficient f . Thus, in the steady-state following equation holds:

$$f \cdot u_i = - \frac{d\mu_i}{dz} \quad (14)$$

where u_i is the flow velocity of the species i . The flux is given by:

$$J_i = u_i \cdot c_i \quad (15)$$

To relate the chemical potential μ_i to the concentration c_i , the partial pressure p_i must be considered, resulting in:

$$\mu_i = \mu_i^0 + RT \ln(p_i/[p]) \quad (16)$$

Using eq. (14), eq. (16) and the relation $c_i = \frac{dc_i}{d \ln(c_i/[c])}$ the flux in the steady-state can be written as:

$$J_i = u_i \cdot c_i = - \frac{1}{f} \frac{RT d \ln(p_i/[p])}{dz} \cdot \frac{dc_i}{d \ln(c_i/[c])} = - \frac{RT d \ln(p_i/[p])}{f d \ln(c_i/[c])} \cdot \frac{dc_i}{dz} \quad (17)$$

By comparison with eq. (10) the transport diffusivity D_i can be expressed as:

$$D_i = \frac{RT d \ln(p_i/[p])}{f d \ln(c_i/[c])} \quad (18)$$

where $\frac{d \ln(p_i/[p])}{d \ln(c_i/[c])}$ represents the gradient of the equilibrium isotherm in logarithmic coordinates.[55, 56]

The difference in the chemical potential as the driving force is also presumed in the Stefan-Maxwell formulation. This model has the advantage that the diffusivities \mathfrak{D}_{ij} have values found from binary experiments and that the model does not require designating one species as solvent. For isothermal conditions the Stefan-Maxwell formulation can be simplified to:

$$J_i = -\mathfrak{D}_{ij} \frac{d \ln(p_i/[p])}{d \ln(c_i/[c])} \cdot \frac{dc_i}{dz} \quad (19)$$

with J_i as the flux of the component i , \mathfrak{D}_{ij} as the Stefan-Maxwell diffusivity for both components i and j , $\frac{d \ln(p_i/[p])}{d \ln(c_i/[c])}$ as the equilibrium isotherm of the component i and $\frac{dc_i}{dz}$ as the concentration gradient in the z direction. Eq. (19) can also be used to describe the diffusion of a single component i in a porous adsorbent k . In this case, the Stefan-Maxwell diffusivity \mathfrak{D}_{ik} means the diffusivity of the component i . Furthermore, in a microporous adsorbent there is no clear distinction between molecules adsorbed on the surface and those free in the gas phase. Therefore, only a total “intracrystalline” concentration c is considered. Assuming an ideal vapor phase, the transport equation then takes the form:

$$J = -D \frac{dc}{dz} = -\left(D_0 \frac{d \ln(p/[p])}{d \ln(c/[c])}\right) \frac{dc}{dz} \quad (20)$$

D_0 is defined as the corrected diffusivity and $\frac{d \ln(p/[p])}{d \ln(c/[c])} = \Gamma$ is the thermodynamic factor which arises from the nonlinearity of the relationship between the partial pressure and the concentration.[55]

1.2.6 Gas separation performance of ZIF membranes

ZIF membranes were tested for many important industrial separation applications such as natural gas sweetening, carbon dioxide capture, and hydrogen purification. Until now only a few ZIFs could be synthesized as dense membranes, namely ZIF-7, ZIF-8, ZIF-9, ZIF-22, ZIF-69, ZIF-71, ZIF-78, ZIF-90, ZIF-95 and ZIF-100.[18, 36, 57-74] The advantage of ZIF membranes in

comparison to commonly used polymer membranes is a size and shape discrimination resulting from their narrow pore distributions. Additionally, ZIF membranes can also be modified to achieve enhanced solubility-based separations. Hydrogen, for example, is purified under conditions that require membrane operation under high temperatures, pressures, and aggressive gases. The purification involves separating hydrogen from a variety of mixtures, including H_2/CO_2 , H_2/CH_4 , and H_2/N_2 . In the H_2/CO_2 separation, ZIF-7, ZIF-8, ZIF-22, ZIF-78, ZIF-90, and ZIF-95 membranes exceed the present Robeson plot. [58-78] The ZIF-8 performance in the H_2/CH_4 separation is median relative to other materials and does not reach the polymeric upper bound.[36, 38]

In general, ZIF-8 appears uniquely suited for several potential gas separation applications that include CO_2 removal from CH_4 streams (acid gas removal) or N_2 (post-combustion CO_2 capture) and separating N_2 from O_2 . The expectations stems from the similarity between the crystallographic pore diameter of ZIF-8 (3.4 Å) that falls between these pairs (critical diameter of O_2 : 3.5 Å, N_2 : 3.6 Å, CO_2 : 3.3 Å, and CH_4 : 3.8 Å). Unfortunately, ZIF-8 performance falls short of expectations since the material framework is quite flexible. Consequently, the trend of gas diffusivity in ZIFs is different from that observed for rigid zeolites that have a sharp decrease for gas molecules with critical diameters similar to the crystallographic pore size. ZIF apertures have been modeled as a temporal distribution of pore sizes, in which large pore openings are rare. Thus, it becomes increasingly difficult for large molecules to pass.[41-48, 75]

1.3 Mixed Matrix Membranes (MMMs)

1.3.1 The advantages of MMMs

MMMs consist of an inorganic or MOF phase in the form of nano- or micro-crystals (discrete phase) which are embedded in a polymeric matrix (continuous phase). The combination of two different materials with different fluxes and selectivities provides the possibility to fabricate more stable and highquality membranes.[76, 77] If, for example, porous additives like zeolites or MOFs are combined with low permeable, glassy polymers, a strong improvement of

permeability is expected, which is economically attractive for large scale separations. MMMs in general attracted attention as a promising means to improve the properties of polymer membranes. Polymeric membranes suffer from a trade-off relationship between the permeability and the selectivity, which is clearly illustrated in the so-called Robeson plots.[9] The separation abilities of the MMMs, however, can be far above these plots.[78] In addition, MMMs are often mechanically more stable than the pure inorganic or MOF membranes and easier to produce. Furthermore, it is possible to fabricate hollow fibre membranes out of MMMs, which is nearly impossible for the inorganic or MOF membranes.[79] In some cases the new materials offer enhanced physical, thermal and mechanical properties in the face of aggressive environments and could therefore be used to stabilize polymer membranes against variations in permeability and selectivity by temperature.[80,81] However, there are still some difficulties to overcome. One significant problem is the compatibility of the polymer and the additive to get a mechanically stable membrane with a homogenous particle dispersion. Agglomerates, however, represent unselective pathways for gas molecules.[22, 23] Additionally, unlinked additives tend to get separated from the polymer solution during the drying process due to gravitation. This phenomenon allows only moderate particle volume fractions of around 30 vol-% and a highly viscous MMM solution for the membrane preparation. The drying process is also very crucial since fast drying leads to solvent entrapments in the polymer, whereas slow drying promotes the segregation of additives.

1.3.2 MMM Classification

1.3.2.1 MMMs with rubbery and glassy polymer

MMMs can be synthesized using rubbery and glassy polymer matrices. But the choice of the polymer has far reaching implications for the separation performance of the resulting membranes. Different studies show a high correlation between the chemical structure of the polymer and the observed gas permeation parameters.[80-83] As to the rubbery polymers, most detailed studies were performed for siloxane with different side chains.[76, 84-86] It was shown

that when the size of the side groups increases, the chain becomes less flexible, the glass transition temperature, as a result, increases and the gas permeability decreases, while the selectivities sometimes increase. In this, rubbery polymers differ from glassy polymers, where the introduction of larger side groups often results in a strongly increased permeability.[82] An explanation for such a behavior can be given on the basis of the free volume theory.[87, 88] So far, only the effect of nonpolar side chains have been considered. The introduction of functional groups which are capable of dipole-dipole interactions or which can form hydrogen bonds can strongly influence the gas permeability due to increasing interchain interactions or interactions with some penetrants. Thus, an increase of the selectivity is possible.[89] Generally, rubbery polymers have a high gas permeability and only a moderate gas separation selectivity, while glassy polymers often show great selectivities but a moderate or low gas permeability.[9] Beside the correlation between the structure of the polymer and the observed permeation, the polymer structure also influences the matrix-additive interaction.[23] For example, if the glass transition temperature of a solvent-swollen polymer is higher than the MMM synthesis temperature, the evaporation of the solvent during the MMM synthesis process can lead to considerable tensile stresses in the glassy polymer matrix. These stresses can tend to void-forming between the polymer and the additive surface, but only if the interactions of the polymer and the additives are not too strong as, for example, between zeolites and glassy polymers.[90, 91] On the other hand, if the polymer is rubbery at the MMM synthesis temperature, it is still flexible and can adapt to the sieve surface even when all the solvent has left. The formation of defects is unlikely with this. Nevertheless, repulsive interactions between the polymer and the additive may also lead to poor MMMs.[92]

1.3.2.2 MMMs with inorganic fillers

The integration of zeolites into a polymeric membrane has attracted much attention since it is possible to combine the size and shape selectivity of zeolites with the mechanical stability of polymers. However, the interaction between polymer and zeolite is often poor, thus leading to void spaces between both

components. Another problem arises from the partial pore blockage of the zeolite pores. This phenomenon has, for example, been observed with 3A, 4A and 5A zeolites in polyethersulfone matrices, where the permeabilities of the gases decreased with an increase in additive amount. Only the 5A zeolite got constant permeability values.[76, 82] Because of these challenges, the zeolite MMMs have never attracted industrial usage.

1.3.2.3 MMMs with inorganic-organic fillers

Because of their hybrid nature with organic parts, MOFs are of increasing interest as porous fillers in MMMs. It is possible to functionalize the ligands of the MOFs accessing a better interaction between the polymeric phase and the disperse MOF phase. Thus, the formation of micro-gaps between an inorganic-organic MOF and an organic polymer phase can be avoided. The first incorporation of a MOF into a polymer for the fabrication of gas selective MMMs has been that of copper(II) biphenyl-dicarboxylate-triethylenediamine into poly-(3-acetoxyethylthiophene). [93]

1.3.3 Limitations of the MMM synthesis

1.3.3.1 Particle size, sedimentation, and agglomeration

The effect of different particle sizes on the separation ability of MMMs has been investigated for silicalite in PDMS.[94] It was shown that the permeability of MMMs decreases with decreasing particle size of silicalite. This behavior may be due to the rigidified polymer layers around the zeolite. The importance of using small filler particles to achieve a good $n\text{-C}_4\text{H}_{10}/\text{CH}_4$ separation in PMP has been demonstrated in [95]. Significant increase in permeability has been observed only for particles smaller than 50 nm. Obviously small particles show a tendency to agglomerate, which leads to defective MMMs.[96]

One of the most influential factors during the MMM preparation is the particle agglomeration due to small particle sizes, sedimentation or migration to the surface. Due to different physical properties or different densities between the

filler and the polymer, precipitation of the additive may occur, resulting in the formation of inhomogeneous membranes. Furthermore, agglomeration of the filler particles will result in empty, non-selective voids in the MMM. One solution to eliminate the problem of sedimentation was to increase the viscosity of the MMM solution in order to slow down the process.[97, 98] Another solution is to form and dry the membranes rapidly [99] or to match the polarity of the polymer matrix and the filler's surface groups as well as a covalent binding between both phases.[100] As a rule agglomeration gets serious, when extending the filler loadings up to 30 vol-% of the MMM and when the fillers and polymers do not show any attractive interaction between each other. In contrast to sedimentation, particles agglomerates move to the membrane surface when the membranes were formed at high temperatures. This phenomenon is the result of convection cells which are formed during the film formation due to different surface tensions.[81, 101, 102]

1.3.3.2 Interface morphologies

The permeabilities of MMMs strongly depend on the nanoscale morphology of the interface between the polymer and the filler. Fig. 6 shows a schematic diagram of various nanoscale interface structures.



Fig. 6: The schematic diagram of various morphology of the mixed matrix structure.[22] Case 1 is the ideal case without morphology changes; case 2 shows a rigidified polymer due to the incorporation of filler particles; case 3 shows a reduced permeability region on the surface of the porous filler particles and case 4 illustrates the void-forming between the polymer matrix and the filler particles.

The case 1 is the ideal case, in which the filler particles and the polymer have a defect-free, structural unchanged transition. Its separation results correspond to the ideal Maxwell model predictions (see chapter 1.3.4). The second case of the diagram shows a rigidified polymer layer around the filler, which can be induced by strongly attractive interactions between the polymer and the filler surface. Case three displays a situation in which the filler pores have been partially closed by polymer chains or additives. This case is sometimes observed with zeolites in polymer matrices.[103-105] The last case shows an interface void between the filler and the polymer, caused by repulsive interactions or stress-induced void-formation.

In general, pore blockage of porous fillers always decreases the gas permeability of the MMMs, while its effect on the selectivity of MMMs is different.[104, 106] Pore blockage considerably decreases the selectivity if the original pore size of the filler is comparable to the molecular diameter of the gas molecule. On the other hand, pore blockage may increase the selectivity if the original pore size of the filler is larger than the molecular diameter of the studied gases. Since pore blockage disturbs sometimes the separation function of the inorganic filler, investigations are necessary to suppress this effect. Li et al., for example, modified the zeolite surface by using a silane coupling agent (APDEMS = (3-amino-propyl)-diethoxymethylsilane), which induced a distance of about 5-9 Å between the polymer chains and the zeolite, thus reducing the partial pore blockage.[106, 107, 108]

1.3.4 Mass transport and permeability

In the area of membrane-based gas separation, non-porous polymeric membranes separate according to the solution-diffusion model.[107-109] Herein, the gas permeation is controlled by the diffusivity coefficient (D) and the solubility coefficient (S). The diffusivity is the mobility of individual molecules passing the polymer chains. The solubility (S), in contrast, is the ratio of the dissolved penetrant concentration in the upstream face of the polymer $c_{i,z=0}$ to the upstream penetrant partial pressure p_i :

$$c_{i,z=0} = S_i \cdot p_i \quad (21)$$

The permeability (P) represents the ability of molecules to pass through a membrane:

$$P = D \cdot S \quad (22)$$

The ability of a membrane to separate two molecules i and j can be described by the ratio of their permeabilities, called the membrane selectivity α_{ij} [49]:

$$\alpha_{ij} = \frac{P_i}{P_j} \quad (23)$$

Accordingly, the difference in the permeabilities of the two gas species results not only from the diffusivity difference, but also from the differences in the

interactions with the polymer. An upper limit for the performance of polymeric membranes in gas separation was predicted by Robeson in the early 1990s.[10] Improvements have been achieved by using MMMs. To predict the MMM performance various models are available, including the Maxwell model, the Higuchi model, Landauer model, and the effective medium theory. Several studies have compared the predictions of MMMs with these studies and found that the predictions were very similar.[22, 98, 110, 111] Nevertheless, the Maxwell model is the most appropriate model to estimate the predicted MMM behavior, because of the simplicity of the expression and its well-fitting predictions. The Maxwell model first analyzed the steady-state dielectric properties in a conducting dilute suspension of identical spheres.[112] When this analysis is extended to find the composite permeability of a composite containing a dispersion of spheres, the following expression results:

$$P_{eff} = P_c \left[\frac{P_d + 2P_c - 2\phi_d(P_c - P_d)}{P_d + 2P_c + \phi_d(P_c - P_d)} \right] \quad (24)$$

where P_{eff} is the effective composite permeability, ϕ_d the volume fraction of the dispersed phase, P_c the permeability of the continuous polymer matrix and P_d the permeability of the dispersed filler material. By defining a “reduced permeation polarizability” β as [86]:

$$\beta = \frac{P_d - P_c}{P_d + 2P_c} \quad (25)$$

the effective composite permeability can also be written as

$$P_{eff} = P_c \left[\frac{1 + 2\beta\phi_d}{1 - \beta\phi_d} \right]. \quad (26)$$

For the “reduced permeation polarizability”, three different cases exist: For highly permeable fillers ($P_d \gg P_c$) β becomes 1, for equal permeability in both phases β becomes 0 and for non-permeable filler $P_d = 0$ β becomes -0.5.[113] The Maxwell model is intended to be applicable for low filler loadings ($\phi_d \leq 0.2$) since it assumes that the diffusion mass transport around filler particles is not affected by the presence of nearby particles. The Bruggeman model is an improved version of the Maxwell model for higher loads and correlates the effective permeability (P_{eff}) with the volume fraction (ϕ_d) of the dispersed phase:

$$\left[\frac{\left(\frac{P_{eff}}{P_c}\right) - \left(\frac{P_d}{P_c}\right)}{1 - \left(\frac{P_d}{P_c}\right)} \right] \cdot \left(\frac{P_{eff}}{P_c}\right)^{-\frac{1}{3}} = (1 - \phi_d) \quad (27)$$

The above Maxwell and Bruggeman models give similar results up to $\phi_d \approx 0.2$. [114] For non-ideal MMMs with interface voids, polymer chain rigidification and pore blockage, the Maxwell model can be modified to a model for a three-phase system. The permeability P_{3MMM} of this three-phase membrane was obtained by applying the Maxwell model twice. At first the permeability of the combined interface void/rigidified polymer phase and the molecular sieve can be described with a revised version of the Maxwell model, in which the molecular sieve is the dispersed phase and the interface void/rigidified polymer is the continuous phase:

$$P_{eff} = P_I \left[\frac{P_d + 2P_I - 2\phi_s(P_I - P_d)}{P_d + 2P_I + \phi_s(P_I - P_d)} \right] \quad (28)$$

Herein, P_{eff} is the permeability of the combined sieve and interface (void or rigidified polymer phase), P_d is the permeability of the dispersed sieve phase, P_I is the permeability of the interphase and ϕ_s is the volume fraction of the molecular sieve in the combined phase (molecular sieve plus interphase). Finally, the permeability of the three-phase membrane (polymer plus interphase plus molecular sieve) can be described by the permeability of the continuous polymer phase P_c and the permeability of the dispersed and combined inter- and molecular sieve phase P_{eff} . Thus, P_{3MMM} is given by:

$$P_{3MMM} = P_c \left[\frac{P_{eff} + 2P_c - 2(\phi_d + \phi_I)(P_c - P_{eff})}{P_{eff} + 2P_c + (\phi_d + \phi_I)(P_c - P_{eff})} \right] \quad (29)$$

with ϕ_d as volume fraction of the sieve phase and ϕ_I as volume fraction of the interface in the three-phase membrane.[22, 23]

References:

1. R. W. Rousseau, Handbook of separation process technology, first ed., Wiley-Interscience, New York, 1987.
2. S. P. Nunes, K.-V. Peinemann, Membrane technology: In the chemical industry, second ed., Wiley-VCH, Weinheim, 2001.
3. M. Mulder, Basic principles of membrane technology, second ed., Kluwer Academic Publishers, Dordrecht, 2000.
4. K. Scott, Handbook of industrial membranes, first ed., Elsevier Advanced Technology, Oxford, 2006.
5. A. Caetano, M. N. de Pinho, H. Muntau, Membrane technology: Applications to industrial wastewater treatment, first ed., Kluwer Academic Publishers, Dordrecht, 1995.
6. W. Koros, G. Fleming, Membrane-based gas separation, *J. Membr. Sci.* 1993, 83, 1.
7. T. Melin, R. Rautenbach, Membranverfahren Grundlagen der Modul- und Anlagenauslegung, third ed., Springer, Heidelberg, 2007.
8. N. C. Mat, Y. Lou, G. G. Lipscomb, Hollow fiber membrane modules, *Curr. Opin. Chem. Eng.* 2014, 4, 18.
9. L. Robeson, The upper bound revisited, *J. Membr. Sci.* 2008, 320, 390.
10. L. Robeson, Polymer membranes for gas separation, *Curr. Opin. Solid State Mater. Sci.* 1999, 4, 549.
11. J. E. Koresh, A. Soffer, Mechanism of permeation through molecular-sieve carbon membrane. Part 1. The effect of adsorption and the dependence on pressure, *J. Chem. Soc. Faraday Trans. I* 1986, 82, 2057.
12. H. L. Guo, G. S. Zhu, I. J. Hewitt, S. L. Qiu, “Twin copper source” growth of metal–organic framework membrane: $\text{Cu}_3(\text{BTC})_2$ with high permeability and selectivity for recycling H_2 , *J. Am. Chem. Soc.* 2009, 131, 1646.
13. R. Ranjan, M. Tsapatsis, Microporous metal organic framework membrane on porous support using the seeded growth method, *Chem. Mater.* 2009, 21, 4920.

14. Y. Y. Liu, E. P. Hu, E. A. Khan, Z. P. Lai, Synthesis and characterization of ZIF-69 membranes and separation for CO₂/CO mixture, *J. Membr. Sci.* 2010, 353, 36.
15. M. C. McCarthy, V. Varela-Guerrero, G. V. Barnett, H. K. Jeong, Synthesis of zeolitic imidazolate framework films and membranes with controlled microstructures, *Langmuir* 2010, 26, 14636.
16. S. R. Venna, M. A. Carreon, Highly permeable zeolite imidazolate framework-8 membranes for CO₂/CH₄ separation, *J. Am. Chem. Soc.* 2010, 132, 76.
17. Y. Pan, T. Li, G. Lestari, Z. P. Lai, Effective separation of propylene/propane binary mixtures by ZIF-8 membranes, *J. Membr. Sci.* 2012, 390-391, 93.
18. Y.-S. Li, F.-Y. Liang, H. Bux, A. Feldhoff, W.-S. Yang, J. Caro, Molecular sieve membrane: Supported metal–organic framework with high hydrogen selectivity, *Angew. Chem. Int. Ed.* 2010, 122, 558.
19. X. Zou, F. Zhang, S. Thomas, G. Zhu, V. Valtchev, S. Mintova, Co₃(HCOO)₆ microporous metal–organic framework membrane for separation of CO₂/CH₄ mixtures, *Chem. Eur. J.* 2011, 17, 12076.
20. S. Aguado, C.-H. Nicolas, V. Moizan-Baslé, C. Nieto, H. Amrouche, N. Bats, N. Audebrand, D. Farrusseng, Facile synthesis of an ultramicroporous MOF tubular membrane with selectivity towards CO₂, *New J. Chem.* 2011, 35, 41.
21. M. A. Aroon, A. F. Ismail, T. Matsuura, M. M. Montazer-Rahnati, Performance studies of mixed matrix membranes for gas separation: A review, *Sep. Purif. Technol.* 2010, 75, 229.
22. R. Mahajan, W. Koros, Mixed matrix membrane materials with glassy polymers. Part 1, *Polym. Eng. Sci.* 2002, 42, 1420.
23. R. Mahajan, W. Koros, Mixed matrix membrane materials with glassy polymers. Part 2, *Polym. Eng. Sci.* 2002, 42, 1432.
24. H. K. Chae, D. Y. Siberio-Pérez, J. Kim, Y. B. Go, M. Eddaoudi, A. J. Matzger, M. O’Keeffe, O. M. Yaghi, A route to high surface area, porosity and inclusion of large molecules in crystals, *Nature* 2004, 427, 523.

25. H. C. Zhou, J. Long, O. M. Yaghi, Introduction to metal-organic frameworks, *Chem. Rev.* 2012, 112, 673.
26. O. M. Yaghi, G. M. Li, Selective binding and removal of guests in a microporous metal-organic framework, *Nature* 1995, 378, 703.
27. Y. Kinoshita, I. Matsubara, T. Higuchi, Y. Saito, The crystal structure of Bis(Adiponitrilo)Copper(I) Nitrate, *Bull. Chem. Soc. Jpn.* 1959, 32, 1221.
28. S. R. Batten, N. R. Champness, X. M. Chen, J. Garcia-Martinez, S. Kitagawa, L. Öhrström, M. O’Keeffe, M. P. Suh, J. Reedijk, Terminology of metal-organic frameworks and coordination polymers (IUPAC Recommendations 2013), *Pure Appl. Chem.* 2013, 85, 1715.
29. S. R. Batten, N. R. Champness, X. M. Chen, J. Garcia-Martinez, S. Kitagawa, L. Öhrström, M. O’Keeffe, M. P. Suh, Coordination polymer, metal-organic frameworks and the need for terminology guidelines, *Cryst. Eng. Comm.* 2012, 14, 3001.
30. S. Kitagawa, R. Kitaura, S. Noro, Functional porous coordination polymers, *Angew. Chem. Int. Ed.* 2004, 43, 2334.
31. G. Férey, Hybrid porous solids: Past, present, future, *Chem. Soc. Rev.* 2008, 37, 191.
32. R. Banerjee, A. Phan, B. Wang, C. Knobler, H. Furukawa, M. O’Keeffe, O. M. Yaghi, High-throughput synthesis of zeolitic imidazolate frameworks and application to CO₂ capture, *Science* 2008, 319, 939.
33. K. S. Park, Z. Ni, A. P. Côté, J. Y. Choi, R. D. Huang, F. J. Uribe-Romo, H. K. Chae, M. O’Keeffe, O. M. Yaghi, Exceptional chemical and thermal stability of zeolitic imidazolate frameworks, *Proc. Natl. Acad. Sci. USA* 2006, 103, 10186.
34. W. Morris, C. J. Doonan, H. Furukawa, R. Banerjee, O. M. Yaghi, Crystals as molecules, postsynthesis covalent functionalization of zeolitic imidazolate frameworks, *J. Am. Chem. Soc.* 2008, 130, 12626.
35. J. J. Low, A. I. Benin, P. Jakubczak, J. F. Abrahamian, S. A. Faheem, R. R. Willis, Virtual high throughput screening confirmed experimentally: Porous coordination polymer hydration, *J. Am. Chem. Soc.* 2009, 131, 15834.

36. H. Bux, F. Liang, Y. S. Li, J. Cravillon, M. Wiebcke, J. Caro, Zeolitic imidazolate framework membrane with molecular sieving properties by microwave-assisted solvothermal synthesis, *J. Am. Chem. Soc.* 2009, 131, 16000.
37. A. M. Ortiz, A. Boutin, A. H. Fuchs, F. X. Coudert, Investigating the pressure-induced amorphization of zeolitic imidazolate framework ZIF-8: Mechanical instability due to shear mode softening, *J. Phys. Chem. Lett.* 2013, 4, 1861.
38. L. Diestel, H. Bux, D. Wachsmuth, J. Caro, Pervaporation studies of n-hexane, benzene, mesitylene and their mixtures on zeolitic imidazolate framework-8 membranes, *Micropor. Mesopor. Mater.* 2012, 164, 288.
39. D. I. Kolokolov, L. Diestel, J. Caro, D. Freude, A. G. Stepanov, Rotational and translational motion of benzene in ZIF-8 studied by ^2H NMR: Estimation of microscopic self-diffusivity and its comparison with macroscopic measurements, *J. Phys. Chem. C* 2014, 118, 12873.
40. K. Zhang, R. P. Lively, C. Zhang, R. R. Chance, W. J. Koros, D. S. Sholl, Exploring the framework hydrophobicity and flexibility of ZIF-8: From biofuel recovery to hydrocarbon separations, *J. Phys. Chem. Lett.* 2013, 4, 3618.
41. C. Gücüyener, J. van der Bergh, J. Gascon, F. Kapteijn, Ethane/ethene separation turned on its head: Selective ethane adsorption on the metal-organic framework ZIF-7 through a gate-opening mechanism, *J. Am. Chem. Soc.* 2010, 132, 17704.
42. D. Fairen-Jimenez, S. A. Moggach, M. T. Wharmby, P. A. Wright, S. Parsons, T. Düren, Opening the gate: Framework flexibility in ZIF-8 explored by experiments and simulations, *J. Am. Chem. Soc.* 2011, 133, 8900.
43. S. A. Moggach, T. D. Bennett, A. K. Cheetham, The effect of pressure on ZIF-8: Increasing pore size with pressure and the formation of a high-pressure phase at 1.47 GPa, *Angew. Chem. Int. Ed.* 2009, 38, 7087.
44. T. Chokbunpiam, R. Chanajaree, T. Remsungnen, O. Saengsawang, S. Fritsch, C. Chemlik, J. Caro, W. Janke, S. Hannongbua, N_2 in ZIF-8:

- Sorbate induced structural changes and self-diffusion, *Micropor. Mesopor. Mater.* 2014, 187, 1.
45. S. Aguado, G. Bergeret, M. P. Titus, V. Moizan, C. Nieto-Draghi, N. Bats, D. Farrusseng, Guest-induced gate-opening of a zeolitic imidazolate framework, *New J. Chem.* 2011, 35, 546.
46. J. van den Bergh, C. Gücüyener, E. A. Pidko, E. J. M. Hensen, J. Gascon, F. Kapteijn, Understanding the anomalous alkane selectivity of ZIF-7 in the separation of light alkane/alkene mixtures, *Chem. Eur. J.* 2011, 17, 8832.
47. D. L. Chen, N. Wang, F. F. Wang, J. Xie, Y. Zhong, W. Zhu, J. K. Johnson, R. Krishna, Utilizing the gate-opening mechanism in ZIF-7 for adsorption discrimination between N₂O and CO₂, *J. Phys. Chem. C* 2014, 118, 17831.
48. C. O. Ania, E. García-Pérez, M. Haro, J. J. Gutiérrez-Sevillano, T. Valdés-Solís, J. B. Parra, S. Calero, Understanding gas-induced structural deformation of ZIF-8, *J. Phys. Chem. Lett.* 2012, 3, 1159.
49. W. J. Koros, Y. H. Ma, T. Shimidzu, Terminology for membranes and membrane processes, *Pure Appl. Chem.* 1996, 68, 1479.
50. J. M. van de Graaf, F. Kapteijn, J. A. Moulijn, Methodological and operational aspects of permeation measurements on Silicalite-1 membranes, *J. Membr. Sci.* 1998, 144, 87.
51. P. W. Atkins, J. de Paula, *Physikalische Chemie*, fourth ed., Wiley-VCH, Weinheim, 2006.
52. J. Rouquérol, D. Avnir, C. W. Fairbridge, D. H. Everett, J. M. Haynes, N. Pernicone, J. D. F. Ramsay, K. S. W. Sing, K. K. Unger, Recommendations for the characterization of porous solids, *Pure Appl. Chem.* 1994, 66, 1739.
53. K. S. W. Sing, D. H. Everett, R. A. W. Haul, L. Moscou, R. A. Pierotti, J. Rouquérol, T. Siemieniewska, Reporting physisorption data for gas/solid systems with special reference to the determination of surface area and porosity, *Pure Appl. Chem.* 1985, 57, 603.
54. L. Onsager, Theories and problems of liquid diffusion, *Ann. N. Y. Acad. Sci.* 1945, 46, 241.

55. J. Kärger, D. M. Ruthven, D. N. Theodorou, Diffusion in nanoporous materials Volume 1, first ed., Wiley-VCH, Weinheim, 2012.
56. J. Kärger, Leipzig, Einstein, Diffusion, first ed., Leipziger Universitätsverlag, Leipzig, 2007.
57. Y. Li, F. Liang, H. Bux, W. Yang, J. Caro, Zeolitic imidazolate framework ZIF-7 based molecular sieve membrane for hydrogen separation, *J. Membr. Sci.* 2010, 354, 48.
58. V. M. Aceituno Melgar, H. T. Kwon, J. Kim, Direct spraying approach for synthesis of ZIF-7 membranes by electrospray deposition, *J. Membr. Sci.* 2014, 459, 190.
59. Z. Xie, J. Yang, J. Wang, J. Bai, H. Yin, B. Yuan, J. Lu, Y. Zhang, L. Zhou, C. Duan, Deposition of chemically modified α -Al₂O₃ particles for high performance ZIF-8 membrane on a macroporous tube, *Chem. Commun.* 2012, 48, 5977.
60. H. Bux, A. Feldhoff, J. Cravillon, M. Wiebcke, Y. Li, J. Caro, Oriented zeolitic imidazolate framework-8 membrane with sharp H₂/C₃H₈ molecular sieve separation, *Chem. Mater.* 2011, 23, 2262.
61. Y. Pan, B. Wang, Z. Lai, Synthesis of ceramic hollow fiber supported zeolitic imidazolate framework-8 (ZIF-8) membranes with high hydrogen permeability, *J. Membr. Sci.* 2012, 421, 292.
62. K. Tao, L. Cao, Y. Lin, C. Kong, L. Chen, A hollow ceramic fiber supported ZIF-8 membrane with enhanced gas separation performance prepared by hot dip-coating seeding, *J. Mater. Chem. A* 2013, 1, 13046.
63. L. Ge, A. Du, M. Hou, V. Rudolph, Z. Zhu, Enhanced hydrogen separation by vertically-aligned carbon nanotube membranes with zeolite imidazolate frameworks as a selective layer, *RSC Adv.* 2012, 2, 11793.
64. Y. Pan, Z. Lai, Sharp separation of C₂/C₃ hydrocarbon mixtures by zeolitic imidazolate framework-8 (ZIF-8) membranes synthesized in aqueous solutions, *Chem. Commun.* 2011, 47, 10275.
65. K. Tao, C. Kong, L. Chen, High performance ZIF-8 molecular sieve membrane on hollow ceramic fiber via crystallizing-rubbing seed deposition, *Chem. Eng. J.* 2013, 220, 1.

66. M. Shah, H. T. Kwon, T. Vu, S. Sachdeva, H. K. Jeong, One step in situ synthesis of supported zeolitic imidazolate framework ZIF-8 membranes: Role of sodium formate, *Micropor. Mesopor. Mater.* 2013, 165, 63.
67. K. Huang, Z. Dong, Q. Li, W. Jin, Growth of a ZIF-8 membrane on the inner-surface of a ceramic hollow fiber via cycling precursors, *Chem. Commun.* 2013, 49, 10326.
68. A. Huang, H. Bux, F. Steinbach, J. Caro, Molecular-sieve membrane with hydrogen permselectivity: ZIF-22 in LTA topology prepared with 3-aminopropyltriethoxysilane as covalent linker, *Angew. Chem. Int. Ed.* 2010, 49, 4958.
69. X. Dong, K. Huang, S. Liu, R. Ren, W. Jin, Y. S. Lin, Synthesis of zeolitic imidazolate framework-78 molecular-sieve membrane: Defect formation and elimination, *J. Mater. Chem.* 2012, 22, 19222.
70. A. Huang, J. Caro, Covalent post-functionalization of zeolitic imidazolate framework ZIF-90 membrane for enhanced hydrogen selectivity, *Angew. Chem. Int. Ed.* 2011, 50, 4979.
71. A. Huang, W. Dou, J. Caro, Steam-stable zeolitic imidazolate framework ZIF-90 membrane with hydrogen selectivity through covalent functionalization, *J. Am. Chem. Soc.* 2010, 132, 15562.
72. A. Huang, N. Wang, C. Kong, J. Caro, Organosilica-functionalized zeolitic imidazolate framework ZIF-90 membrane with high gas-separation performance, *Angew. Chem. Int. Ed.* 2012, 51, 10551.
73. A. J. Brown, J. R. Johnson, M. E. Lydon, W. J. Koros, C. W. Jones, S. Nair, Continuous polycrystalline zeolitic imidazolate framework-90 membranes on polymeric hollow fibers, *Angew. Chem. Int. Ed.* 2012, 51, 10615.
74. A. Huang, Y. Chen, N. Wang, Z. Hu, J. Jiang, J. Caro, A highly permeable and selective zeolitic imidazolate framework ZIF-95 membrane for H₂/CO₂ separation, *Chem. Commun.* 2012, 48, 10981.
75. B. R. Pimentel, A. Parulkar, E. Zhou, N. A. Brunelli, R. P. Lively, Zeolitic imidazolate frameworks: Next-generation materials for energy-efficient gas separations, *Chem. Sus. Chem.* 2014, 7, 3202.

76. D. R. Paul, D. R. Kemp, The diffusion time lag in polymer membranes containing adsorptive fillers, *J. Polym. Sci.: Polym. Phys.* 1973, 41, 79.
77. S. Kulprathipanja, R. W. Neuzil, N. N. Li, Separation of fluids by means of mixed matrix membranes, US patent 4740219, 1988.
78. R. Mahajan, W. J. Koros, Factors controlling successful formation of mixed-matrix gas separation materials, *Ind. Eng. Chem. Res.* 2000, 39, 2692.
79. V. Bhardwaj, A. Macintosh, I. D. Sharpe, S. A. Gordeyev, S. J. Shilton, Polysulfone hollow fiber gas separation membranes filled with submicron particles, *Ann. N. Y. Acad. Sci.* 2003, 984, 318.
80. R. D. Noble, Perspectives on mixed matrix membranes, *J. Membr. Sci.* 2011, 378, 393.
81. T. S. Chung, L. Y. Jiang, Y. Li, S. Kulprathipanja, Mixed matrix membranes (MMMs) comprising organic polymers with dispersed inorganic fillers for gas separation, *Prog. Polym. Sci.* 2007, 32, 483.
82. P. Bernardo, E. Drioli, G. Golemme, Membrane gas separation: A review/state of the art, *Ind. Eng. Chem. Res.* 2009, 48, 4638.
83. H. Vinh-Thang, S. Kaliaguine, Predictive models for mixed matrix membrane performance: A review, *Chem. Rev.* 2013, 113, 4980.
84. A. Car, C. Stropnik, K. V. Peinemann, Hybrid membrane materials with different metal-organic frameworks (MOFs) for gas separation, *Desalination* 2006, 200, 424.
85. T. H. Bae, J. S. Lee, W. Qiu, W. J. Koros, C. W. Jones, S. Nair, A high-performance gas-separation membrane containing submicrometer-sized metal-organic framework crystals, *Angew. Chem. Int. Ed.* 2010, 49, 9863.
86. S. Basu, A. Cano-Odena, I. F. J. Vankelecom, Asymmetric Matrimid[®]/[Cu₃(BTC)₂] mixed-matrix membranes for gas separations, *J. Membr. Sci.* 2010, 362, 478.
87. Y. Yampolskii, Methods for investigation of the free volume in polymers, *Russ. Chem. Rev.* 2007, 76, 59.
88. I. F. J. Vankelecom, E. Mercks, M. Luts, J. B. Uytterhoeven, Incorporation of zeolite in polyimide membranes, *J. Phys. Chem.* 1995, 99, 13187.

89. Y. Yampolskii, Polymeric gas separation membranes, *Macromolecules* 2012, 45, 3298.
90. T. C. Merkel, B. D. Freeman, R. J. Spontak, Z. He, I. Pinnau, P. Meakin, A. J. Hill, Ultrapermeable, reverse-selective nanocomposite membranes, *Science* 2002, 296, 519.
91. T. T. Moore, W. J. Koros, Non-ideal effects in organic-inorganic materials for gas separation membranes, *J. Mol. Struct.* 2005, 739, 87.
92. T. C. Merkel, Z. He, I. Pinnau, B. D. Freeman, P. Meakin, A. J. Hill, Sorption and transport in poly(2,2-bis(trifluoromethyl)-4,5-difluoro-1,3-dioxole-co-tetrafluoro-ethylene) containing nanoscale fumed silica, *Macromolecules* 2003, 36, 8406.
93. H. Yehia, T. J. Pisklak, J. P. Ferraris, K. J. Balkus, I. H. Musselman, Methane facilitated transport using copper(II)biphenyldicarboxylate-triethylenediaminepoly(3-acetoxyethylthiophene) mixed matrix membranes, *Polym. Prepr.* 2004, 45, 35.
94. Ş. B. Tantekin-Ersolmaz, Ç. Alalay-Orala, M. Tather, A. Erdem-Şenatalar, B. Schoeman, J. Sterte, Effect of zeolite particle size on the performance of polymer-zeolite mixed matrix membranes, *J. Membr. Sci.* 2000, 175, 285.
95. Z. He, I. Pinnau, A. Morisato, Nanostructured poly(4-methyl-2-pentyne)/silica hybrid membranes for gas separation, *Desalination* 2002, 146, 11.
96. B. Zornoza, C. Téllez, J. Coronas, J. Gascon, F. Kapteijn, Metal organic framework based mixed matrix membranes: An increasingly important field of research with a large application potential, *Micropor. Mesopor. Mater.* 2013, 166, 67.
97. J. P. Boom, Transport through zeolite filled polymeric membranes. Ph. D. thesis, The Netherlands: University of Twente, 1994.
98. R. Mahajan, Formation, characterization and modeling of mixed matrix membrane materials, Ph. D. thesis, USA: University of Texas at Austin, 2000.

99. D. Q. Vu, W. J. Koros, S. J. Miller, Mixed matrix membranes using carbon molecular sieves. I. Preparation and experimental results, *J. Membr. Sci.* 2003, 211, 311.
100. T. C. Merkel, B. D. Freeman, R. J. Spontak, Z. He, I. Pinnau, Ultrapermeable, reverse-selective nanocomposite membranes, *Science* 2002, 296, 519.
101. R. Mahajan, R. Burns, M. Schaeffer, W. J. Koros, Challenges in forming successful mixed matrix membranes with rigid polymeric materials, *J. Appl. Poly. Sci.* 2002, 86, 881.
102. V. G. Levich, V. S. Krylov, Surface-tension-drive phenomena, *Annu. Rev. Fluid Mech.* 1969, 1, 293.
103. R. Mahajan, W. J. Koros, Factors controlling successful formation of mixed-matrix gas separation materials, *Ind. Eng. Chem. Res.* 2000, 39, 2692.
104. Y. Li, H. M. Guan, T. S. Chung, S. Kulprathipanja, Effects of novel silane modification of zeolite surface on polymer chain rigidification and partial pore blockage in polyethersulfone (PES)-zeolite A mixed matrix membranes, *J. Membr. Sci.* 2006, 275, 17.
105. G. Clarizia, C. Algieri, E. Drioli, Filler-polymer combination: A route to modify gas transport properties of a polymeric membrane, *Polymer*, 2004, 45, 5671.
106. Y. Li, T. S. Chung, C. Cao, S. Kulprathipanja, The effects of polymer chain rigidification, zeolite pore size and pore blockage on polyethersulfone (PES)-zeolite A mixed matrix membrane, *J. Membr. Sci.* 2005, 260, 45.
107. R. W. Spillman, Economics of gas separation membranes, *Chem. Eng. Prog.* 1989, 85, 41.
108. G. W. Meindersma, M. Kuczynski, Implementing membrane technology in process industry: Problems and opportunities, *J. Membr. Sci.* 1996, 113, 285.
109. B. D. Freeman, I. Pinnau, *Polymer membrane for gas and vapor separations: Chemistry and material science*, first ed., American Chemical Society, Washington D.C., 1999.

110. J. H. Petropoulos, A comparative study of approaches applied to the permeability of binary composite polymeric materials, *J. Polym. Sci.: Polym. Phys.* 1985, 23, 1309.
111. C. M. Zimmerman, A. Singh, W. J. Koros, Tailoring mixed matrix composite membranes for gas separations, *J. Membr. Sci.* 1997, 137, 145.
112. J. C. Maxwell, *A treatise on electricity and magnetism*, third ed., Dover Publications Inc., New York, 1954.
113. H. B. T. Jeazet, T. Koschine, C. Staudt, K. Raetzke, C. Janiak, Correlation of gas permeability in a metal-organic framework MIL-101 (Cr)-Polysulfone mixed-matrix membrane with free volume measurements by positron annihilation lifetime spectroscopy (PALS), *Membr.* 2013, 3, 331.
114. R. H. B. Bouma, A. Checchetti, G. Chidichimo, E. Drioli, Permeation through a heterogeneous membrane: The effect of the dispersed phase, *J. Membr. Sci.* 1997, 128, 141.

2 Pervaporative separation of benzene containing mixtures on ZIF-8 membranes

2.1 Summary

The separation of alkanes and aromatics is a popular topic, which gets increasingly important since a recent regulation of the US Environmental Protection Agency called most refiners on to reduce the benzene content in gasoline to less than 0.62 vol-% till 2013. Unfortunately, it is difficult to meet the demands only with pre-fraction of the naphtha stream. The pervaporation or vapor permeation of the n-alkane/aromatic mixture by nanoporous membranes would be a less-energy intensive solution for this problem.

In chapter 2.2 ZIF-8 was evaluated as a selective membrane for the pervaporative separation of n-hexane/benzene and n-hexane/mesitylene. Although the size of the pore window of ZIF-8 is 3.4 Å from crystallographic data, it was found no sharp separation between the n-alkane and the bulky benzene molecule, whereas mesitylene was not adsorbed. This experimental finding can be explained by a marked framework flexibility of ZIF-8.

Additional ^2H NMR experiments were carried out by our cooperation partners from the Boreskov Institute of Catalysis in Novosibirsk, who characterized and quantified the molecular dynamics of benzene adsorbed in ZIF-8 (chapter 2.3). It could be observed that the benzene molecule undergoes fast rotations within the ZIF-8 cage and relatively slow isotropic reorientations by collisions with the walls. Furthermore, benzene undergoes also translational jump diffusions between neighboring cages. The benzene mobility could be estimated by the self-diffusion coefficient of $D_{self}^0 \approx 4 \cdot 10^{-16} \text{m}^2 \text{s}^{-1}$ at $T = 323 \text{ K}$. The macroscopic pervaporation measurements of our group, however, showed a diffusivity of $3.5 \cdot 10^{-15} \text{m}^2 \text{s}^{-1}$ at $T = 298 \text{ K}$ and a fractional occupancy of $\Theta = 0.99$. This experimental finding could demonstrate the limits of macroscopic measurements.

2.2 Pervaporation studies of n-hexane, benzene, mesitylene and their mixtures on zeolitic imidazolate framework-8 membranes

Lisa Diestel, Helge Bux, Dennis Wachsmuth and Jürgen Caro

Microporous and Mesoporous Materials 2012, 192, 288-293.

Reprinted (adapted) with permission from *Microporous and Mesoporous Materials*. Copyright (2012) Elsevier.

[doi:10.1016/j.micromeso.2012.06.031](https://doi.org/10.1016/j.micromeso.2012.06.031)



Pervaporation studies of *n*-hexane, benzene, mesitylene and their mixtures on zeolitic imidazolate framework-8 membranes

Lisa Diestel, Helge Bux, Dennis Wachsmuth, Jürgen Caro*

Leibniz University Hannover, Institute of Physical Chemistry and Electrochemistry, Callinstr. 3a, 30167 Hannover, Germany

ARTICLE INFO

Article history:
Available online 28 July 2012

Keywords:
ZIF-8 membrane
Pervaporation
Breathing
Gate opening

ABSTRACT

The metal–organic framework (MOF) ZIF-8 (ZIF-8 = zeolitic imidazolate framework-8) was evaluated as molecular sieve membrane in the pervaporation of the two liquid mixtures *n*-hexane/benzene and *n*-hexane/mesitylene. Though it is known from permeation studies of light gases that ZIF-8 membranes show no sharp separation cut-off at the estimated crystallographic pore size of 3.4 Å, highly branched or aromatic hydrocarbons > C₅ could be expected therefore to become rejected by the ZIF-8 pores thus remaining in the retentate. However, the ZIF-8 membrane shows for *n*-hexane and benzene remarkable fluxes. Under consideration of the leakage of the apparatus, we can state that *n*-hexane and benzene can pass the ZIF-8 membrane. Benzene had a lower flux than *n*-hexane, whereas for mesitylene we could only observe a very small leakage rate through the O-ring gasket. Correspondingly, medium mixture separation factors have been found for the pervaporation separation of a liquid *n*-hexane/benzene mixture. Additional mixed gas hydrogen/methane separations, adsorption experiments and leak rate measurements were carried out to evaluate the results.

© 2012 Elsevier Inc. All rights reserved.

1. Introduction

The separation of alkanes and aromatics is a popular topic, which nowadays gets even more important. One of the US EPA's (EPA = Environmental Protection Agency) recent regulation (MSAT II) calls refiners to further reduce aromatic compounds to less than 0.62 vol.% in US gasoline until 2013 [1]. A survey published by EPA showed that most of the refiners plan to install additional naphtha pre-fractionation capacities [2]. The catalytic conversion of aromatics as proposed by Weitkamp can be a competing technology [3]. Molecular sieving of *n*-alkane/aromatic mixtures by nanopore membranes in pervaporation or vapour permeation might be another competing technology to distillation.

Molecular sieve membranes, such as zeolite membranes, are based on the principle of physical separation by size exclusion [4]. Additionally, also the interplay of mixed component adsorption and diffusion can result in remarkable separation effects [5]. However, up to now, only LTA zeolite membranes are used in the de-watering of bio-ethanol [6]. There is still no commercial zeolite membrane-based gas separation process on the market. It is hoped that metal–organic framework (MOFs)-based membranes can solve the problems encountered in the development of zeolite membranes [7,8]. MOFs are porous hybrid organic–inorganic

materials consisting of metal cations or metal oxide clusters bridged by organic linker molecules [9–11]. Their mechanical properties are located between inorganic zeolites and organic polymers [12]. MOFs show remarkable properties such as ultra-high inner surfaces, framework flexibility (e.g., breathing or gate opening effects) [13], and chirality [14]. It is, therefore, not surprising that MOFs are currently discussed for multiple purposes, such as carriers for drug delivery [15,16], as a storages for hydrogen [17,18] or for capturing greenhouse gases [19,20], and as future catalyst materials [21,22]. MOF syntheses are widely template-free and can be even performed at room temperature by non-classical methods as layer-by-layer growth [23–25]. This might open new and efficient pathways for membrane productions that are impossible to realize with classical molecular sieves as zeolites. Recently, several groups reported breakthroughs in the preparation of polycrystalline MOF molecular sieve membranes showing selectivity above Knudsen in gas separation experiments [26–36]. However, there are up to now only a few examples utilizing polycrystalline MOF membranes for liquid phase separation by pervaporation [37].

In our recent publications, we discussed the separation properties of polycrystalline MOF membranes employing ZIF-8 (ZIF-8 = zeolitic imidazolate framework-8 [38]) in several light gas permeation experiments [39]. On the basis of these experiments and reports from other groups [29–31], it can be concluded that the framework flexibility of ZIF-8 prevents sharp molecular sieving (cut off) like it is observed for zeolite membranes with a more rigid

* Corresponding author.

E-mail address: juergen.caro@pci.uni-hannover.de (J. Caro).

framework. In this report, to the best of our knowledge, we present the first liquid separation experiments with polycrystalline ZIF-8 membranes by pervaporation. In our investigations, we focused on the separation of liquid mixtures of *n*-hexane (critical diameter¹ $\sigma = 4.3 \text{ \AA}$ [40]) with benzene ($\sigma = 5.8 \text{ \AA}$ [40]) and with mesitylene (1,3,5-trimethylbenzene, $\sigma = 8.4 \text{ \AA}$ [41]), respectively. Although the size of the pore window of ZIF-8 is estimated to be 3.4 \AA from crystallographic data, several reports have shown that the framework structure of ZIF-8 is in fact more flexible rather than static and even large molecules like CH_4 (critical diameter 3.8 \AA) can enter the pore network [42,43]. In their report on chromatography by ZIF-8, Luebbbers et al. demonstrated that *n*-alkanes (critical diameter 4.3 \AA) become easily adsorbed by ZIF-8 [44]. Another chromatographic study showed that more bulky branched alkanes (critical diameter $> 5.4 \text{ \AA}$) are not able to pass the narrow pore windows of ZIF-8 whereas the linear ones are adsorbed [46]. The consideration of framework flexibility is crucial to predict correct separations on MOF membranes. Permeation studies on ZIF-22 [47] and ZIF-90 [48] membranes also showed that no sharp cut-off exists for hydrocarbons with critical diameters larger than the crystallographic pore size. A more appropriate expression for the terminus "breathing" might be "gate opening" [49]. In a recent paper of Kapteijn's group, it was shown that ethane is adsorbed by ZIF-7 at a lower pressure in comparison to the only slightly lighter and stiffer ethylene [50].

It is, therefore, the aim of this paper to study for the first time single component pervaporation of *n*-hexane, benzene, and mesitylene as well as of their binary mixtures on a supported ZIF-8 membrane. Additional mixed gas studies will be done for membrane evaluation.

2. Experimental

2.1. Synthesis of ZIF-8 nanocrystals and seeding suspension

ZIF-8 nanocrystals were prepared by the method reported by Cravillon et al. [51]. $0.73 \text{ g ZnNO}_3 \cdot 6\text{H}_2\text{O}$ (2.45 mmol , 1 eq.) in 50 mL methanol and 0.81 g 2-methylimidazole (9.86 mmol , 4 eq.) in 50 mL methanol were mixed under vigorous stirring and kept for 2 h at room temperature. Afterwards, the precipitate was collected by centrifugation and washed two times with 50 mL methanol. Meanwhile, 0.12 g sodium hydrogen carbonate and 1.20 g polyethyleneimine (PEI, $\sim 50\%$ in water, 4 wt.%) were solved in 30 mL water. Eventually, 0.80 g wet ZIF-8 nanoparticles (2.5 wt.%) were added to the solution, and the suspension was stirred overnight.

2.2. ZIF-8 membrane preparation

The polycrystalline ZIF-8 membranes were prepared on the basis of a fine-tuned procedure we published recently [39]. As porous support, asymmetric $\alpha\text{-Al}_2\text{O}_3$ microfiltration disc membranes ($18 \text{ mm} \times 1 \text{ mm}$; Fraunhofer IKTS, former Hermsdorfer HITK, Germany) were used. The previously cleaned supports (acetone, dried at $90 \text{ }^\circ\text{C}$) were dipped in the seeding suspension at $30 \text{ }^\circ\text{C}$ and 15% RH. The dipping parameters were set as following: up speed = 200 mm min^{-1} , down speed = 300 mm min^{-1} , lower delay = 10 s, and upper delay = 3 min. The coated supports were dried overnight at room temperature. For the secondary growth process 0.54 g ZnCl_2 (3.94 mmol , 1 eq.), 0.49 g 2-methylimidazole

¹ The critical diameter is the smallest cross-sectional diameter. It can be calculated from the Lennard-Jones potential under consideration of the electron clouds [40]. Another approach for the determination of critical parameters is the determination of the "shadow" of a molecule from the projection of the molecule to different planes [45].

(5.92 mmol , 1.5 eq.) and 0.27 g sodium formate (3.94 mmol , 1 eq.) were solved in 80 mL methanol. The solution was filled in a 200 mL Teflon autoclave and one of the coated supports was put vertically in the solution. The closed autoclave was heated in the microwave oven with a heating rate of $7.5 \text{ }^\circ\text{C min}^{-1}$ at $100 \text{ }^\circ\text{C}$ for 1.5 h. After the autoclave was cooled down to room temperature, the membrane was washed with 20 mL methanol and dried overnight at room temperature.

2.3. Characterizations

X-ray diffraction (XRD analysis of a typical ZIF-8 membrane was carried out on a Bruker D8 Advance diffractometer (reflection mode, $\text{Cu K}\alpha$ radiation). The 2θ range from 5 to 50 was scanned with a step size of 0.02. For scanning electron microscopy (SEM), a typical membrane was manually broken for cross sectional view. The images were taken on a JEOL JSM-6700F instrument (acceleration voltage = 10 kV , current = $10 \text{ }\mu\text{A}$).

2.4. Gas permeation measurements on ZIF-8 membranes

For an evaluation and comparison with previously prepared supported ZIF-8 membranes, mixed gas separation was measured in a modified Wicke-Kallenbach apparatus using an equimolar H_2/CH_4 feed with a total flow rate of 100 ml min^{-1} at 1.6 bar pressure. N_2 was used as sweep gas with 50 ml min^{-1} at a pressure of 1 bar.

2.5. Pervaporation experiments on ZIF-8 membranes

For the pervaporation experiments, we used a home-built apparatus as shown in Fig. 1. To seal the membranes within the pervaporation module, rubber O-ring gaskets made from different materials were tested (Table 1). For FKM50 O-Rings a leak rate of $0.3\text{--}1.2 \times 10^{-7} \text{ mol/min cm}^2$ have been determined for *n*-hexane, benzene and mesitylene. In the following hydrocarbon pervaporation studies, FKM50 has been used to seal the membrane.

The feed mixtures contained different vol.% ratios of (i) *n*-hexane and benzene and (ii) *n*-hexane and mesitylene. The driving force for mass transfer across the membrane was applied by using reduced pressure (vacuum) of about 4 mbar. The permeate was collected in liquid nitrogen cooling traps, and the collecting process were stopped after 30 min. The collected samples were weighted by a precision balance and their composition analyzed by gas chromatography (GC).

The ideal permselectivity $\alpha_{ij}^{\text{ideal}}$ can be calculated from the pure component fluxes N_i and N_j and is defined as follows [52]:

$$\alpha_{ij}^{\text{ideal}} = \frac{N_i}{N_j} \quad (1)$$

The corresponding binary mixture separation factor $\alpha_{ij}^{\text{real}}$ can be calculated by dividing the molar ratio of the permeate x_i/x_j by the molar ratio of the retentate y_i/y_j .

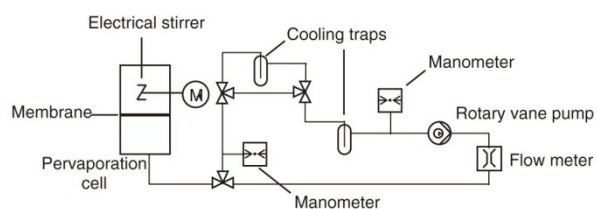


Fig. 1. Experimental setup of the pervaporation equipment.

2. Pervaporative separation of benzene containing mixtures on ZIF-8 membranes

290

L. Diestel et al. / *Microporous and Mesoporous Materials* 164 (2012) 288–293

Table 1

Leakage rates of different O-ring gasket materials in mesitylene, hexane and benzene “pervaporation” at 23 °C using a metal plate instead of a ZIF-8 membrane.

Gasket material	Liquid	Leakage [mol/min cm ²]
VMQ70	Mesitylene	2.8×10^{-7}
FKM70	Mesitylene	2.5×10^{-7}
Kalrez [®] 6375	Mesitylene	3.0×10^{-7}
FKM50	Mesitylene	0.3×10^{-7}
FKM50	Hexane	1.2×10^{-7}
FKM50	Benzene	0.8×10^{-7}

$$\alpha_{ij}^{real} = \frac{X_i/X_j}{Y_i/Y_j} \quad (2)$$

2.6. Liquid phase adsorption studies

To prove the adsorption of hexane, benzene and mesitylene by ZIF-8 we did some liquid phase adsorption studies. Therefore, we put 0.1 g activated ZIF-8 microcrystals, which were dried for 7 days at 90 °C, in glass vials and add equimolar liquid mixtures of ethanol and hexane, benzene or mesitylene, respectively. The vials were closed air-tight and stored for 24 h at room temperature. Afterwards, the remaining liquids were weighted and analyzed by GC. The adsorbed amounts of alkane, aromatics and ethanol were calculated from the molar amount of the liquid mixture in the beginning minus the molar amount of the remained liquid divided by the mass of added ZIF-8.

3. Results and discussion

3.1. Characterization of the ZIF-8 membranes

The top and the cross-section views of the supported ZIF-8 membrane prepared as described in Section 2.2 are shown in Fig. 2. The SEM images illustrate that the ZIF-8 membrane layer of about 15 μm thickness is continuously and densely grown on top of the α-Al₂O₃ microfiltration support.

The XRD patterns (Fig. 3) show the phase purity of the ZIF-8 layer formed.

In the mixed gas permeation of an equimolar hydrogen/methane mixture after Wicke–Kallenbach a mixed gas separation factor α_{H_2/CH_4}^{real} of 15 has been measured analyzing the retentate and permeate compositions by gas chromatography. The individual fluxes amount $N_{H_2} \approx 0.244$ ml/min cm² and $N_{CH_4} \approx 0.015$ ml/min cm². Both this separation factor and the fluxes are characteristic of high-quality ZIF-8 membranes [39].

It has to be noted that – as already discussed in the Introduction – the critical size of methane is with 3.8 Å too big to

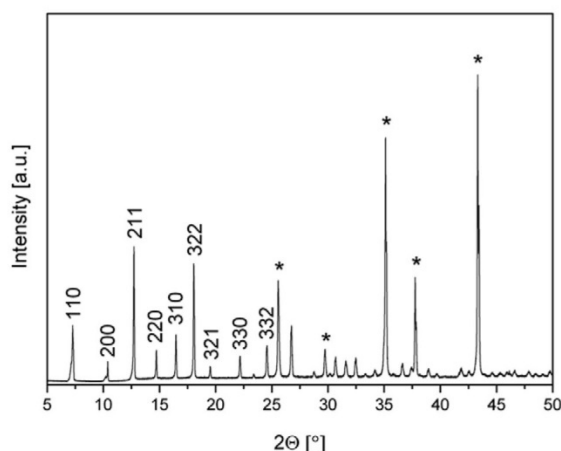


Fig. 3. XRD pattern of the ZIF-8 membrane under study. Reflections marked by asterisks denote signals from the α-Al₂O₃ microfiltration support.

enter a ZIF-8 pore assuming a rigid 3.4 Å pore size (see Fig. 4b). This pore size originates from single crystal studies of ZIF-8 as shown in Fig. 4a [53]. However, from pioneering in situ XRD studies it is known that the imidazolite linkers show a swing effect upon gas adsorption, thus the pores open and give access to the cavity [49].

3.2. Pervaporation

3.2.1. *n*-Hexane/benzene

The permeate flux N_i in mol min⁻¹ cm⁻² across the ZIF-8 membrane was calculated from the total amount of the permeate collected by freezing. First experiments with the pure components *n*-hexane and benzene showed significant mass transfers for both species. The flow rates were found to amount $N_{nCG} \approx 8.5 \times 10^{-6}$ mol min⁻¹ cm⁻² for hexane (nCG) and $N_{bnz} \approx 4.4 \times 10^{-7}$ mol min⁻¹ cm⁻² for benzene (bnz). After subtracting the leakage rates (Table 1), fluxes of $N_{nCG} \approx 8.4 \times 10^{-6}$ mol min⁻¹ cm⁻² and $N_{bnz} \approx 3.6 \times 10^{-7}$ mol min⁻¹ cm⁻² remain. From this corrected fluxes, for *n*-hexane/benzene separation, an ideal permselectivity $\alpha_{nCG, bnz}^{ideal} \approx 23$ can be predicted. For the equimolar *n*-hexane/benzene mixture, the real mixture separation factor $\alpha_{nCG, bnz}^{real}$ was found to be much less and amounts to only 8.4 if taking the small leakage effect into consideration. This finding, that the real mixture separation factor is much less than the ideal permselectivity, is characteristic of a physical situation if mass transport of a mobile component – like *n*-hexane – is blocked by a less mobile one – like benzene. It follows indeed from the liquid phase adsorption studies

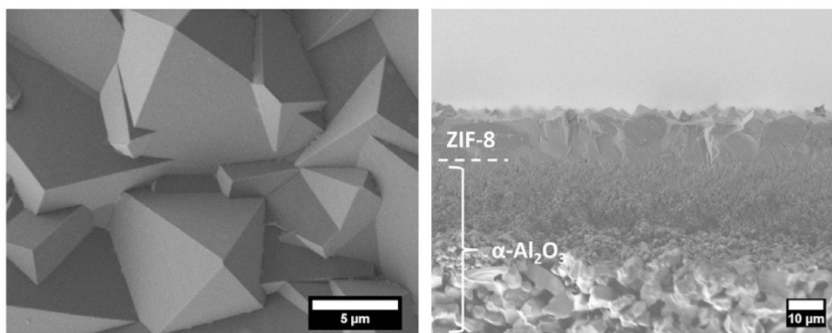


Fig. 2. SEM top view and cross section of the ZIF-8 membrane under study. The ZIF-8 membrane layer is located on an α-Al₂O₃ microfiltration support.

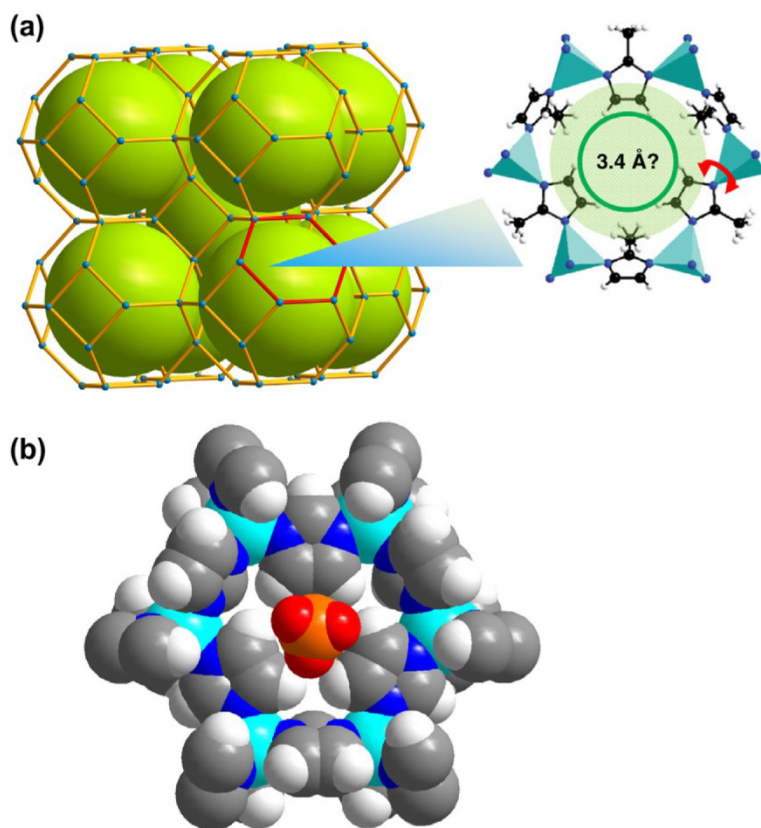


Fig. 4. (a) Orientation of the methylimidazolite ring in the 6-membered Zn-methylimidazolite-Zn ring as determined from single crystal XRD data [53]. By adding the covalent radius of hydrogen, an open pores size of 3.4 Å is estimated. (b) A methane molecule (central molecule with van der Waals radii) with a critical size of 3.8 Å seems unable to pass the ZIF-8 pore (outer 6-membered ring with the corresponding van der Waals radii) assuming a rigid framework.

shown in Fig. 5 that benzene – as the less mobile component in comparison with *n*-hexane – becomes adsorbed by ZIF-8.

To investigate the possibility of the adsorption of benzene and mesitylene in ZIF-8, liquid adsorption studies were carried out as described in Section 2.6. For this purpose, the corresponding adsorbates *n*-hexane, benzene and mesitylene, were mixed with the solvent ethanol. To prevent competition in adsorption between the solvent and the adsorbates under study, ethanol was employed as

solvent since ZIF-8 favors non-polar adsorbates over polar ones [54]. This assumption is in complete accordance with the findings from the adsorption of liquid mixtures (Fig. 6). Though the experiments are quite simple and do not allow quantitative statements, they qualitatively confirm the expectation that *n*-hexane and benzene, but not mesitylene, are adsorbed by ZIF-8. Interestingly and in contrast to the finding from Luebbers et al. [44], the

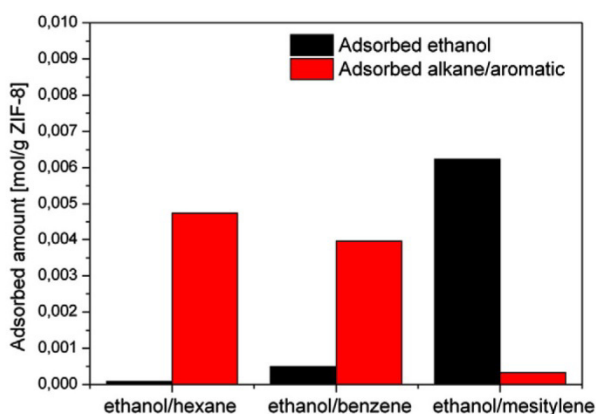


Fig. 5. Adsorption of binary equimolar mixtures of *n*-hexane, benzene and mesitylene with ethanol on ZIF-8 powder at 23 °C for 24 h contact time.

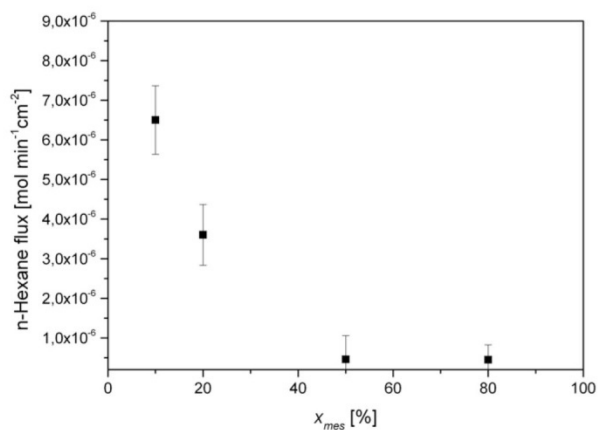


Fig. 6. *n*-Hexane fluxes from an *n*-hexane/mesitylene mixture through a supported ZIF-8 membrane as function of the molar mesitylene ratio x_{mes} in the liquid *n*-hexane/mesitylene feed at room temperature.

2. Pervaporative separation of benzene containing mixtures on ZIF-8 membranes

292

L. Diestel et al. / *Microporous and Mesoporous Materials* 164 (2012) 288–293

measurements show that despite its molecular size benzene can be adsorbed within the ZIF-8 framework. It is interesting to note that the volume of the adsorbed *n*-hexane corresponds to the published pore volume of ZIF-8 of 0.66 cm³/g [38]. The whole amount of the adsorbed amounts of ethanol and benzene occupies a volume of about 0.4 cm³/g which means that not the whole pore volume of ZIF-8 is occupied which might be a kinetic effect. However, there is no doubt that benzene becomes remarkably adsorbed under our experimental conditions by ZIF-8. This experimental finding is in complete accordance with the results of recent breakthrough experiments showing that *p*-xylene is adsorbed by ZIF-8 although its kinetic diameter is almost twice as large as the formal pore size [55].

3.2.2. *n*-Hexane/mesitylene

Since the single component flux of mesitylene $N_{mes} \approx 3.0 \times 10^{-8}$ mol min⁻¹ cm⁻² was found to be in the order of the leak flux, it is not useful to calculate ideal permselectivities and real mixture separation factors. However, we studied the pervaporation of *n*-hexane/mesitylene on a ZIF-8 membrane for different feed compositions (Fig. 6). With increasing mesitylene concentrations up to molar ratio *n*-hexane:mesitylene ≈ 0.5 , the *n*-hexane flux decreases continuously. For molar mesitylene concentrations >50%, the *n*-hexane flux does not further decrease. Obviously, a critical mesitylene concentration of $N_{mes} \leq 50\%$ is necessary to form the blocking mesitylene layer for the uptake of *n*-hexane by the ZIF-8 membrane. This finding is in complete accordance with the model that a non-transporting bulky molecule blocks the pore entrances for the mobile component as observed for the sorption kinetics of *n*-decane on 5A zeolites from nonadsorbing solvents [56].

From the adsorptions studies of the ethanol/benzene mixture it followed clearly (see Section 3.2.1 and Fig. 5) that benzene becomes adsorbed by ZIF-8. However, no remarkable adsorption was found for mesitylene but with increasing mesitylene concentration in the feed, pore blocking by mesitylene reduces the pervaporation flux of *n*-hexane.

4. Conclusions

Supported polycrystalline ZIF-8 membranes were evaluated by separating liquid mixtures of *n*-hexane/benzene and *n*-hexane/mesitylene as feed in pervaporation experiments at room temperature. Even considering the framework flexibility that already has proven to spoil a clear cut off in the separation performance of ZIF-8 in light gas permeation experiments, bulky aromatic compounds should not be able to enter the framework and a molecular sieve exclusion separation was expected. Surprisingly, this sharp separation could not be found experimentally. Accordingly, simple liquid adsorption experiments were carried out with mixtures of the hydrocarbons under study and ethanol. The measurements qualitatively show that *n*-hexane and benzene become adsorbed by ZIF-8, but mesitylene not. This corresponds to the trend found in pervaporation experiments, showing that the real mixture separation factor is lower than the predicted ideal permselectivity for *n*-hexane/benzene in comparison with *n*-hexane/mesitylene since the mobile component *n*-hexane is blocked by the less mobile one benzene. In contrast, for *n*-hexane/mesitylene, molecular sieving takes place and with increasing mesitylene concentration in the binary mixture, the *n*-hexane flux is increasingly reduced by pore entrance blocking.

Acknowledgements

This work was financed by DFG in the frame of Priority Program 1362 (Porous Metal–Organic Frameworks), organized by S. Kaskel

(Dresden). We thank F. Kapteijn and J. Gascon (Delft) for the construction and manufacture of the permeation module.

References

- [1] Summary and Analysis of the 2009 Gasoline Benzene Pre-Compliance Reports, EPA United States Environmental Protection Agency, Washington, 2009.
- [2] Summary and Analysis of the 2011 Gasoline Benzene Pre-Compliance Reports, EPA United States Environmental Protection Agency, Washington, 2011.
- [3] J. Weitkamp, A. Raichle, Y. Traa, M. Rupp, F. Fuder, *Chem. Commun.* (2000) 1133–1134.
- [4] D.M. Ruthven, *Chem. Ing. Tech.* 83 (2011) 44–52.
- [5] C. Chmelik, J. Kärger, *Chem. Soc. Rev.* 39 (2010) 4864–4884.
- [6] M. Tsapatsis, *Science* 334 (2011) 767–768.
- [7] J. Caro, *Curr. Opin. Chem. Eng.* 1 (2011) 77–83.
- [8] J. Gascon, F. Kapteijn, *Angew. Chem. Int. Ed.* 49 (2010) 1530–1532.
- [9] M. O’Keeffe, M.A. Peskov, S.J. Ramsden, O.M. Yaghi, *Acc. Chem. Res.* 41 (2008) 1782–1789.
- [10] G. Férey, *Chem. Soc. Rev.* 37 (2008) 191–214.
- [11] S. Horike, S. Shimomura, S. Kitagawa, *Nat. Chem.* 1 (2009) 695–704.
- [12] J.C. Tan, A.K. Cheetham, *Chem. Soc. Rev.* 40 (2011) 1059–1080.
- [13] M. Pera-Titus, D. Farrusseng, *J. Phys. Chem. C* 116 (2012) 1638–1649.
- [14] G. Nickler, A. Henschel, R. Grünker, K. Gedrich, S. Kaskel, *Chem. Ing. Tech.* 83 (2011) 90–103.
- [15] P. Horcajada, T. Chalati, C. Serre, B. Gillet, C. Sebrie, T. Baati, J.F. Eubank, D. Heurtaux, P. Clayette, C. Kreuz, J.S. Chang, Y.K. Hwang, V. Marsaud, P.N. Bories, L. Cynober, S. Gil, G. Férey, P. Couvreur, R. Gref, *Nat. Mater.* 9 (2010) 172–178.
- [16] A.C. McKinlay, R.E. Morris, P. Horcajada, G. Férey, R. Gref, P. Couvreur, C. Serre, *Angew. Chem. Int. Ed.* 49 (2010) 6260–6266.
- [17] L.J. Murray, M. Dinca, J.R. Long, *Chem. Soc. Rev.* 38 (2009) 1294–1314.
- [18] M.P. Suh, H.J. Park, T.K. Prasad, D.-W. Lim, *Chem. Rev.* 12 (2012) 782–835.
- [19] G. Férey, C. Serre, T. Devic, G. Maurin, H. Jobic, P.L. Llewellyn, G. De Weireld, A. Vimont, M. Daturi, J.-S. Chang, *Chem. Soc. Rev.* 40 (2011) 550–562.
- [20] J.-R. Li, Y. Ma, M.C. McCarthy, J. Sculley, J. Yu, H.K. Jeong, P.B. Balbuena, H.-C. Zhou, *Coord. Chem. Rev.* 255 (2011) 1791–1823.
- [21] J. Juan-Alcañiz, J. Gascon, F. Kapteijn, *J. Mater. Chem.* (2012). 10.1039/c2jm15563j.
- [22] L. Ma, C. Abney, W. Lin, *Chem. Soc. Rev.* 38 (2009) 1248–1256.
- [23] D. Bradshaw, A. Garai, J. Huo, *Chem. Soc. Rev.* 41 (2012) 2344–2381.
- [24] A. Betard, H. Bux, S. Henke, D. Zacher, J. Caro, R.A. Fischer, *Micropor. Mesopor. Mater.* 150 (2012) 76.
- [25] A. Schoedel, C. Scherb, T. Bein, *Angew. Chem. Int. Ed.* 49 (2010) 7225–7228.
- [26] H.L. Luo, G.S. Zhu, I.J. Hewitt, S.L. Qiu, *J. Am. Chem. Soc.* 131 (2009) 1646–1647.
- [27] R. Ranjan, M. Tsapatsis, *Chem. Mater.* 21 (2009) 4920–4924.
- [28] Y.Y. Liu, E.P. Hu, E.A. Khan, Z.P. Lai, *J. Membr. Sci.* 353 (2010) 36–40.
- [29] M.C. McCarthy, V. Varela-Guerrero, G.V. Barnett, H.K. Jeong, *Langmuir* 26 (2010) 14636–14641.
- [30] S.R. Venna, M.A. Carreon, *J. Am. Chem. Soc.* 132 (2010) 76–78.
- [31] Y. Pan, T. Li, G. Lestari, Z.P. Lai, *J. Membr. Sci.* 390–391 (2012) 93–98.
- [32] Y.-S. Li, F.-Y. Liang, H. Bux, A. Feldhoff, W.-S. Yang, *J. Caro, Angew. Chem. Int. Ed.* 122 (2010) 558–561.
- [33] Y.-S. Li, H. Bux, A. Feldhoff, G.-L. Li, W.-S. Yang, *J. Caro, Adv. Mater.* 22 (2010) 3322–3326.
- [34] X. Zou, F. Zhang, S. Thomas, G. Zhu, V. Valtchev, S. Mintova, *Chem. Eur. J.* 17 (2011) 12076–12083.
- [35] S. Aguado, C.-H. Nicolas, V. Moizan-Baslé, C. Nieto, H. Amrouche, N. Bats, N. Audebrand, D. Farrusseng, *New J. Chem.* 35 (2011) 41–44.
- [36] M. Shah, M.C. McCarthy, S. Sachdeva, A.K. Lee, H.K. Jeong, *Ind. Eng. Chem. Res.* 51 (2012) 2179–2199.
- [37] Y. Hu, X. Dong, J. Nan, W. Jina, X. Ren, N. Xu, Y.M. Lee, *Chem. Commun.* 47 (2011) 737–739.
- [38] K.S. Park, Z. Ni, A.P. Côté, J.Y. Choi, R.D. Huang, F.J. Uribe-Romo, H.K. Chae, M. O’Keeffe, O.M. Yaghi, *Proc. Natl. Acad. Sci. USA* 103 (2006) 10186–10191.
- [39] H. Bux, A. Feldhoff, J. Cravillon, M. Wiebcke, Y.S. Li, J. Caro, *Chem. Mater.* 23 (2011) 2262–2269.
- [40] D.W. Breck, *Zeolite Molecular Sieves*, Wiley, New York, 1974.
- [41] M. Noack, P. Kölsch, D. Venzke, P. Toussaint, J. Caro, *Micropor. Mater.* 3 (1994) 201–206.
- [42] K. Li, D.H. Olson, J. Seidel, T.J. Emge, H. Gong, H. Zeng, J. Li, *J. Am. Chem. Soc.* 131 (2009) 10368–10369.
- [43] W. Zhou, H. Wu, T.J. Udovic, J.J. Rush, T. Yildirim, *J. Phys. Chem.* 112 (2008) 12602–12606.
- [44] M.T. Luebbbers, T. Wu, L. Shen, R.I. Masel, *Langmuir* 26 (2010) 15625–15633.
- [45] R.H. Rohrbaugh, *J. Jurs, Anal. Chim. Acta* 199 (1987) 99.
- [46] N. Chang, Z.Y. Gu, X.P. Yan, *J. Am. Chem. Soc.* 132 (2010) 13645–13647.
- [47] A. Huang, H. Bux, F. Steinbach, J. Caro, *Angew. Chem. Int. Ed.* 49 (2010) 4958–4961.
- [48] A. Huang, W. Dou, J. Caro, *J. Am. Chem. Soc.* 132 (2010) 15562–15564.
- [49] D. Fairen-Jimenez, S.A. Moggach, M.T. Wharmby, P.A. Wright, S. Parsons, T. Düren, *J. Am. Chem. Soc.* 133 (2011) 8900–8902.
- [50] C. Gücüyener, J. van den Bergh, J. Gascon, F. Kapteijn, *J. Am. Chem. Soc.* 132 (2010) 17704–17706.

2. Pervaporative separation of benzene containing mixtures on ZIF-8 membranes

L. Diestel et al. / Microporous and Mesoporous Materials 164 (2012) 288–293

293

- [51] J. Cravillon, S. Münzer, S.J. Lohmeier, A. Feldhoff, K. Huber, M. Wiebcke, *Chem. Mater.* 21 (2009) 1410–1412.
- [52] W.J. Koros, Y.H. Ma, T. Shimidzu, *Pure & Appl. Chem.* 86 (1995) 1479–1489.
- [53] X.-C. Huang, Y.-Y. Lin, J.-P. Zhang, X.-M. Chen, *Angew. Chem.* 118 (2006) 1587–1589.
- [54] C. Chmelik, H. Bux, J. Caro, L. Heinke, F. Hibbe, T. Titze, J. Kärger, *Phys. Rev. Lett.* 104 (2010) 085902–1–4.
- [55] D. Peralta, G. Chaplais, A. Simon-Masseron, K. Barthelet, C. Chizallet, A. Quoineaud, G. Pirngruber, *J. Am. Chem. Soc.* 134 (2012) 8115–8126.
- [56] J. Caro, M. Bülow, J. Kärger, *AIChE J.* 26 (1980) 1044–1046.

2.3 Rotational and translational motion of benzene in ZIF-8 studied by ^2H NMR: Estimation of microscopic self-diffusivity and its comparison with macroscopic measurements

Daniil I. Kolokolov, Lisa Diestel, Jürgen Caro, Dieter Freude, and Alexander G. Stepanov

The Journal of Physical Chemistry C 2014, 118, 12873-12879.

Reprinted (adapted) with permission from the Journal of Physical Chemistry C, Copyright (2014) American Chemical Society.

[doi:10.1021/jp5026834](https://doi.org/10.1021/jp5026834)

Rotational and Translational Motion of Benzene in ZIF-8 Studied by ^2H NMR: Estimation of Microscopic Self-Diffusivity and Its Comparison with Macroscopic Measurements

Daniil I. Kolokolov,^{†,‡} Lisa Diestel,[§] Juergen Caro,[§] Dieter Freude,^{||} and Alexander G. Stepanov^{*,†,‡}

[†]Boreskov Institute of Catalysis, Siberian Branch of the Russian Academy of Sciences, Prospekt Akademika Lavrentieva 5, Novosibirsk 630090, Russia

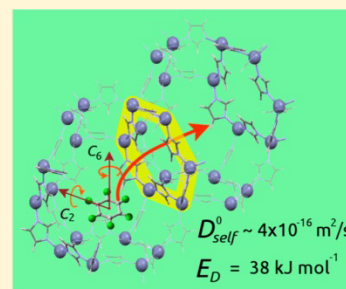
[‡]Faculty of Natural Sciences, Department of Physical Chemistry, Novosibirsk State University, Pirogova Street 2, Novosibirsk 630090, Russia

[§]Institute of Physical Chemistry and Electrochemistry, Leibniz University Hannover, Callinstrasse 3A, 30167 Hannover, Germany

^{||}Universität Leipzig, Fakultät für Physik und Geowissenschaften, Linnéstrasse 5, 04103 Leipzig, Germany

Supporting Information

ABSTRACT: In relation to unique properties of metal–organic framework (MOF) ZIF-8 to adsorb and separate hydrocarbons with kinetic diameters notably larger than the entrance windows of the porous system of this microporous material, the molecular dynamics of benzene adsorbed on ZIF-8 has been characterized and quantified with ^2H nuclear magnetic resonance. We have established that within the ZIF-8 cage the benzene molecule undergoes fast rotations, hovering in the symmetric potential of the spherical cage and relatively slow isotropic reorientations by collisions with the walls. Benzene performs also translational jump diffusion between neighboring cages characterized by an activation barrier $E_D = 38 \text{ kJ mol}^{-1}$ and a pre-exponential factor $\tau_{D0} = 4 \times 10^{-10} \text{ s}$. This microscopic measurement of benzene mobility allows us to estimate the self-diffusion coefficient for benzene in ZIF-8 ($D_{\text{self}}^0 \approx 4 \times 10^{-16} \text{ m}^2 \text{ s}^{-1}$ at $T = 323 \text{ K}$). Macroscopic measurements of diffusivities derived from membrane permeation studies ($3.5 \times 10^{-15} \text{ m}^2 \text{ s}^{-1}$ at $T = 298 \text{ K}$ for fractional occupancy $\Theta \approx 0.99$) and sorption uptake ($D_{\text{i,MS}} \approx 10^{-20} \text{ m}^2 \text{ s}^{-1}$ at 323 K) are several orders of magnitude larger or smaller than the microscopic self-diffusion coefficient D_{self}^0 which was derived from relaxation time analysis. This experimental finding is attributed to the limits of macroscopic measurements.



1. INTRODUCTION

Zeolitic imidazolate frameworks (ZIFs) are an important subclass of metal–organic framework (MOF) materials, characterized by zeolite-like topologies.^{1,2} Such framework organization coupled with very high pore volume, exceptional for a MOF chemical and thermal stability (up to $\sim 550 \text{ }^\circ\text{C}$) and tunable organic building blocks, make them highly attractive for applications as gas storage, chemicals encapsulation, sensing, and separation.^{3–7}

Although about 100 different ZIF structures were already discovered, one of the most studied is ZIF-8.^{1,2} It is composed of zinc cations coordinated to four 2-methylimidazolate ligands, resulting in a hybrid material with sodalite topology (SOD) with large spherical cavities of $\sim 11.6 \text{ \AA}$ diameter connected by small windows with a dimension of $\sim 3.4 \text{ \AA}$.

Such framework composition makes ZIF-8 particularly interesting as a molecular sieve. Indeed it was demonstrated recently that ZIF-8 is capable to separate light paraffins/olefins with high selectivity.⁸ These results stimulated further adsorption and membrane permeation studies that revealed ZIF-8 was capable to fit molecules like linear and branched alkanes⁹ with kinetic diameter of $d_{\text{crit}} \approx 4.3 \text{ \AA}$ and even larger

aromatic molecules with $d_{\text{crit}} \approx 5 \text{ \AA}$.^{6,10} This spectacular effect was related to the “flexibility” of the framework.

The MOF type materials are remarkable to show different kinds of flexibility including the (i) substantial change of the unit cell size, called “breathing”,^{11–13} (ii) small or no change of the unit cell size for linker reorientation, called “gate opening”,^{14–17} and (iii) the overcoming of the window barrier by slightly larger molecules with sufficient kinetic energy under consideration of lattice vibrations.^{18,19} However, for molecules with critical diameters larger than 3.4 \AA (Rietveld pore opening of ZIF-8), the gate opening is most likely the key phenomenon. Indeed, the application of excessive pressure, temperature, or adsorption of guest molecules was demonstrated to induce deformations of linker orientation relative to their equilibrium position.^{14,20,21} Pirngruber et al.⁹ described this gate opening effect as the “transitory tilt” of the imidazolate ligands, which allows to increase the formal pore window size of 3.4 \AA by almost the factor of 2 and tried to correlate this phenomenon

Received: March 18, 2014

Revised: May 15, 2014

Published: May 29, 2014

with separation of *n*-alkanes/aromatic molecules by ZIF-8 in breakthrough experiments.¹⁰ This linker “tilting” also qualitatively explains the relatively high value of the flux of benzene ($N_{\text{benzene}} \approx 3.6 \times 10^{-7} \text{ mol min}^{-1} \text{ cm}^{-2}$) permeating through the ZIF-8 membrane.²²

However, despite the importance of the problem and numerous macroscopic measurements, no *microscopic* study of the molecular dynamics of benzene inside the ZIF-8 pores was reported yet. Moreover, the only attempt to estimate the diffusion of aromatic molecules inside ZIF-8 was made by gas phase sorption uptake experiments.⁶ These macroscopic measurements estimated a rather low corrected diffusivity of $D_{\text{trans}}^0 \sim 10^{-20} \text{ m}^2 \text{ s}^{-1}$ for a loading ~ 1 molecule per cage at 323 K, with a relative high activation energy $E_{D_{\text{trans}}} \sim 40 \text{ kJ mol}^{-1}$. These corrected diffusivities from macroscopic studies should be comparable with self-diffusivities derived from microscopic studies.

Measuring such slow translational dynamics, and differentiating it from fast internal rotations expected for adsorbed benzene, is not a trivial task, and we need some adequate experimental tool. A particularly good solution could be provided by solid-state ^2H nuclear magnetic resonance (NMR) since it covers a very broad time scale of molecular motions, 10^{-4} – 10^{-10} s. ^2H NMR line shape is very sensitive to the mode and the rate of the motion in which the molecule is involved.^{23–26} Therefore, ^2H NMR patterns can be used to probe the actual mechanism of reorientational motion and thus serve as a marker of the molecule surrounding in the confined area. Benzene as the basic and most important representative among aromatic molecules is often used as a model guest to probe molecular interactions and organization in different classes of porous materials. So far the benzene dynamics was characterized by ^2H NMR in bulk/condensed state^{27,28} and adsorbed into mesoporous silica gels,^{28,29} active alumina,^{30,31} graphite,³² zeolites,^{33–38} and MOFs.³⁹ Those results clearly demonstrated that benzene mobility was extremely sensitive to the inner potential provided by the interior of porous material.

In this work we report the successful use of ^2H NMR technique to probe molecular mobility of benzene inside the ZIF-8 micropores and estimate the time scale of rotational and translational motion of adsorbed benzene. For correlation, also macroscopic measurements of benzene pervaporation through ZIF-8 membranes have been performed and the derived transport diffusion coefficient can be compared with the microscopic estimation of the self-diffusivity derived from ^2H NMR relaxation measurements.

2. EXPERIMENTAL SECTION

2.1. Materials. Nanocrystals of ZIF-8 have been prepared following the recipe of Cravillon et al.⁴⁰ First, 0.73 g of $\text{ZnNO}_3 \cdot 6\text{H}_2\text{O}$ (2.45 mmol, 1 equiv) in 50 mL of methanol and 0.81 g of 2-methylimidazole (9.86 mmol, 1 equiv) in 50 mL of methanol were mixed under vigorous stirring and stored for 2 h at room temperature. The precipitate was collected by centrifugation and washed twice with 50 mL of methanol. Further material was dried in nitrogen at 373 K overnight. X-ray diffraction analysis (XRD) proved that it was pure ZIF-8 with a crystal size of 40 nm. SEM image of the nanosized ZIF-8 and the corresponding XRD pattern are given in the Supporting Information.

Perdeuterated benzene- d_6 with 99.6% ^2H isotope enrichment purchased from Sigma-Aldrich Inc. was used in this work.

2.2. Sample Preparation. In order to prepare a sample for the NMR experiments, approximately 0.064 g of ZIF-8 powder was loaded in a glass tube, 5 mm outer diameter, and connected to a vacuum system. The sample was then heated at 423 K for 8 h under vacuum to a final pressure above the sample of 10^{-2} Pa. After cooling the sample back to room temperature, the material was exposed to the vapor of previously degassed benzene- d_6 (30 mbar) in the calibrated volume (38.7 mL). It took ~ 20 min for complete consumption of benzene- d_6 vapor to occur (4 mg of benzene was adsorbed). The quantity of adsorbed benzene corresponded to 1 molecule per cavity of ZIF-8. After adsorption, the neck of the tube was sealed off, while the material sample was maintained in liquid nitrogen in order to prevent its heating by the flame. The sealed sample was then transferred into the NMR probe.

2.3. NMR Measurements. ^2H NMR experiments were performed at the Larmor frequency $\omega_z/2\pi = 61.42 \text{ MHz}$ on a Bruker Avance-400 spectrometer, using a high power probe with 5 mm horizontal solenoid coil. All ^2H NMR spectra were obtained by Fourier transformation of quadrature-detected phase-cycled quadrupole echoes arising in the pulse sequence $(90^\circ_x - \tau_1 - 90^\circ_y - \tau_2 - \text{acquisition} - t)$, where $\tau_1 = 20 \mu\text{s}$, $\tau_2 = 21 \mu\text{s}$, and t is a repetition time of the sequence during the accumulation of the NMR signal.⁴¹ The duration of the $\pi/2$ pulse was 1.8–2.1 μs . Spectra were typically obtained with 500–1000 scans with repetition time ranging from 1 to 10 s. Inversion–recovery experiments for determination of the spin–lattice relaxation times (T_1) were carried out using the pulse sequence $(180^\circ_x - \tau_v - 90^\circ_{\pm x} - \text{acquisition} - t)$, where τ_v was a variable delay between the 180° and 90° pulses. T_2 values were derived from the Lorentzian-type spectra according to the well-known relation $T_2 = 1/\pi\Delta\nu_{1/2}$, where $\Delta\nu_{1/2}$ is the width at a half-height of the Lorentzian line shape. Some experimental values of T_2 were additionally measured by a Carr–Purcell–Meiboom–Gill (CPMG)⁴² pulse sequence. A good coincidence of T_2 measured with CPMG with that derived from the line width was found. T_1 values were measured with an accuracy of 5–8%, while the estimation of the accuracy of T_2 values are in a 7–10% interval with regard to the measured values.

The temperature of the samples was controlled with a flow of nitrogen gas, stabilized with a variable-temperature unit BVT-3000 with a precision of about 1 K.

3. RESULTS AND DISCUSSION

3.1. Mobility Characterization and Estimation of Benzene Self-Diffusivity with ^2H NMR. Figure 1 shows ^2H NMR line shapes expected for benzene molecule involved in different reorientational motions. The actual reorientation mechanism of benzene molecules depends strongly on environmental media. In the gas state, the benzene molecule represents an axially symmetric rotor with the rotation around the C_6 symmetry axis being the most favorable. In the solid state, the benzene molecule is immobile on the ^2H NMR time scale (i.e., $\tau_c > 10^{-6}$ s) only below 90 K,^{27,28} exhibiting the line shape like that shown in Figure 1a. At the temperature as high as 100 K the molecules of solid benzene become involved in the rotation around their C_6 axes with the line shape shown in Figure 1b, and this rotation is retained up to the melting point of benzene.^{27,28}

The presence of other modes of benzene molecule reorientation, including the random isotropic reorientation, depends strongly on the particular system. The ^2H NMR line shape of benzene adsorbed in ZSM-5 cannot be described by

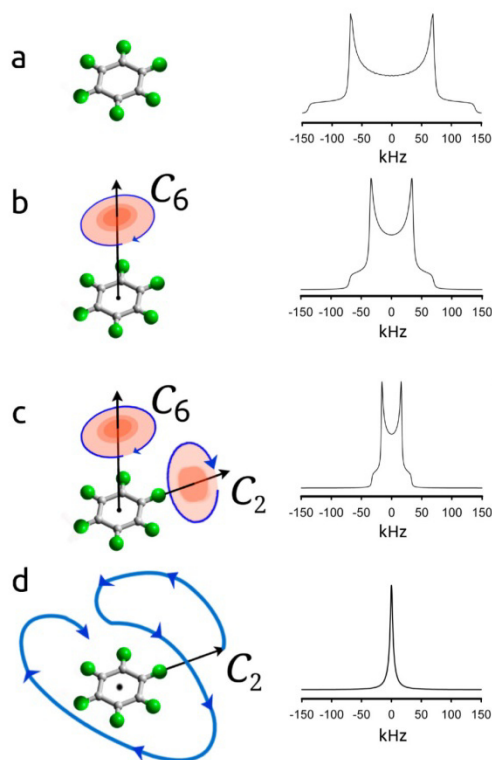


Figure 1. Theoretical ^2H NMR line shapes for deuterated benzene molecules undergoing different types of motion: static molecules (a); fast planar rotation around C_6 symmetry axis (b); fast rotation around both C_6 and C_2 axes (c); and fast isotropic reorientation (d).

isotropic reorientation at temperatures $T < 440$ K.³⁷ However, it can be described by an isotropic motion at $T > 200$ K in SBA-15,²⁸ Al_2O_3 ,⁴³ and NaX zeolite^{33,36} since Lorentzian type line shapes were observed in these cases. Below 200 K, the random reorientation of benzene is very slow ($\tau_c > 10^{-4}$ s) in the porous materials mentioned above, even in MIL-47(V) type material with relatively large pores ($\sim 10 \text{ \AA} \times 10 \text{ \AA}$) and low loading of 1 molecule per MOF unit cell.³⁹

Figure 2 shows the evolution of the ^2H NMR spectra of benzene- d_6 adsorbed on ZIF-8 in dependence of the temperature. Contrary to other adsorptive systems reported so far,^{28,33,36,37,43} the adsorbed benzene exhibits a Lorentzian line shape already at $T \approx 100$ K. This indicates that benzene in ZIF-8 is involved in isotropic motion already at a temperature as low as 100 K. Such results is a direct spectroscopic evidence that benzene molecules are indeed isolated from each other and rapidly isotropically rotating, hovering in the internal potential of the cavity like a weakly bonded molecular top. From this finding by ^2H NMR we can conclude that the benzene molecules have entered the ZIF-8 pore system and do not form any surface layer on the outer surface of the ZIF-8 nanocrystallites.

The information on benzene dynamics in ZIF-8 can be obtained from the analysis of the spin–lattice (T_1) and spin–spin (T_2) relaxation times as a function of temperature (Figure

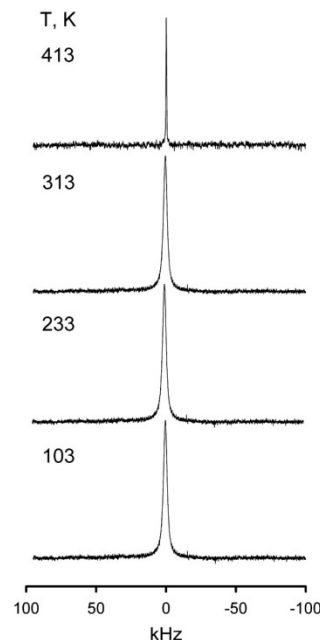


Figure 2. Evolution with temperature of ^2H NMR spectrum of benzene- d_6 adsorbed on ZIF-8 with loading of ~ 1 molecule per cavity.

3). The behavior of two curves for T_1 and T_2 shows that, in contrast with a typical liquid state situation,⁴⁴ the benzene

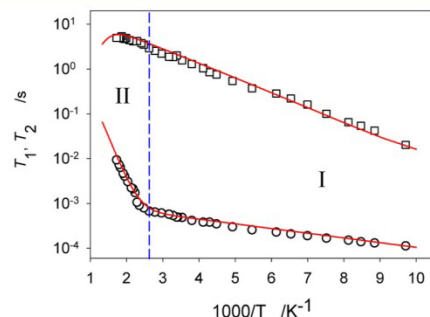


Figure 3. Temperature dependences of ^2H NMR T_1 (\square) and T_2 (\circ) relaxation times for benzene- d_6 adsorbed in ZIF-8.

molecules in ZIF-8 framework exhibit both (i) very fast motional modes, governing the T_1 relaxation times, and (ii) much slower modes that affect the transverse relaxation T_2 . Such behavior of T_1 and T_2 was already observed for linear alkanes in 5A zeolite with a cavity–window–cavity structural topology similar to ZIF-8.⁴⁵

T_1 smoothly changes with temperature without any bending of the curve within the temperature range of 100–400 K. This means that the relaxation is regulated in this temperature window by a single fast motional mode. However, at 450 K the T_1 stops to further increase and tends to decrease with

temperature, which indicates the presence of another motional mode.

T_2 relaxation shows clearly two regions of its evolution with temperature. In the temperature region I from 100 to 400 K, the evolution of T_2 is characterized by a very low slope, and in the temperature region II between 400 and 500 K, with a much steeper monotonic growth. Thus, we have again two motional modes that define the T_2 evolution with temperature. It is important to note that the evolution of T_2 in the temperature region II is clearly meeting the change of evolution of T_1 in temperature region II. This indicates that both T_1 and T_2 evolutions in the temperature region II reflect essentially the same motion. In order to correctly describe the experimental results we need a dynamical model that can fit both relaxation curves simultaneously.

Let us first deal with the T_1 relaxation. The spin–lattice relaxation is most sensitive to motions with characteristic time $\sim \omega_z^{-1}$, i.e., $\sim 10^{-9}$ s, for our experimental conditions. Since T_1 evolves smoothly between 100 and 450 K we can assume that only one internal fast motion controls the molecular motion of adsorbed benzene. It can be assumed that this fast motion represents the rotation of the benzene ring around its C_6 axis. However, our fitting test for T_1 and T_2 has shown (see Supporting Information, Figure S1) that one cannot fit both experimental curves, provided that the T_1 curve reflects only a single fast rotation. So we have to assume in addition to the fast C_6 another more slow rotation around the C_2 symmetry axis. Since we could not estimate the parameters of the C_6 rotation, we have assumed that the kinetics of the rotation around C_6 axis is similar to those measured for benzene in MOF MIL-47 system³⁹ ($E_{C_6} = 3$ kJ mol⁻¹; $\tau_{C_6,0} \approx 10^{-13}$ s). We have to note, however, that the parameters of the C_6 rotation were not essential for T_1 and T_2 curves fitting, provided that benzene is involved in a second, much slower rotation around its C_2 axis. It follows that the parameters of C_6 rotation just have to be at least 10 times faster at 100 K than the second rotation around C_2 axis. We have inferred that the rotation around C_2 axis is responsible for the observed T_1 relaxation curve with fitting parameters $E_{C_2} = 6.5$ kJ mol⁻¹ and $\tau_{C_2,0} = 1.6 \times 10^{-12}$ s. The geometry of this rotation is defined by the benzene geometry (see Supporting Information for fitting details).

The situation for the T_2 relaxation is more complicated. Adsorbed benzene exhibits a liquid-like line shape. This means that T_2 is defined by an isotropic reorientation of benzene molecules. However, the fast internal rotations of benzene alone are not able to explain the observed isotropic pattern. So some additional motion of benzene must exist. This isotropic reorientation can arise basically from two types of motion. The first one is the random collision of benzene molecules with the walls within one cage of ZIF-8, and the second one is the translational migration of benzene over the pore system, e.g., by jumps from cage to cage passing the window. The second motion could be considered as translational jump diffusion with a self-diffusion coefficient D_{self}^0 . It can be assumed that reorientation by collisions with cage walls could be characterized by a small activation barrier and thus governs the temperature region I of the T_2 relaxation curve. The translational jump diffusion through narrow “gates” could require much higher activation energy. Therefore, it is fast enough only at relatively high temperatures.

The relaxation model that takes into account four different modes of benzene motion in ZIF-8 allows us to perfectly fit

simultaneously both T_1 and T_2 experimental curves. Reorientation by random collision with cage walls is characterized by a very low activation barrier $E_R = 2$ kJ mol⁻¹ and a rather high pre-exponential factor $\tau_{R0} = 10^{-5}$ s. Such long characteristic time indicates that either this motion is not very effective in terms of random reorientation or that the benzene molecule is literally suspended in the spherical potential of the ZIF-8 cavity. Its collisions with walls are quite rare, compared to internal rotations. The translational motion by jumps between the cages is characterized by an activation barrier of $E_D = 38$ kJ mol⁻¹ and a pre-exponential factor $\tau_{D0} = 4 \times 10^{-10}$ s as derived from T_1 and T_2 fitting. Such parameters of translational motion indicate that we are indeed monitoring the microscopic, local diffusion between the cages. This is essentially the main result of the present study.

Having got the kinetic parameters for translational diffusion characteristic time τ_{D0} , we can estimate the self-diffusion coefficient D_{self}^0 of benzene in ZIF-8 and compare it with results of macroscopic measurements. Assuming that the diffusion occurs by jumps between the centers of the cages, the self-diffusion coefficient D_{self}^0 can be estimated from Einstein equation $D_{\text{self}}^0 = \langle l \rangle^2 / 6\tau_D$, where l is the mean distance between the centers of neighboring cages and τ_D is the mean residence time of the molecule in the cage. We have estimated from this equation that $D_{\text{self}}^0 \approx 4 \times 10^{-16}$ m² s⁻¹ at 323 K. Such low diffusivity can hardly be monitored by pulsed-field gradient (PFG) NMR. The arguments for this are described in the following paragraph.

The PFG NMR diffusometry determines the self-diffusion coefficient D by measuring the decay of the amplitude S (S_0 for zero gradient) of a stimulated echo in dependence of the field gradient intensity g by the well-known equation (see ref 47) $\psi = S/S_0 = \exp[-D(\delta g)^2(\Delta - (\delta/3))]$. Here, δ denotes the gradient pulse duration and Δ is the observation time between the first and third $\pi/2$ pulses of the stimulated echo pulse sequence. The value of the gyromagnetic ratio amounts for ¹H nuclei $\gamma = 26.7522128 \times 10^7$ s⁻¹ T⁻¹. We consider now benzene in ZIF-8 at 323 K with our experimentally estimated self-diffusion coefficient of $D_{\text{self}}^0 \approx 4 \times 10^{-16}$ m² s⁻¹. In order to calculate the expected PFG NMR echo decay for the benzene, we use a gradient pulse duration of 1 ms, which has to be shorter than the transverse relaxation time (the experimentally under MAS determined value is 2.9 ms), and an observation time of 1 s, which has to be shorter than the experimentally obtained longitudinal relaxation time of 2 s. In addition, we assume a maximum gradient of 50 T m⁻¹. Then we obtain $\psi \approx 0.07$. However, a value of $\psi \approx 1$ is necessary for the accurate determination of the self-diffusion coefficient by PFG NMR. A maximum gradient of about 200 T m⁻¹ would be needed, but is not yet realized in PFG NMR diffusometry.

Hence, because of the impossibility to measure the self-diffusion coefficient by PFG NMR for benzene in ZIF-8, we further compared our ²H NMR relaxation estimate of self-diffusivity with diffusion coefficients derived from (i) membrane permeation and (ii) sorption uptake.

3.2. Determination of Transport Diffusion Coefficient from Pervaporation Studies of Benzene through ZIF-8 Membrane. ZIF-8 membrane has been grown as a supported dense layer on top of a porous ceramic as shown in Figure 4, and pervaporation studies of benzene on this membrane have been carried out. Details of the membrane synthesis and pervaporation are given in ref 22 and in the Supporting Information.

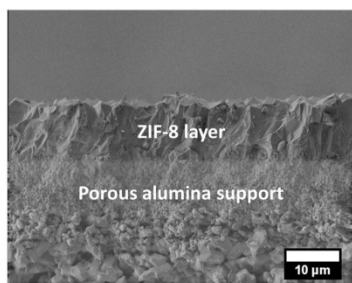


Figure 4. Cross section of a 15 μm ZIF-8 membrane on a ceramic macroporous support.

In single component benzene pervaporation experiments, a benzene flux of $N_{\text{benzene}} \approx 3.6 \times 10^{-7} \text{ mol min}^{-1} \text{ cm}^{-2}$ through the ZIF-8 membrane has been measured at room temperature. From these pervaporation experiments, Fickian or “transport” diffusion coefficients $D_{i,\text{Fick}}$ and Maxwell–Stefan or “corrected” diffusion coefficients $D_{i,\text{MS}}$ can be derived (for details, see the Supporting Information).

According to refs 46 and 47 for constant driving force, the first Fickian Law gives the permeation flux density N_i ,

$$N_i = -D_{i,\text{Fick}} \nabla q_i \quad (1)$$

with ∇q_i as the gradient of the molar loading. $D_{i,\text{Fick}}$ is related to the $D_{i,\text{MS}}$ by the thermodynamic factor Γ_i ,⁴⁸

$$D_{i,\text{Fick}} = D_{i,\text{MS}} \Gamma_i \quad (2)$$

Γ_i characterizes the curvature of the adsorption isotherm and is defined by

$$\Gamma_i = \frac{q_i}{p_i} \frac{dp_i}{dq_i} = \frac{d \ln p_i}{d \ln q_i} \quad (3)$$

If the adsorption system behaves ideally, i.e., if there is a linear (Henry) adsorption isotherm, $d \ln p_i/d \ln q_i$ becomes 1, and under this condition, the Fickian or “transport” diffusivity is equal to the Maxwell–Stefan or “corrected” diffusivity (ref 47).

Molecular dynamics simulation showed that at zero loading the three diffusion coefficients $D_{i,\text{Fick}}$, $D_{i,\text{MS}}$, and the self-diffusion coefficient $D_{i,\text{self}}^0$ were identical but with increasing loading $D_{i,\text{Fick}} > D_{i,\text{MS}} \geq D_{i,\text{self}}^0$. However, for most adsorbate systems the self- and Maxwell–Stefan diffusion coefficients become similar again at high loadings⁴⁶ since at pore saturation the correlation effects become dominant. Krishna⁴⁹ showed for mixtures that, as the concentration of guest molecules within the pores approached saturation, the molecular jumps became increasingly correlated. When substituting in a thought experiment the binary mixture components by tagged and untagged species, this virtual experiment leads to the physically expected and mathematically exact relationship $D_{i,\text{self}}^0 = D_{i,\text{MS}}$.⁵⁰

For the flux density N_i , eq 1 can be simplified to

$$N_i = \frac{\varepsilon \rho q_{\text{sat}}}{\delta} D_{i,\text{MS}} \Gamma_i (\Theta_{\text{feed}} - \Theta_{\text{permeate}}) \quad (4)$$

with the membrane porosity $\varepsilon = 0.62$, the ZIF-8 framework density $\rho = 924 \text{ kg m}^{-3}$, the saturation capacity for benzene $q_{\text{sat}} = 4.5 \text{ mol kg}^{-1}$, the ZIF-8 membrane thickness $\delta = 15 \mu\text{m}$, and the thermodynamic factor Γ_i . For a single-site Langmuir isotherm, eq 3 gives $\Gamma_i = 1/(1 - \Theta_i)$ with Θ as the fractional

occupancy. Published isotherm data of benzene in ZIF-8⁵¹ can be used for the calculation of Γ_i . As a rough estimate, the downstream fractional loading of the membrane can be assumed to be zero, i.e., $\Theta_{\text{permeate}} = 0$. By assuming different values of fractional occupancy Θ_i on the upstream side of the membrane, the corresponding $D_{i,\text{MS}}$ can be calculated. As outlined above, for high loadings, the Maxwell–Stefan diffusivity $D_{i,\text{MS}}$ derived from pervaporation studies should come near to the self-diffusivity $D_{i,\text{self}}^0$ estimated from NMR relaxation time experiments. This expectation is indeed found as a tendency in Figure S1, Supporting Information. However, there is still 1 order of magnitude difference between $D_{i,\text{MS}} \approx 3.5 \times 10^{-15} \text{ m}^2 \text{ s}^{-1}$ from pervaporation at $\Theta = 0.99$ loading and the level of $D_{i,\text{self}}^0 \approx 4 \times 10^{-16} \text{ m}^2 \text{ s}^{-1}$ from NMR relaxation.

However, when comparing our result on benzene diffusivity in ZIF-8 as derived from pervaporation studies with the $D_{i,\text{MS}}$ data obtained from gas phase sorption uptake experiments,⁶ we see that the activation barrier of the process is basically the same $\sim 40 \text{ kJ mol}^{-1}$, whereas the corrected diffusion coefficient $D_{i,\text{MS}} \approx 10^{-20} \text{ m}^2 \text{ s}^{-1}$ at 323 K is several orders of magnitude smaller than the microscopic self-diffusion coefficient $D_{i,\text{self}}^0 \approx 4 \times 10^{-16} \text{ m}^2 \text{ s}^{-1}$ as derived from NMR relaxation analysis, which underlines the limits of macroscopic transient uptake measurements. Often discrepancies between macroscopic and microscopic diffusivity measurements are reported, which can be explained in terms of structural defects leading to surface and intracrystalline barriers, exhibiting dramatic effects on sorption uptake kinetics on the macroscale but with only minimal influence on the microscale.^{47,52}

4. CONCLUSIONS

We were able to demonstrate by means of solid-state ^2H NMR that the benzene molecules are indeed adsorbed inside the ZIF-8 cages proving the gate opening effect in this MOF on a microscopic level. At low loadings (~ 1 molecule per cage) the adsorbed benzene molecules are located in separate cages and thus isolated from each other. Within the ZIF-8 cage, the benzene molecule quickly rotates hovering in the symmetric potential of the spherical cage and performs relatively slow isotropic reorientations by collisions with its walls. Finally benzene performs translational jump diffusion between the neighboring cages with an activation barrier $E_D = 38 \text{ kJ mol}^{-1}$ and a pre-exponential factor $\tau_{D0} = 4 \times 10^{-10} \text{ s}$. These are the first microscopic measurements of benzene diffusivity in ZIF-type materials since the direct measurement of the slow benzene self-diffusion by pulsed field gradient NMR is not possible. Our self-diffusivity ($D_{i,\text{self}}^0 \approx 4 \times 10^{-16} \text{ m}^2 \text{ s}^{-1}$ at $T = 323 \text{ K}$) estimated from relaxation time analysis using the model of activated jumps between neighboring cavities lies in between the Maxwell–Stefan or “corrected” diffusivities derived from membrane permeation ($D_{i,\text{MS}} \approx 3.5 \times 10^{-15} \text{ m}^2 \text{ s}^{-1}$ at $T = 298 \text{ K}$ for fractional occupancy $\Theta \approx 0.99$) and sorption uptake studies ($D_{i,\text{MS}} \approx 10^{-20} \text{ m}^2 \text{ s}^{-1}$ at 323 K).

■ ASSOCIATED CONTENT

Supporting Information

Technical details on ^2H NMR T_1 and T_2 relaxation time simulation procedure, motion models implementation, SEM image and XRD analysis of used ZIF-8 material, ZIF-8 membrane preparation and pervaporation experiments on ZIF-8 membranes, interpretation and correlation of Fickian or “transport” diffusion coefficients, and Maxwell Stefan diffusion coefficients and self-diffusion coefficients. This

material is available free of charge via the Internet at <http://pubs.acs.org>.

AUTHOR INFORMATION

Corresponding Author

*(A.G.S.) Tel: +7 952 905 9559. Fax: +7 383 330 8056. E-mail: stepanov@catalysis.ru.

Notes

The authors declare no competing financial interest.

ACKNOWLEDGMENTS

This work was supported by Russian Foundation for Basic Research (Grant Nos. 14-03-91333). L.D. and J.C. thank DFG Priority Program 1362 (Porous Metal–Organic Frameworks). We are grateful to Rajamani Krishna (Van't Hoff Institute, University Amsterdam) for help in the correlation and interpretation of the different diffusion studies.

REFERENCES

- Huang, X. C.; Lin, Y. Y.; Zhang, J. P.; Chen, X. M. Ligand-Directed Strategy for Zeolite-Type Metal–Organic Frameworks: Zinc(II) Imidazolates with Unusual Zeolitic Topologies. *Angew. Chem., Int. Ed.* **2006**, *45*, 1557–1559.
- Park, K. S.; Ni, Z.; Cote, A. P.; Choi, J. Y.; Huang, R. D.; Uribe-Romo, F. J.; Chae, H. K.; O'Keeffe, M.; Yaghi, O. M. Exceptional Chemical and Thermal Stability of Zeolitic Imidazolate Frameworks. *Proc. Natl. Acad. Sci. U.S.A.* **2006**, *103*, 10186–10191.
- Chen, B. L.; Liang, C. D.; Yang, J.; Contreras, D. S.; Clancy, Y. L.; Lobkovsky, E. B.; Yaghi, O. M.; Dai, S. A Microporous Metal–Organic Framework for Gas-Chromatographic Separation of Alkanes. *Angew. Chem., Int. Ed.* **2006**, *45*, 1390–1393.
- Férey, G. Hybrid Porous Solids: Past, Present, Future. *Chem. Soc. Rev.* **2008**, *37*, 191–214.
- Cunha, D.; Ben Yahia, M.; Hall, S.; Miller, S. R.; Chevreau, H.; Elkaim, E.; Maurin, G.; Horcajada, P.; Serre, C. Rationale of Drug Encapsulation and Release from Biocompatible Porous Metal–Organic Frameworks. *Chem. Mater.* **2013**, *25*, 2767–2776.
- Zhang, K.; Lively, R. P.; Zhang, C.; Chance, R. R.; Koros, W. J.; Sholl, D. S.; Nair, S. Exploring the Framework Hydrophobicity and Flexibility of ZIF-8: From Biofuel Recovery to Hydrocarbon Separations. *J. Phys. Chem. Lett.* **2013**, *4*, 3618–3622.
- Bae, T. H.; Lee, J. S.; Qiu, W. L.; Koros, W. J.; Jones, C. W.; Nair, S. A High-Performance Gas-Separation Membrane Containing Submicrometer-Sized Metal–Organic Framework Crystals. *Angew. Chem., Int. Ed.* **2010**, *49*, 9863–9866.
- Bohme, U.; Barth, B.; Paula, C.; Kuhnt, A.; Schwieger, W.; Mundstock, A.; Caro, J.; Hartmann, M. Ethene/Ethane and Propene/Propane Separation via the Olefin and Paraffin Selective Metal–Organic Framework Adsorbents CPO-27 and ZIF-8. *Langmuir* **2013**, *29*, 8592–8600.
- Peralta, D.; Chaplais, G.; Simon-Masseron, A.; Barthelet, K.; Chizallet, C.; Quoineaud, A. A.; Pirngruber, G. D. Comparison of the Behavior of Metal–Organic Frameworks and Zeolites for Hydrocarbon Separations. *J. Am. Chem. Soc.* **2012**, *134*, 8115–8126.
- Peralta, D.; Chaplais, G.; Paillaud, J. L.; Simon-Masseron, A.; Barthelet, K.; Pirngruber, G. D. The Separation of Xylene Isomers by ZIF-8: A Demonstration of the Extraordinary Flexibility of the ZIF-8 Framework. *Microporous Mesoporous Mater.* **2013**, *173*, 1–5.
- Kitagawa, S.; Uemura, K. Dynamic Porous Properties of Coordination Polymers Inspired by Hydrogen Bonds. *Chem. Soc. Rev.* **2005**, *34*, 109–119.
- Serre, C.; Millange, F.; Thouvenot, C.; Nogués, M.; Marsolier, G.; Louer, D.; Férey, G. Very Large Breathing Effect in the First Nanoporous Chromium(III)-Based Solids: MIL-53 or CrIII(OH)₂{O₂C-C₆H₄-CO₂}₂{HO₂C-C₆H₄-CO₂H}_xH₂O_y. *J. Am. Chem. Soc.* **2002**, *124*, 13519–13526.
- Mu, B.; Li, F.; Huang, Y. G.; Walton, K. S. Breathing Effects of CO₂ Adsorption on a Flexible 3D Lanthanide Metal–Organic Framework. *J. Mater. Chem.* **2012**, *22*, 10172–10178.
- Fairen-Jimenez, D.; Moggach, S. A.; Wharmby, M. T.; Wright, P. A.; Parsons, S.; Duren, T. Opening the Gate: Framework Flexibility in ZIF-8 Explored by Experiments and Simulations. *J. Am. Chem. Soc.* **2011**, *133*, 8900–8902.
- van den Bergh, J.; Gucuyener, C.; Pidko, E. A.; Hensen, E. J. M.; Gascon, J.; Kapteijn, F. Understanding the Anomalous Alkane Selectivity of ZIF-7 in the Separation of Light Alkane/Alkene Mixtures. *Chem.—Eur. J.* **2011**, *17*, 8832–8840.
- Aguado, S.; Bergeret, G.; Titus, M. P.; Moizan, V.; Nieto-Draghi, C.; Bats, N.; Farrusseng, D. Guest-Induced Gate-Opening of a Zeolite Imidazolate Framework. *New J. Chem.* **2011**, *35*, 546–550.
- Gucuyener, C.; van den Bergh, J.; Gascon, J.; Kapteijn, F. Ethane/Ethene Separation Turned on Its Head: Selective Ethane Adsorption on the Metal–Organic Framework ZIF-7 through a Gate-Opening Mechanism. *J. Am. Chem. Soc.* **2010**, *132*, 17704–17706.
- Haldoupis, E.; Watanabe, T.; Nair, S.; Sholl, D. S. Quantifying Large Effects of Framework Flexibility on Diffusion in MOFs: CH₄ and CO₂ in ZIF-8. *ChemPhysChem* **2012**, *13*, 3449–3452.
- Chokbunpiam, T.; Chanajaree, R.; Saengsawang, O.; Reimann, S.; Chmelik, C.; Fritzsche, S.; Caro, J.; Reimsungnen, T.; Hannongbua, S. The Importance of Lattice Flexibility for the Migration of Ethane in ZIF-8: Molecular Dynamics Simulations. *Microporous Mesoporous Mater.* **2013**, *174*, 126–134.
- Pera-Titus, M.; Lescouet, T.; Aguado, S.; Farrusseng, D. Quantitative Characterization of Breathing upon Adsorption for a Series of Amino-Functionalized MIL-53. *J. Phys. Chem. C* **2012**, *116*, 9507–9516.
- Finsy, V.; Kirschhock, C. E. A.; Vedts, G.; Maes, M.; Alaerts, L.; De Vos, D. E.; Baron, G. V.; Denayer, J. F. M. Framework Breathing in the Vapour-Phase Adsorption and Separation of Xylene Isomers with the Metal–Organic Framework MIL-53. *Chem.—Eur. J.* **2009**, *15*, 7724–7731.
- Diestel, L.; Bux, H.; Wachsmuth, D.; Caro, J. Pervaporation Studies of *n*-Hexane, Benzene, Mesitylene and Their Mixtures on Zeolitic Imidazolate Framework-8 Membranes. *Microporous Mesoporous Mater.* **2012**, *164*, 288–293.
- Spieß, H. W. Rotation of Molecules and Nuclear Spin Relaxation. In *NMR Basic Principles and Progress*; Diehl, P., Fluck, E., Kosfeld, R., Eds.; Springer-Verlag: New York, 1978; Vol. 15, p 55.
- Smith, I. C. P. Deuterium NMR. In *NMR of Newly Accessible Nuclei*; Laszlo, P., Ed.; Academic Press: London, U.K., 1983; Vol. 2, p 1.
- Jelinski, L. W. Deuterium NMR of Solid Polymers. In *High Resolution NMR Spectroscopy of Synthetic Polymers in Bulk (Methods and Stereochemical Analysis)*; Komoroski, R. A., Ed.; VCH Publishers: New York, 1986; Vol. 7, p 335.
- Barnes, R. G. Deuteron Quadrupole Coupling Tensors in Solids. *Adv. Nucl. Quadrupole Reson.* **1974**, *1*, 335–355.
- Ok, J. H.; Vold, R. R.; Vold, R. L.; Etter, M. C. Deuterium Nuclear Magnetic-Resonance Measurements of Rotation and Libration of Benzene in a Solid-State Cyclamer. *J. Phys. Chem.* **1989**, *93*, 7618–7624.
- Gedat, E.; Schreiber, A.; Albrecht, J.; Emmeler, T.; Shenderovich, I.; Findenegg, G. H.; Limbach, H. H.; Buntkowsky, G. ²H Solid-State NMR Study of Benzene-*d*₆ Confined in Mesoporous Silica SBA-15. *J. Phys. Chem. B* **2002**, *106*, 1977–1984.
- Zibrowius, B.; Bulow, M.; Pfeifer, H. Microdynamical Behavior of Benzene Molecules Adsorbed on Silicalite as Studied by C-13 NMR. *Chem. Phys. Lett.* **1985**, *120*, 420–423.
- Gottlieb, H. E.; Luz, Z. Deuterium NMR of Molecules Adsorbed on Active Alumina. *J. Magn. Reson.* **1983**, *54*, 257–271.
- Boddenberg, B.; Beerwerth, B. Proton and Deuteron Magnetic Resonance Relaxation of Benzene Adsorbed on Alumina and on a Platinum/Alumina Catalyst. *J. Phys. Chem.* **1989**, *93*, 1440–1447.
- Boddenberg, B.; Grosse, R. Deuterium NMR Study on the Rotational Dynamics and the Orientation of Benzene Molecules

Adsorbed on Graphite and Boron Nitride. *Z. Naturforsch., A: Phys. Sci.* **1986**, *41*, 1361–1368.

(33) Hasha, D. I.; Miner, V. W.; Garces, J. M.; Rocke, S. C. Dynamics of Benzene in X-Type Zeolites. *ACS Symp. Ser.* **1985**, *288*, 485–497.

(34) Eckman, R. R.; Vega, A. J. Deuterium Solid-State NMR Study of the Dynamics of Molecules Sorbed by Zeolites. *J. Phys. Chem.* **1986**, *90*, 4679–4683.

(35) Boddenberg, B.; Burmeister, R. ^2H NMR Study on the Rotation and Diffusion Kinetics of Propene and Benzene in NaX and Ag NaX Zeolites. *Zeolites* **1988**, *8*, 488–494.

(36) Zibrowius, B.; Caro, J.; Pfeifer, H. Deuterium Nuclear Magnetic-Resonance Studies of the Molecular-Dynamics of Benzene in Zeolites. *J. Chem. Soc., Faraday Trans. I* **1988**, *84*, 2347–2356.

(37) Kustanovich, I.; Vieth, H. M.; Luz, Z.; Vega, S. NMR-Studies of the Sorption of *p*-Xylene, Toluene, and Benzene on ZSM5 Zeolite. *J. Phys. Chem.* **1989**, *93*, 7427–7431.

(38) Geil, B.; Isfort, O.; Boddenberg, B.; Favre, D. E.; Chmelka, B. F.; Fujara, F. Reorientational and Translational Dynamics of Benzene in Zeolite NaY as Studied by One- and Two-Dimensional Exchange Spectroscopy and Static-Field-Gradient Nuclear Magnetic Resonance. *J. Chem. Phys.* **2002**, *116*, 2184–2193.

(39) Kolokolov, D. I.; Jobic, H.; Stepanov, A. G.; Ollivier, J.; Rives, S.; Maurin, G.; Devic, T.; Serre, C.; Ferey, G. Experimental and Simulation Evidence of a Corkscrew Motion for Benzene in the Metal-Organic Framework MIL-47. *J. Phys. Chem. C* **2012**, *116*, 15093–15098.

(40) Cravillon, J.; Munzer, S.; Lohmeier, S. J.; Feldhoff, A.; Huber, K.; Wiebcke, M. Rapid Room-Temperature Synthesis and Characterization of Nanocrystals of a Prototypical Zeolitic Imidazolate Framework. *Chem. Mater.* **2009**, *21*, 1410–1412.

(41) Powles, J. G.; Strange, J. H. Zero Time Resolution Nuclear Magnetic Resonance Transients in Solids. *Proc. Phys. Soc. London* **1963**, *82*, 6–15.

(42) Farrar, T. C.; Becker, E. D. *Pulse and Fourier Transform NMR. Introduction to Theory and Methods*; Academic Press: New York, 1971.

(43) Boddenberg, B.; Beerwerth, B. Proton and Deuteron Magnetic-Resonance Relaxation of Benzene Adsorbed on Alumina and on a Platinum Alumina Catalyst. *J. Phys. Chem.* **1989**, *93*, 1440–1447.

(44) Harris, R. K. *Nuclear Magnetic Resonance Spectroscopy. A Physico-Chemical View*; Pitman: London, U.K., 1983.

(45) Kolokolov, D. I.; Arzumanov, S. S.; Stepanov, A. G.; Jobic, H. Dynamics of linear $n\text{-C}_6\text{-}n\text{-C}_{22}$ alkanes inside 5A zeolite studied by ^2H NMR. *J. Phys. Chem. C* **2007**, *111*, 4393–4403.

(46) Krishna, R.; van Baten, J. M. Influence of Adsorption Thermodynamics on Guest Diffusivities in Nanoporous Crystalline Materials. *Phys. Chem. Chem. Phys.* **2013**, *15*, 7994–8016.

(47) Kärger, J.; Ruthven, D. M.; Theodorou, D. N. *Diffusion in Nanoporous Materials*; Wiley-VCH: Weinheim, Germany, 2012.

(48) Krishna, R.; Wesselingh, J. A. Review Article Number 50: The Maxwell–Stefan Approach to Mass Transfer. *Chem. Eng. Sci.* **1997**, *52*, 861–911.

(49) Krishna, R.; van Baten, J. M. Describing Mixture Diffusion in Microporous Materials under Conditions of Pore Saturation. *J. Phys. Chem. C* **2010**, *114*, 11557–11563.

(50) Krishna, R. Personal information.

(51) Zhu, A. X.; Lin, R. B.; Qi, X. L.; Liu, Y.; Lin, Y. Y.; Zhang, J. P.; Chen, X. M. Zeolitic Metal Azolate Frameworks (MAFs) from $\text{ZnO}/\text{Zn}(\text{OH})_2$ and Monoalkyl-Substituted Imidazoles and 1,2,4-Triazoles: Efficient Syntheses and Properties. *Microporous Mesoporous Mater.* **2012**, *157*, 42–49.

(52) Heitjans, P.; Kärger, J. *Diffusion in Condensed Matter: Methods, Materials, Models*; Springer: Berlin, Germany, 2005.

3 Mixed matrix membranes as alternative for MOF and polymeric membranes

3.1 Summary

Despite the superior performance of the crystalline MOF membranes with their well-defined pore systems, low flux polymeric membranes rule the commercial scene because of their reproducibility, processing and mechanical strength. Furthermore, the scale-up of neat MOF membranes is still a major bottleneck. However, the existing polymeric membrane materials are not optimal since improvements of the permeability are always at the expense of selectivity, and vice versa. During the last few decades, various polymers have been modified with inorganic or MOF fillers forming MMMs to improve the performance of the polymeric membranes. MOFs are very promising nanoporous filler materials because these materials have high surface areas, high pore volumes and a chemical nature that can be fine-tuned by a special linker selection or post-synthetic modification. Moreover, MOFs exhibit an intrinsic hybrid nature which leads to enhanced interactions between the polymer and the filler materials.

In chapter 3.2 rubbery polymer MMMs made of polymethylphenylsiloxane (PMPS) and ZIF-8 nanoparticles are studied for the separation of different practice-relevant gas mixtures in comparison with the neat polymer membrane and the neat ZIF-8 membrane. The neat ZIF-8 membrane showed the best size selective separation, whereas the neat PMPS membrane had higher separation factors for the CO₂ separations from other gases. It was anticipated that the selectivity of the 9 vol-% ZIF-8-PMPS MMM results from an interplay of PMPS and ZIF-8. But actually, the permeability of the MMM was higher than that of the PMPS membrane and sometimes also higher than the permeability of the neat ZIF-8 membrane while the selectivity was comparable to that of the neat PMPS. Thus, these results indicate an increase in free volume for the PMPS polymer after introducing ZIF-8 nanoparticles.

In chapter 3.3 glassy polymer MMMs consisting of Matrimid[®] 5218 and ZIF-8 or ZIF-90 nanoparticles, respectively, are studied for the H₂/CO₂ separation and compared with the neat polymer and the neat ZIF membranes. It was found that

the embedding of the nanoparticles modifies the separation performance of the neat Matrimid membrane due to well fittings between the glassy polymer and the nanoparticles. Thus, the separation behavior of these MMMs should be able to be described by the Maxwell-Stefan model. However, the MMMs showed slightly higher selectivities and lower permeabilities than expected. Even better separation results could be obtained by binding ZIF-90 particles covalently with ethyleneamine to the Matrimid matrix.

To verify and explain these surprising results additional separation studies were carried out. In chapter 3.4 the separation of the binary mixture H_2/CH_4 on neat ZIF-8 and ZIF-90, neat glassy Matrimid and 10 to 30 vol-% ZIF-8 and ZIF-90 nanoparticle/Matrimid MMMs are compared. Again surprisingly high separation performances could be found for the MMMs with particle loadings ≤ 20 vol-%. Higher loadings lead to agglomerations and segregations, which result in MMMs with a lower selectivity. After analyzing the polymer structure around the ZIF nanoparticles, which showed no structural changes, it was concluded that the polymer matrix seems to prevent the framework flexibility of ZIF-8 and ZIF-90. To verify this assumption, neat ZIF-8 and ZIF-90 membranes were coated with a Matrimid polymer layer (dual-layer membrane). Indeed, the polymer coating caused a suppression of the linker distortion of the ZIF layer in contact with the polymer which results in enhanced H_2/CH_4 selectivity.

3.2 Comparative permeation studies on three supported membranes: Pure ZIF-8, pure polymethylphenylsiloxane, and mixed matrix membranes

Lisa Diestel, Xinlei Liu, Yanshuo Li, Weishen Yang and Jürgen Caro

Microporous and Mesoporous Materials 2014, 189, 210-215.

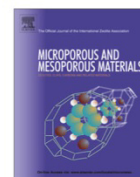
Reprinted (adapted) with permission from *Microporous and Mesoporous Materials*. Copyright (2014) Elsevier.

[doi:10.1016/j.micromeso.2013.09.012](https://doi.org/10.1016/j.micromeso.2013.09.012)



Contents lists available at ScienceDirect

Microporous and Mesoporous Materials

journal homepage: www.elsevier.com/locate/micromeso

Comparative permeation studies on three supported membranes: Pure ZIF-8, pure polymethylphenylsiloxane, and mixed matrix membranes

L. Diestel^{a,*}, X.L. Liu^b, Y.S. Li^b, W.S. Yang^b, J. Caro^a^a Institute of Physical Chemistry and Electrochemistry, Leibniz University Hannover, Hannover, Germany^b Dalian Institute of Chemical Physics, Chinese Academy of Sciences, Dalian, China

ARTICLE INFO

Article history:

Available online 21 September 2013

Dedicated to Dr. Michael Stöcker on the occasion of his retirement as Editor-in-Chief of Microporous and Mesoporous Materials.

Keywords:

Permeation
ZIF-8 membrane
PMPS membrane
Mixed matrix membrane
Increased free volume

ABSTRACT

We studied the separation of four practice-relevant gas mixtures on three different membranes which were prepared on porous alumina supports: (i) a pure ZIF-8 (zeolitic imidazolate framework), (ii) a pure PMPS (polymethylphenylsiloxane) polymer, and (iii) a mixed matrix membrane (MMM, with 8.3 wt.% \approx 8.8 vol.% ZIF-8 (density 0.93 g cm^{-3}) in PMPS (density 1.00 g cm^{-3})). The four gas mixtures under study were: CO_2/CH_4 , CO_2/N_2 , H_2/CO_2 , and O_2/N_2 . Whereas the pure ZIF-8 membrane shows the best separation factor $\alpha = 11$ for H_2/CH_4 , the pure PMPS membrane has higher separation factors for the CO_2 separation from other gases. It was anticipated that the separation behavior of the MMM results from an interplay of the permeation through the PMPS polymer matrix and the embedded ZIF-8 nanocrystals. Actually, the separation factors of the MMM were found to be equal to the separation factors of the pure polymer membrane. However, we measured much higher gas fluxes through the MMM than through the pure polymer membrane. This experimental finding could indicate an increase of the free volume of the PMPS polymer after introduction of ZIF-8 nanoparticles.

© 2013 Elsevier Inc. All rights reserved.

1. Introduction

The energy-efficient and environmentally friendly separation of practice-relevant model gas mixtures such as CO_2/CH_4 for natural gas processing, CO_2/N_2 for exhaust gas treatment, H_2/CO_2 for hydrogen recovery and purification, and O_2/N_2 for the production of oxygen-enriched air and nitrogen as protecting gas is a challenging research field [1]. Membrane technology has become a workhorse in gas purification as it requires less energy for the separation and has less environmental impacts since it needs no additional chemicals and produces no waste [2]. Compared with inorganic membranes, commonly used organic polymer membranes have the benefit of a relatively simple manufacture and an easy scale-up. But membranes show a trade-off between permeability and selectivity. This means that thin membranes with a high permeability have a low separation quality and vice versa [3]. This trade-off behavior was illustrated by Robeson in a so-called Robeson plot [4], which was updated in 2008 [5]. Observing the development of the polymer membrane technology, there have been great efforts during the last three decades in permeability and selectivity [6] by using different monomers [7–13], thermal post treatment [14], chemical and photochemical crosslinking [15] and by creating mixed matrix membranes (MMM) with porous

and non-porous fillers [16–18]. Especially porous filler materials bear a significant research interest in the field of gas and liquid separation processes [19–23] as these fillers can improve the separation behavior of membranes by size exclusion and adsorption effects [24,25]. Besides, the pore size of some porous filler materials – MOFs (metal organic frameworks) for example – can be varied and their affinities towards certain molecules can be fit for the separation tasks [26]. MOFs are nanoporous materials, which consist of metal ions or clusters and covalent linking organic molecules. ZIFs (zeolitic imidazolate frameworks) are a sub-class of MOFs with an exceptional chemical stability. This makes ZIFs attractive as membrane and as filler material. Until now many ZIF membranes could be successfully prepared [27–36]. Especially ZIF-8 is interesting for separation applications as it shows the best stability towards temperature and chemicals. ZIF-8 consists of Zn(II) ions and 2-methylimidazolate linkers, giving a sodalite structure with a pore cavity of 11.6 Å and a theoretical pore aperture of 3.4 Å [37]. It has been demonstrated as capable separation medium for smaller gas molecules like H_2/CH_4 with a selectivity of 11–15 [29,38,39] and CO_2/CH_4 with a selectivity of 4–7 [27]. However, the separation qualities of the ZIF-8 membrane are not yet satisfactory for industrial applications as the scaling-up is difficult and the gas permeability through the membrane is low [28,30,32–34].

New MMM consist of nanoparticulate fillers, for example zeolite, MOF, ionic liquid or carbon, which are embedded in a continuous polymer phase thus combining the molecular sieving property of

* Corresponding author. Tel.: +49 0511 762 2943.

E-mail address: lisa.diestel@pci.uni-hannover.de (L. Diestel).

the filler with the established processability of the polymer in one membrane [40–42]. The manufacture of ZIF-8 based MMM has already been tried by different groups using different materials. Zhang et al. [43] for example made 6FDA-DAM/ZIF-8 mixed matrix membranes, which showed high performance in the separation of C_3H_6 and C_3H_8 . Ordoñez et al. [44] mixed ZIF-8 and Matrimid® for several gas separations. They found increased permeability values for H_2 , CO_2 , O_2 , N_2 , CH_4 and C_3H_8 at loadings of 50 wt.% 100 nm ZIF-8 and improved ideal selectivities of gas pairs containing small molecules, such as H_2/O_2 , H_2/CO_2 , H_2/CH_4 , CO_2/CH_4 , CO_2/C_3H_8 , and H_2/C_3H_8 . Song et al. [45] made MMM with 20 wt.% 60 nm ZIF-8 particles and Matrimid®, which showed enhanced permeabilities of the pure gases H_2 , CO_2 , O_2 , N_2 and CH_4 with negligible losses in selectivity. First vaporization studies have been done by Liu et al. [46] who tested a 9.1 wt.% ZIF-8/PMPS MMM for alcohol/water separation. But until now, there are no attempts to compare and correlate the separation behavior of a pure ZIF-8 membrane, a pure polymer membrane and a MMM under the same conditions

2. Experimental

2.1. Membranes preparation

The pure ZIF-8 membrane was prepared on an α -alumina support by secondary growth using seed crystals. The ZIF-8 nanocrystals used for seeding ZIF-8 were prepared by mixing 0.73 g $Zn(NO_3)_2 \cdot 6H_2O$ in 50 mL methanol and 0.81 g 2-methylimidazole in 50 mL methanol under vigorous stirring and keeping the solution for 2 h at 25 °C [47]. Afterwards, the precipitate was collected by centrifugation and washed with methanol. Meanwhile, 0.12 g sodium hydrogen carbonate and 1.20 g polyethyleneimine ($\approx 50\%$ in water, M_r 600,000–1,000,000) were dissolved in 30 mL water. Then, 0.80 g ZIF-8 nanoparticles were added to the solution, and the clear suspension was stirred overnight. The alumina support with 70 nm Al_2O_3 particles in the top layer was dipped in this suspension at 25 °C and 25% humidity. For the secondary growth process 0.54 g $ZnCl_2$, 0.49 g 2-methylimidazole and 0.27 g sodium formate were dissolved in 80 mL methanol. The solution was filled in a 200 mL Teflon autoclave and the dried seed-coated support was put vertically in the solution. The autoclave was heated up to 100 °C in a microwave oven at a heating rate of 7.5 °C min^{-1} and kept at 100 °C for 1.8 h. After that, the autoclave was cooled down to 25 °C for 6 h and finally the membrane was washed with methanol and activated at 30 °C overnight.

The pure PMPS membrane was prepared by mixing 0.03 g dibutyltin dilaurate, 0.30 g tetraethylorthosilicate, 7.00 g isooctane and 3.00 g PMPS successively at 25 °C in a glass bottle. The mixture was sonicated for 20 min in an ice bath with a probe-type sonicator and kept at room temperature for 10 min. Afterwards an α -alumina support was dipped into the solution for 10 s and withdrawn with 1 $mm\ s^{-1}$. The membrane was cured at 25 °C for 24 h, at 100 °C for 12 h and then kept at 100 °C for additional 24 h under vacuum.

For the mixed matrix membrane (MMM), ZIF-8 nanoparticles were produced at 25 °C by adding 70 mL of a zinc precursor solution (70 mL methanol with 1.03 g $Zn(NO_3)_2 \cdot 6H_2O$) to 70 mL of a stirred 2-methylimidazole solution (70 mL methanol with 2.07 g 2-methylimidazole) [46]. After 1 h the nanoparticles were collected by centrifugation, washed with methanol and re-dispersed in isooctane to get a 4.5 wt.% ZIF-8 suspension. Then, 0.03 g dibutyltin dilaurate, 0.30 g tetraethylorthosilicate, 3.33 g isooctane, 3.00 g PMPS and 6.67 g ZIF-8 solution were mixed successively at 25 °C in a glass bottle. This mixture was sonicated for 20 min in an ice bath and kept at room temperature for 10 min. Afterwards an α -alumina support was dipped into this mixture for 10 s and

withdrawn with 1 $mm\ s^{-1}$. The membrane was activated at 25 °C for 24 h, at 100 °C for 12 h and then kept at 100 °C for additional 12 h under vacuum. Higher nanoparticle loadings in the MMM ($>15\ wt.\%$) have also been tested but the best separation performances have been reached at a content of 8.3 wt.% ZIF-8 nanoparticles due to a homogenous distribution of the particles in the polymer.

2.2. Membrane characterization

All three membranes have been characterized by X-ray diffraction patterns (XRD) and scanning electron microscopy (SEM). The XRD patterns were acquired from 5° to 50° at a rate of 0.02°/min using a Bruker D8 Advance diffractometer with $CuK\alpha$ X-ray radiation. The SEM surface and cross section view of the membranes have been performed on a JEOL JSM-6700F instrument (acceleration voltage = 2 kV, current = 5 μA).

The mixed gas separations and single gas permeation experiments with the three membranes were performed in a modified Wicke–Kallenbach apparatus using equimolar gas feeds with a total flow rate of 100 $mL\ min^{-1}$ at 1.2 bar pressure or a single component gas feed with a flow rate of 50 $mL\ min^{-1}$ at 1.2 bar pressure. For the mixtures H_2/CH_4 , CH_4/CO_2 , and H_2/CO_2 as feed and the single gases H_2 , CH_4 and CO_2 , nitrogen has been used as sweep gas. For the mixtures N_2/CO_2 and N_2/O_2 as feed gas and the single gases N_2 , CO_2 and O_2 , hydrogen has been used as sweep gas. The sweep gas had a flow rate of 50 $mL\ min^{-1}$ at a pressure of 1 bar. The ideal permselectivity α_{ij}^{ideal} can be calculated from the pure component gas permeabilities P_i and P_j and is defined as follows:

$$\alpha_{ij}^{ideal} = \frac{P_i}{P_j} \quad (1)$$

The corresponding binary mixture separation factor α_{ij}^{real} has been calculated by dividing the molar ratio of the permeate x_i/x_j as determined in gas chromatography by the molar ratio of the feed gas mixture y_i/y_j which nearly corresponds to the molar ratio of the retentate since the feed flux \gg permeate flux [50]:

$$\alpha_{ij}^{real} = \frac{x_i/x_j}{y_i/y_j} \quad (2)$$

3. Results

3.1. Membrane preparation

Fig. 1a and b show the SEM and XRD of the ZIF-8 nanoparticles as synthesized before embedding them into the MMM. These ZIF-8 particles have a size of around 40 nm (Fig. 1a) and show the characteristic XRD pattern of ZIF-8 (Fig. 1b).

It can be concluded from the XRD of the activated MMM in Fig. 2b that the embedding of ZIF-8 into PMPS did not change the crystallinity of ZIF-8. On the other hand, the interaction between the ZIF-8 nanoparticles and PMPS did not structure the polymer thus creating a pseudo-crystallinity of PMPS. The XRD of the activated ZIF-8 membrane (Fig. 2a) shows – as expected – the reflections of ZIF-8 and of α -alumina. The XRD of the activated polymer membrane shows a weak broad signal of PMPS (e.g., 10–15° in Fig. 2c) and the reflections of the α -alumina support. From comparing the XRD signal intensities of the supported ZIF-8 membrane layer (Fig. 2a) with those of the non-oriented ZIF-8 powder crystals (Fig. 1b) and those of non-oriented ZIF-8 crystals in the MMM (Fig. 2b) a preferred crystal orientation can be stated. This orientation of the ZIF-8 crystals in the membrane layer is characterized by the so called Crystallographic Preferred

3. Mixed matrix membranes

212

L. Diestel et al. / Microporous and Mesoporous Materials 189 (2014) 210–215

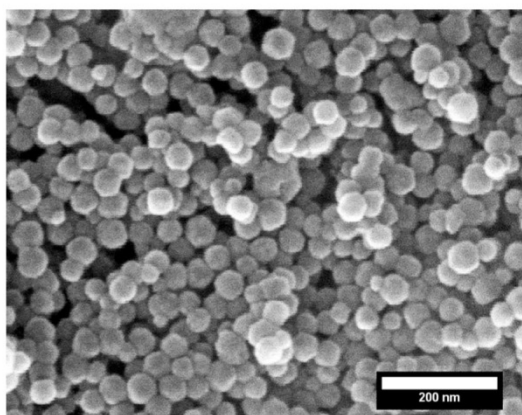


Fig. 1a. Representative SEM picture of the 40 nm ZIF-8 nanoparticles which were used for the preparation of the MMM. The SEM picture of the ZIF-8 seed crystals which were used in the secondary growth membrane synthesis looks quite similar.

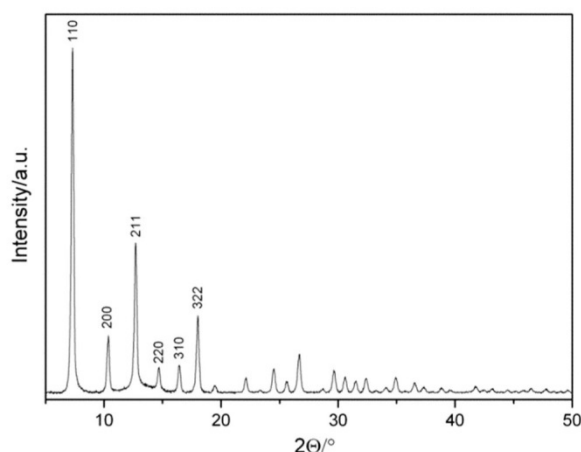


Fig. 1b. XRD pattern of the ZIF-8 nanoparticles shown in (a) which are used for the MMM preparation. Again, the XRD of the ZIF-8 nanoparticle seeds which were used in the secondary growth membrane synthesis compares.

Orientation index $CPO(X)/(Y)$ which is based on the (X) reflection and the (Y) reflection and defined as follows [48]:

$$CPO \frac{(X)}{(Y)} = \frac{\left(\frac{I_M^{(X)}}{I_M^{(Y)}} \right) - \left(\frac{I_P^{(X)}}{I_P^{(Y)}} \right)}{\left(\frac{I_P^{(X)}}{I_P^{(Y)}} \right)} \quad (3)$$

where I refers to the intensity of a reflection X or Y and M and P refer to the membrane or the non-textured powder, respectively. If the CPO index is ≥ 1 then the crystals in the membrane have a preferred [X] orientation. For $CPO = 0$ in contrast, the membrane is non-textured and for a negative CPO index the crystals in the membrane even prefer [Y] orientation. For the CPO of the ZIF-8 membrane under study, we compare the intensity of the dominant (200) reflection with the intensities of the (110) and (211) reflections. The CPO indices are $CPO(200/110) = 28$ and $CPO(200/211) = 8$ which clearly demonstrates the organization of the {100} plane of the ZIF-8 crystals lengthwise to the alumina support. The preferred crystallographic orientation can be explained by the evolutionary crystal growth by van der Drift [49]. Starting from a randomly oriented seed crystal layer on top of the α -alumina support, the crystals touch each other during the growth process. Right from this

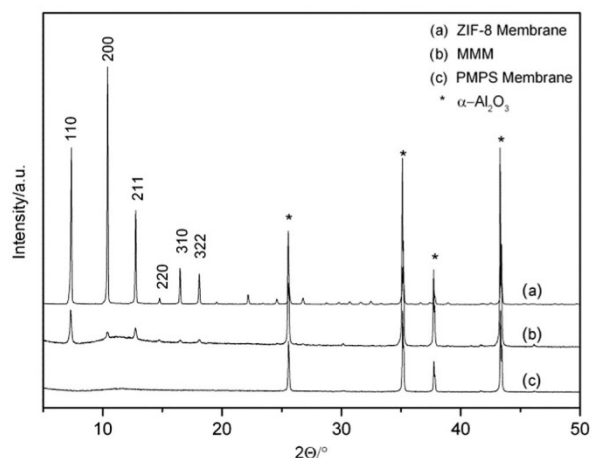


Fig. 2. XRD patterns of the three supported membranes under study: (a) the pure ZIF-8 membrane, (b) the MMM, and (c) the pure PMPS polymer membrane. Asterisks denote the pattern of the α -alumina support.

moment, all crystals which have the fastest growth direction perpendicular to the supporting surface, will overgrow the other crystals thus forming the top of the membrane. According to this experimental finding, the fastest growing direction of our ZIF-8 crystals is the $\langle 100 \rangle$ direction which is in complete accordance with Ref. [31]. From the absence of major defects like pinholes or cracks in the SEM pictures of the three membranes under study (Fig. 3) it follows that all membranes seem to be dense and deserve further testing in the gas permeation. The surface of the ZIF-8 membrane (Fig. 3a) shows a dense layer of well intergrown 5–10 μm large ZIF-8 crystals. From the cross section, the thickness of this membrane is estimated to be about 20 μm as shown in Fig. 3b. The polymer membrane in contrast, consists of a dense polymer layer with a thickness of 5 μm (Fig. 3c). In the MMM, the continuous polymer with embedded ZIF-8 nanoparticles forms a 10 μm thick layer (Fig. 3d). The adherence of the polymer layer and the MMM layer on the alumina support is very good, because of the intrusion of the polymer into the pores of the support evidenced by EDXS analysis [46].

3.2. Permeation studies

The permeation experiments showed that the pure ZIF-8 membrane separates gas mixtures especially by molecular sieving. This effect is not as accurate as for zeolite membranes with a sharp cut off, since the ZIF-8 framework is a coordination polymer and much more flexible than a covalent zeolite framework. Therefore, larger molecules like CH_4 which has a critical diameter of 3.8 Å, can enter the ZIF-8 pore network with a pore size of 3.4 Å. In contrast, for the pure PMPS polymer and the MMM we observed mainly an absorption-based gas separation which results in a permeation preference of the molecule with the higher molecular mass like CO_2 .

3.2.1. H_2/CH_4 separation

The single gas measurements on the three membranes propose that a proper separation of H_2 and CH_4 is only possible with the ZIF-8 membrane. The single component permeabilities through the ZIF-8 membrane were $P_{\text{H}_2} \approx 2598$ Barrer and $P_{\text{CH}_4} \approx 234$ Barrer Table 1. From these permeabilities an ideal permselectivity of $\alpha_{\text{H}_2, \text{CH}_4}^{\text{ideal}} \approx 11$ can be calculated for the H_2/CH_4 mixture on the ZIF-8 membrane (Table 2). The real mixture separation factor as obtained from gas chromatographic analysis was indeed $\alpha_{\text{H}_2, \text{CH}_4}^{\text{real}} \approx 11$ (Table 2). This experimental finding of

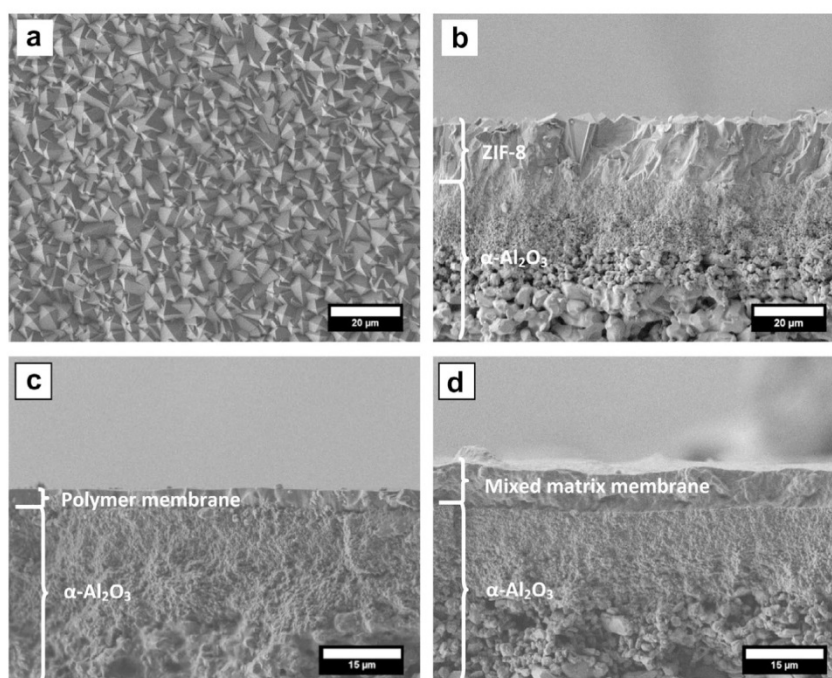


Fig. 3. SEM pictures of (a) top view and (b) cross section of the supported ZIF-8 membrane on the α - Al_2O_3 support with a ZIF-8 crystal size of 5–10 μm and a membrane thickness of about 20 μm , (c) the cross section of the supported PMPS polymer membrane with a thickness of about 5 μm , and (d) the cross section of the supported dense MMM (8.3 wt.% ZIF-8 in PMPS) with a thickness of about 10 μm .

Table 1

Gas permeabilities P of different single gases through the three supported membranes under study at room temperature: ZIF-8, MMM and PMPS polymer membranes.

Gas	P (ZIF-8)/Barrer	P (MMM)/Barrer	P (PMPS)/Barrer
H_2	2598	103	34
CH_4	234	114	37
CO_2	623	827	305
N_2	260	118	35
O_2	468	190	58

preferred hydrogen permeation is in full agreement with the Configurational-Bias Monte Carlo and Molecular Dynamics simulations of Krishna and van Baten [51]. In contrast to this finding, no separations could be reached for the H_2/CH_4 mixture by using the PMPS polymer membrane or the MMM. The pure polymer membrane had single component permeabilities of $P_{\text{H}_2} \approx 34$ Barrer and $P_{\text{CH}_4} \approx 37$ Barrer and the MMM had permeabilities of $P_{\text{H}_2} \approx 103$ Barrer and $P_{\text{CH}_4} \approx 114$ Barrer (Table 1). Accordingly, ideal separation factors of only 0.9 could be calculated for both membranes. Also the real separation factors from gas chromatographic analysis were found to be near 1 (Table 2). It is noticeable that the selectivity of the MMM is the same as that of the pure polymer membrane, which is not

surprising since PMPS is the main component of the MMM (91.7 wt.% \approx 91.2 vol.%). However, the MMM has a surprisingly higher gas permeability than the pure polymer membrane. This higher permeability could be explained by an increased free volume of the PMPS polymer after the introduction of ZIF-8 nanoparticles [45,52,53].

3.3. CO_2 separation from N_2 , CH_4 and H_2

Molecular sieving explains also the other separation patterns of the pure ZIF-8 membrane. CO_2 is a small molecule with a critical diameter of 3.3 Å. Thus it is a little bit smaller than N_2 and CH_4 (critical diameters 3.6 Å and 3.8 Å) but bigger than H_2 (critical diameter 2.9 Å). For the pure ZIF-8 membrane we measured single gas permeabilities of $P_{\text{N}_2} \approx 260$ Barrer, $P_{\text{H}_2} \approx 2598$ Barrer, $P_{\text{CH}_4} \approx 234$ Barrer and $P_{\text{CO}_2} \approx 623$ Barrer (Table 1). From these values we calculated relatively low ideal separation factors of $\alpha_{\text{CO}_2, \text{N}_2}^{\text{ideal}} \approx 2$, $\alpha_{\text{CO}_2, \text{H}_2}^{\text{ideal}} \approx 0.2$, $\alpha_{\text{H}_2, \text{CO}_2}^{\text{ideal}} \approx 5$, and $\alpha_{\text{CO}_2, \text{CH}_4}^{\text{ideal}} \approx 3$ (Table 2). The real separation factors measured for the binary mixtures with gas chromatographic analysis were similar. It should be noted that $\alpha_{\text{CO}_2, \text{H}_2} < 1$ has been predicted by Krishna and van Baten on thesis of Monte Carlo and Molecular Dynamics simulations [51,54]. The PMPS polymer and the MMM separate the gas mixtures by absorp-

Table 2

Separation factors α^{real} (derived from mixed gas permeation) and α^{ideal} (calculated as ratio of the single gas permeabilities) for different gas mixtures on the three supported membranes under study at room temperature: ZIF-8, MMM and PMPS polymer membranes.

Gas mixture	α^{ideal} (ZIF-8)	α^{ideal} (ZIF-8)	α^{ideal} (MMM)	α^{real} (MMM)	α^{real} (PMPS)	α^{real} (PMPS)
H_2/CH_4	11	11	0.9	1	0.9	0.9
CO_2/N_2	2	2	7	7	9	8
CO_2/H_2	0.2	0.2	8	8	9	9
CO_2/CH_4	3	4	7	7	8	8
O_2/N_2	2	2	2	2	2	2

tion based separation. Thus as an interplay of solubility and diffusivity selectivity, CO₂ permeates much faster through the PMPS and MMM than N₂, H₂ and CH₄. For the PMPS polymer membrane single component permeabilities of $P_{N_2} \approx 35$ Barrer, $P_{H_2} \approx 34$ Barrer, $P_{CH_4} \approx 37$ Barrer and $P_{CO_2} \approx 305$ Barrer have been measured (Table 1). With these values, ideal separation factors of $\alpha_{CO_2, N_2}^{ideal} \approx 9$, $\alpha_{CO_2, H_2}^{ideal} \approx 9$, and $\alpha_{CO_2, CH_4}^{ideal} \approx 8$ could be calculated and validated in mixed gas separation experiments (Table 2). Our experimental finding of high CO₂ selectivities for PMPS membranes is in accordance with Ref. [55] that recommends polydimethylsiloxane – which is chemically similar to our PMPS (polymethylphenylsiloxane) – for the separation of CO₂ from gas streams. Again the gas permeabilities through the MMM were found to be higher than the gas permeabilities through the pure PMPS polymer membrane (Table 1). The values of the gas permeabilities for the MMM were $P_{N_2} \approx 118$ Barrer, $P_{H_2} \approx 103$ Barrer, $P_{CH_4} \approx 114$ Barrer and $P_{CO_2} \approx 827$ Barrer. With these values ideal separation factors of $\alpha_{CO_2, N_2}^{ideal} \approx 7$, $\alpha_{CO_2, H_2}^{ideal} \approx 8$, and $\alpha_{CO_2, CH_4}^{ideal} \approx 7$ could be calculated for the MMM and validated by the mixed gas separation (Table 2).

3.4. N₂/O₂ separation

As N₂ and O₂ have nearly the same size (3.6 Å and 3.5 Å), ZIF-8 cannot separate this gas mixture. The ideal separation factor was near 2 in favor of oxygen, derived from the permeabilities of the single gases were $P_{N_2} \approx 260$ Barrer and $P_{O_2} \approx 468$ Barrer (Table 1). Also the PMPS polymer membrane does not show better separation patterns. The permeabilities were $P_{N_2} \approx 35$ Barrer and $P_{O_2} \approx 58$ Barrer. Thus an ideal separation factor of $\alpha_{O_2, N_2}^{ideal} \approx 2$ could be calculated. The real separation factor for both ZIF-8 and PMPS membranes were in the same range as the ideal ones (Table 2). The MMM showed a separation factor of 2 but the permeabilities were again higher in comparison with the PMPS membrane ($P_{N_2} \approx 118$ Barrer and $P_{O_2} \approx 190$ Barrer). Our separation factor of $\alpha_{O_2, N_2} \approx 2$ is in complete accordance with the separation factor O₂/N₂ on polydimethylsiloxane which is chemically similar to our PMPS [55].

The existence of undesirable interphases in the polymer after the introduction of nanoparticles is often a common feature in the preparation of MMM and can spoil the expected beneficial effect of the MMM. Therefore, there is recent work to consider the effect of the imperfect embedding by permeation models. If the permeation performance is predicted by applying the original Maxwell and Bruggeman models, due to the frequent presence of interphases, these models often failed [56,57]. To resolve this drawback, numerous permeation models (GPG, Funk-Lloyd, KJN) were developed to specifically consider interphases between filler and matrix. However, the better choice would be to find an experimentally way of eliminating the problem of an increased free volume in the polymer after the introduction of nanoparticles. Possible would be a better adhesion of the filler to the polymer matrix by chemical surface treatment of the filler or even covalent links between filler and polymer, thus rigidifying the polymer [58,59].

4. Conclusions

Three membranes have been prepared on porous α -alumina supports and their permeation behavior has been compared: Pure polymethylphenylsiloxane (PMPS), pure zeolitic imidazolate framework ZIF-8 and a mixed matrix membrane (MMM) with 8.3 wt.% \approx 8.8 vol.% ZIF-8 in the polymer matrix.

The permeation experiments show that the pure ZIF-8 membrane can separate mixed gas systems by molecular sieving as a special kind of diffusion control. Thus, due to their smaller molec-

ular size H₂ permeates faster through the ZIF-8 membrane than CH₄ and CO₂.

For the PMPS polymer membrane we observed mainly an absorption-based separation mechanism. Thus, CO₂ can be separated from the lighter gases H₂, CH₄ and N₂ on the PMPS which is in accordance with literature.

In all separations studied, the selectivity of the MMM was found to be identical with that of the PMPS polymer membrane but the MMM showed remarkably higher fluxes than the pure PMPS membrane. This experimental finding could be explained by an increased free volume of the PMPS due to the incorporation of ZIF-8 nanoparticles.

Acknowledgements

This work was financed by DFG in the frame of Priority Program 1362 (Porous Metal-Organic Frameworks), organized by S. Kaskel (Dresden). X.L. Liu, Y.S. Li, and W.S. Yang acknowledge the financial support from the National Science Fund of China (21176231, 21006101, 21276249 and 21361130018).

References

- [1] P. Bernardo, G. Golemme, E. Drioli, *Ind. Eng. Chem. Res.* 48 (2009) 4638–4663.
- [2] R. Baker, *Ind. Eng. Chem. Res.* 41 (2002) 1393–1411.
- [3] B. Freeman, *Macromolecules* 32 (1999) 375–380.
- [4] L. Robeson, *J. Membr. Sci.* 62 (1991) 165–185.
- [5] L. Robeson, *J. Membr. Sci.* 320 (2008) 390–400.
- [6] W. Koros, R. Mahajan, *J. Membr. Sci.* 175 (2000) 181–196.
- [7] N. Du, H. Park, M. Dal-Cin, M. Guiver, *Energy Environ. Sci.* 5 (2012) 7306–7322.
- [8] P. Budd, K. Msayib, C. Tattershall, B. Ghanem, K. Reynolds, N. McKeown, D. Fritsch, *J. Membr. Sci.* 251 (2005) 263–269.
- [9] N. Du, H. Park, G. Robertson, M. Dal-Cin, T. Visser, L. Scoles, M. Guiver, *Nat. Mater.* 10 (2011) 372–375.
- [10] S. Metz, M. Mulder, M. Wessling, *Macromolecules* 37 (2004) 4590–4597.
- [11] A. Car, C. Stropnik, W. Yave, K. Peinemann, *Adv. Funct. Mater.* 18 (2008) 2815–2823.
- [12] H. Lin, E. Van Wagner, R. Raharjo, B. Freeman, I. Roman, *Adv. Mater.* 18 (2006) 39–44.
- [13] H. Lin, E. Van Wagner, B. Freeman, L. Toy, R. Gupta, *Science* 311 (2006) 639–642.
- [14] H. Park, C. Jung, Y. Lee, A. Hill, S. Pas, S. Mudie, E. Van Wagner, B. Freeman, D. Cookson, *Science* 318 (2007) 254–258.
- [15] J. Wind, D. Paul, W. Koros, *J. Membr. Sci.* 228 (2004) 227–236.
- [16] T. Chung, L. Jiang, Y. Li, S. Kulprathipanja, *Prog. Polym. Sci.* 32 (2007) 483–507.
- [17] T. Merkel, B. Freeman, R. Spontak, Z. He, I. Pinnau, P. Meakin, A. Hill, *Science* 296 (2002) 519–522.
- [18] D. Vu, W. Koros, S. Miller, *J. Membr. Sci.* 211 (2003) 311–334.
- [19] J. Won, J. Seo, J. Kim, H. Kim, Y. Kang, S. Kim, Y. Kim, J. Jegal, *Adv. Mater.* 17 (2005) 80–84.
- [20] D. Gin, R. Noble, *Science* 332 (2009) 674–676.
- [21] B. Zornoza, S. Irueta, C. Téllez, J. Coronas, *Langmuir* 25 (2009) 5903–5909.
- [22] B. Zornoza, O. Esekhiile, W. Koros, C. Téllez, J. Coronas, *Sep. Purif. Technol.* 77 (2011) 137–145.
- [23] T. Bae, J. Liu, J. Lee, W. Koros, C. Jones, S. Nair, *J. Am. Chem. Soc.* 131 (2009) 14662–14663.
- [24] J. Hu, H. Cai, H. Ren, Y. Wie, Z. Xu, H. Liu, Y. Hu, *Ind. Eng. Chem. Res.* 49 (2010) 12605–12612.
- [25] T. Bae, J. Lee, W. Qiu, W. Koros, C. Jones, S. Nair, *Angew. Chem. Int. Ed.* 49 (2010) 9863–9866.
- [26] H. Hayashi, A. Côté, H. Furukawa, M. O’Keeffe, O. Yaghi, *Nat. Mater.* 6 (2007) 501–506.
- [27] S. Venna, N. Carreon, *J. Am. Chem. Soc.* 132 (2010) 76–78.
- [28] A. Huang, W. Dou, J. Caro, *J. Am. Chem. Soc.* 132 (2010) 15562–15564.
- [29] H. Bux, F. Liang, Y. Li, J. Cravillon, M. Wiebcke, J. Caro, *J. Am. Chem. Soc.* 131 (2009) 16000–16001.
- [30] Y. Li, F. Liang, H. Bux, W. Yang, J. Caro, *J. Membr. Sci.* 354 (2010) 48–54.
- [31] H. Bux, A. Feldhoff, J. Cravillon, M. Wiebcke, Y. Li, J. Caro, *Chem. Mater.* 23 (2011) 2262–2269.
- [32] Y. Li, F. Liang, H. Bux, A. Feldhoff, W. Yang, J. Caro, *Angew. Chem. Int. Ed.* 49 (2010) 548–551.
- [33] A. Huang, J. Caro, *Angew. Chem. Int. Ed.* 50 (2011) 4979–4982.
- [34] A. Huang, H. Bux, F. Steinbach, J. Caro, *Angew. Chem. Int. Ed.* 49 (2010) 4958–4961.
- [35] H. Bux, C. Chmelik, R. Krishna, J. Caro, *J. Membr. Sci.* 369 (2011) 284–289.
- [36] A. Thornton, D. Dubbeldam, M. Liu, B. Ladewig, A. Hill, M. Hill, *Energy Environ. Sci.* 5 (2012) 7637–7646.
- [37] K. Park, Z. Ni, A. Côté, J. Choi, R. Huang, F. Uribe-Romo, H. Chae, M. O’Keeffe, O. Yaghi, *Proc. Natl. Acad. Sci. USA* 103 (2006) 10186–10191.

3. Mixed matrix membranes

- [38] M. McCarthy, V. Varela-Guerrero, G. Barnett, H. Jeong, *Langmuir* 26 (2010) 14636–14641.
- [39] L. Diestel, H. Bux, D. Wachsmuth, J. Caro, *Micropor. Mesopor. Mater.* 164 (2012) 288–293.
- [40] H. Jeazet, C. Staudt, C. Janiak, *Dalton Trans.* 41 (2012) 14003–14027.
- [41] B. Zornoza, C. Téllez, J. Coronas, J. Gascon, F. Kapteijn, *Micropor. Mesopor. Mater.* 166 (2013) 67–78.
- [42] B. Zornoza, B. Seoane, J. Zamaro, C. Téllez, J. Coronas, *ChemPhysChem* 12 (2011) 2781–2785.
- [43] C. Zhang, Y. Dai, J. Johnson, O. Karvan, W. Koros, *J. Membr. Sci.* 389 (2012) 34–42.
- [44] M. Ordoñez, K. Balkus Jr., J. Ferraris, I. Musselman, *J. Membr. Sci.* 361 (2010) 28–37.
- [45] Q. Song, *Energy Environ. Sci.* 5 (2012) 8359–8369.
- [46] X. Liu, Y. Li, G. Zhu, Y. Ban, L. Xu, W. Yang, *Angew. Chem. Int. Ed.* 50 (2011) 10636–10639.
- [47] J. Cravillon, S. Münzer, S. Lohmeier, A. Feldhoff, K. Huber, M. Wiebcke, *Chem. Mater.* 21 (2009) 1410–1412.
- [48] J. Verduijn, A. Bons, M. Anthonis, L. Czarnetzki, *Int. Pat. Appl. PCT WO 96/01683*.
- [49] A. van der Drift, *Philips Res. Rep.* 22 (1967) 267–288.
- [50] W. Koros, Y. Ma, T. Shimidzu, *Pure Appl. Chem.* 68 (1996) 1479–1489.
- [51] R. Krishna, J. van Baten, *Phys. Chem. Chem. Phys.* 13 (2011) 10593–10616.
- [52] T. Rodenas, M. van Dalen, E. García-Pérez, P. Serra-Crespo, B. Zornoza, F. Kapteijn, J. Gascon, *Adv. Funct. Mater.* <http://dx.doi.org/10.1002/adfm.201203462>.
- [53] E. Perez, K. Balkus Jr., J. Ferraris, I. Musselman, *J. Membr. Sci.* 328 (2009) 165–173.
- [54] R. Krishna, J. van Baten, *J. Membr. Sci.* 3360 (2010) 323–333.
- [55] K. Scott, R. Hughes (Eds.), *Industrial Membrane Separation Technology*, Springer, 1995.
- [56] R. Mahajan, W. Koros, *Polym. Eng. Sci.* 42 (2002) 1420–1431.
- [57] H. Vinh-Thang, S. Kaliaguine, *Chem. Rev.* <http://dx.doi.org/10.1021/cr3003888>.
- [58] F. Zhang, X. Zou, X. Gao, S. Fan, F. Sun, H. Ren, G. Zhu, *Adv. Funct. Mater.* 22 (2012) 3583–3590.
- [59] X. Chen, H. Vinh-Thang, D. Rodrigue, S. Kaliaguine, *Ind. Eng. Chem. Res.* 51 (2012) 6895–6906.

3.3 Matrimid-based mixed matrix membranes: Interpretation and Correlation of experimental findings for zeolitic imidazolate frameworks as fillers in H₂/CO₂ separation

Lisa Diestel, Nanyi Wang, Alexander Schulz, Frank Steinbach and Jürgen Caro

Industrial and Engineering Chemistry Research 2015, 54, 1103-1112.

Reprinted (adapted) with permission from Industrial and Engineering Chemistry Research. Copyright (2015) American Chemical Society.

[doi:10.1021/ie504096j](https://doi.org/10.1021/ie504096j)

Matrimid-Based Mixed Matrix Membranes: Interpretation and Correlation of Experimental Findings for Zeolitic Imidazolate Frameworks as Fillers in H₂/CO₂ Separation

Lisa Diestel,* Nanyi Wang, Alexander Schulz, Frank Steinbach, and Jürgen Caro

Institute of Physical Chemistry and Electrochemistry, Leibniz University Hannover, Callinstrasse 3a, 30167 Hannover, Germany

ABSTRACT: In this paper we prepare three “neat” supported membranes, ZIF-8, ZIF-90, and Matrimid 5218, on porous alumina disks and compare their permeation behaviors in the separation of H₂/CO₂ with the corresponding zeolitic imidazolate framework (ZIF)/Matrimid mixed matrix membranes (MMMs). These MMMs consist of ZIF-8 and ZIF-90 nanoparticles which are embedded in Matrimid. We found that the embedding of the nanoparticles modifies the separation performance of the Matrimid 5218 membrane for separating H₂ from CO₂. TEM and SEM images of the ZIF-8 and ZIF-90/Matrimid MMMs show that the ZIFs are well embedded into the polymer. Thus, the separation behavior of these MMMs can be described with the Maxwell model. However, better separation results could be obtained by binding ZIF-90 particles covalently with ethylenediamine to the Matrimid matrix. In comparison to the MMMs that contain nonbound ZIFs, the covalent amine binding between the ZIF-90 particles and the Matrimid matrix leads to slightly lower permeabilities but a much higher H₂/CO₂ separation factor.

1. INTRODUCTION

The capture of CO₂ is a crucial step in fossil fuel conversion and can take place by postcombustion or precombustion procedures. The problems which have to be solved for the postcombustion CO₂ capture are (i) the low partial pressure of CO₂, (ii) the huge amount of flue gas, and (iii) the low pressure of the flue gas at medium temperatures. In the precombustion technologies, in contrast, the coal is gasified or the natural gas is steam-reformed. Afterward, the gas is cleaned and shifted several times before the hydrogen is extracted. On the whole, current CO₂ separation technologies cannot fulfill the separation as economically as is required for a large scale CO₂ reduction. Two of the most common techniques are amine absorption and pressure-swing adsorption. Both methods have disadvantages: amine absorption can only work at low temperatures around 40 °C and pressure-swing adsorption has significant energy requirements.^{1–5} In contrast to this, membrane-based technologies work with much less energy. In the case of the precombustion CO₂ capture, H₂ selective membranes work even at moderate temperatures (150–250 °C) in a one-step separation process. This approach offers the advantages that (i) the mixture of CO₂ and H₂ has already a high pressure, and that (ii) the application of H₂ permeable membranes can deliver CO₂ at high pressures, thus reducing compression costs. Generally, polymer membranes have been used successfully in a number of industrial applications, for example, natural gas sweetening, high-purity nitrogen production, gas dehydration, and acid gas removal.^{1,6} For successful use in industrial gas separation chemically and mechanically stable materials—even at high pressures and temperatures—are required, for example, Matrimid 5218.^{7–11} Additionally, Matrimid has permeability and selectivity properties close to the Robeson plot, which illustrates the limit of current polymer membranes in the trade-off between permeability and selectivity.^{12–15} Alternatives to the polymer

membranes are inorganic porous materials, for example, zeolitic imidazolate frameworks (ZIFs), which exhibit comparatively high permeabilities and selectivities. Besides, for the neat ZIF-8—in this ZIF the Zn²⁺ ions are interconnected by methylimidazolate ions¹⁶—some recent reports point out that the framework adsorbs bulky molecules such as benzene or xylenes,^{17,18} despite its pore openings of 3.4 Å as found from Rietveld X-ray diffraction (XRD) analysis. Hence, it is possible that adsorbed molecules can “open the gate” under certain conditions as found in refs 19–26. Nevertheless, neat ZIFs and other inorganic membranes suffer from a lack of reproducibility and problems in the scale-up.^{16,17,27–38}

Due to these limitations, mixed matrix membranes (MMMs) seem to be a viable pathway.^{39,40} MMMs consist of barrier-like or porous additives which are embedded in a continuous polymer matrix. These materials often have shown great benefits compared to neat polymer membranes, but there are still many challenges to overcome.^{1,36,41–53} One significant problem is the compatibility of the polymers and the additives to get homogeneous particle dispersions without agglomerates which represent unselective pathways for gas molecules. Additionally, unlinked additives tend to get separated from the polymer solution during the slow drying process due to gravitation. This phenomenon allows only moderate particle volume fractions of around 30 vol % and highly viscous MMM solutions for the membrane preparation. The drying process is also very crucial since a fast drying leads to solvent entrapments in the polymer whereas a slow drying promotes the segregation of the additives. An ideal particle–polymer interaction can be described with the barrier film model^{54,55} and the Maxwell

Received: October 17, 2014

Revised: January 6, 2015

Accepted: January 7, 2015

Published: January 7, 2015

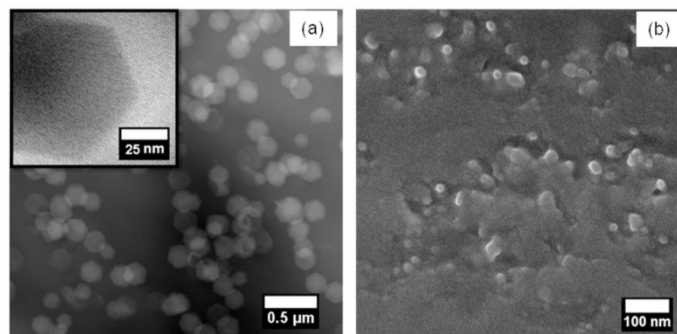


Figure 1. STEM, TEM, and respectively SEM pictures of two 25 vol % MMMs: (a) ZIF-8/Matrimid and (b) ZIF-90/Matrimid. The nanocrystals are homogeneously distributed and well embedded in the Matrimid matrix.

model.^{47–49} The first model illustrates the permeability of gas molecules through polymer membranes with aligned impermeable flakes. In contrast, the second model describes the permeability of gas molecules through a polymer membrane with molecular sieve additives which have aspect ratios near unity. It should be noted that recently a new generation of metal–organic framework (MOF) based MMMs have been developed. These new MMMs consist of parallel ordered MOF layers, through which one kind of gas molecule can permeate whereas the other kind cannot. Based on this concept, recent papers reported on delaminated MOF layers which have been brought into MMMs and led to superior separation performances.^{56–58}

Our aim was to develop MMMs with bulky inorganic molecular sieving additives to improve a Matrimid polymer membrane for the H_2/CO_2 separation and to compare the separation of the MMMs with the separations of the neat polymer and the neat inorganic membrane under the same conditions. Therefore, we used ZIF-8 and ZIF-90 nanocrystals. ZIFs are microporous molecular sieve materials which consist of metal ions and imidazolate linker molecules. Until now many supported ZIF membranes could be successfully prepared.^{27–38} Especially ZIF-8 is interesting for separation applications as it shows the best stability toward temperature (200 °C in N_2) and chemicals. ZIF-90 consists of Zn(II) ions and 2-carboxaldehyde imidazolate linkers, which form a sodalite structure like ZIF-8 but with a pore size of about 3.5 Å.⁵⁹ Both frameworks have interesting H_2/CO_2 membrane separation abilities of 4 or respectively 7 with high hydrogen permeabilities.^{38,28}

2. EXPERIMENTAL DETAILS

2.1. Synthesis of ZIF Powders for MMMs. ZIF-8 Particles. The ZIF-8 nanoparticles were produced at 25 °C by adding 70 mL of a zinc precursor solution (70 mL of methanol with 1.03 g of $Zn(NO_3)_2 \cdot 6H_2O$ (Sigma-Aldrich)) to 70 mL of a stirred 2-methylimidazole solution (70 mL of methanol with 2.07 g of 2-methylimidazole (Sigma-Aldrich)).²⁹ After 1 h the nanoparticles were collected by centrifugation, washed with methanol, and dried at 80 °C for 2 days in a convection oven. Figure 1a shows ZIF-8 particles with a mean size of 90 nm.

ZIF-90 Particles. For the synthesis of ZIF-90 nanoparticles 1.92 g of 2-carboxaldehyde imidazole (Acros) was solved at 70 °C in 50 mL of DMF (*N,N*-dimethylformamide). In between this time 1.48 g of $Zn(NO_3)_2 \cdot 6H_2O$ (Sigma-Aldrich) was

solved at 25 °C in 50 mL of methanol. After the imidazole solution was cooled to 50 °C, the zinc nitrate solution was mixed under vigorous stirring into this solution. Immediately a haze and slowly precipitation could be observed, which was separated after 30 min by centrifugation and washed two times with methanol. The ZIF-90 particles were dried at 80 °C for 2 days in the convection oven.¹⁷ The mean size of the ZIF-90 nanoparticles is 30 nm (see Figure 1b).

2.2. Synthesis of “Neat” Supported Membranes: ZIF-8, ZIF-90, and Matrimid. ZIF-8. The ZIF-8 membranes were produced by the secondary growth method.²⁰ Therefore, 0.12 g of sodium hydrogen carbonate and 1.20 g of polyethylenimine (Sigma-Aldrich, ~50% in water, 4 wt %) were solved in 30 mL of water and mixed with 0.80 g of ZIF-8 nanoparticles. Then, the clear suspension was used for seeding alumina supports (70 nm surface particles; Fraunhofer IKTS, formerly Hermsdorfer HITK, Germany). The dipping parameters were set as follows: up speed = 200 mm min^{-1} , down speed = 300 mm min^{-1} , lower delay = 10 s, and upper delay = 3 min. The coated supports were dried overnight at 25 °C. For the secondary growth process 0.54 g of $ZnCl_2$ (3.94 mmol, 1 equiv), 0.49 g of 2-methylimidazole (5.92 mmol, 1.5 equiv), and 0.27 g of sodium formate (3.94 mmol, 1 equiv) (Sigma-Aldrich) were solved in 80 mL of methanol. The solution was filled in a 200 mL Teflon autoclave, and one of the coated supports was put vertically in the solution. The closed autoclave was heated in a microwave oven with a heating rate of 7.5 °C min^{-1} at 100 °C for 1.5 h. After the autoclave was cooled to room temperature, the membrane was washed with 20 mL of methanol and dried overnight at 25 °C. The supported ZIF-8 membrane is shown in Figure 3.

ZIF-90. The alumina supports (70 nm surface particles; Fraunhofer IKTS, former Hermsdorfer HITK, Germany) were treated at 110 °C for 2 h with 0.46 g APTES (3-aminopropyltriethoxysilane, Sigma-Aldrich) in 10 mL toluol. Afterward the functionalized disks were washed several times with toluol. Then the disks were placed horizontally in a Teflon autoclave which was filled with a solution that consists of 0.43 g $Zn(NO_3)_2 \cdot 4 H_2O$ and 0.23 g imidazole-2-carboxaldehyde (Sigma-Aldrich) solved in 24 mL DMF. The autoclave was heated to 100 °C in a convection oven for 18 h. After the synthesis the membrane was washed with DMF and dried at 60 °C overnight. Figure 4 shows the supported ZIF-90 membrane.

Matrimid. The neat Matrimid membrane was produced by solving 0.30 g of Matrimid 5218 (Huntsman) in 3 mL of DCM

(dichloromethane). The solution was spread on an alumina support (70 nm surface particles; Fraunhofer IKTS, formerly Hermsdorfer HITK, Germany), dried under DCM atmosphere for 48 h, and dried finally for 24 h at 25 °C in ambient atmosphere. The thickness of the neat Matrimid membrane is 150 μm .

2.3. Preparation of Mixed Matrix Membranes (MMMs). The two MMMs ZIF-8/Matrimid and ZIF-90/Matrimid each contained 25 vol % filler and were also fabricated by solution blending. A 0.30 g sample of Matrimid5218 was solved in 2 mL of DCM while 0.08 g of ZIF-8 ($\delta = 0.93 \text{ g cm}^{-3}$) and 0.08 g of ZIF-90 ($\delta = 0.99 \text{ g cm}^{-3}$) were suspended in 1 mL of DCM. The additive and the polymer mixtures were mixed together and sonicated for 24 h. After that alumina supports (70 nm surface particles; Fraunhofer IKTS, formerly Hermsdorfer HITK, Germany) were coated with the honey-like polymer solution and dried under DCM atmosphere for 48 h and under ambient atmosphere conditions for 24 h until the polymer became hard. The ZIF-90 + ethylenediamine/Matrimid MMM was synthesized by solving 0.30 g of Matrimid in 2 mL of DCM and suspending 0.08 g of ZIF-90 in 1 mL of DCM. To the ZIF-90 suspension 50 μL of ethylenediamine (Sigma-Aldrich) was added, stirred for 1 h at 25 °C, and mixed with the Matrimid solution. Afterward the alumina support (70 nm surface particles; Fraunhofer IKTS, formerly Hermsdorfer HITK, Germany) was coated with the polymer mixture and dried at 25 °C in DCM atmosphere for 48 h as well as 24 h under ambient atmosphere conditions. All membranes had a thickness of 150 μm .

2.4. Characterization. Electron Microscopy. For the characterization of the homogeneity and the crystal size, all membranes were manually broken, coated with carbon, and analyzed by scanning electron microscopy (SEM) or transmission electron microscopy (TEM). The SEM images were taken on a JEOL JSM-6700F instrument (acceleration voltage = 5 kV, current = 5 μA). The TEM picture was taken with a field-emission JEOL JEM-2100F instrument. Therefore, the membrane was glued with epoxide on a supporting glass plate, cut with a diamond wire saw, polished by a precision polisher, and further thinned with an argon beam.

XRD. The crystallinity of the neat supported ZIF-8 and ZIF-90 membranes and the ZIF/Matrimid MMMs were characterized by a BRUKER D8Advance X-ray diffractometer (reflection mode, Cu $K\alpha$ radiation). The 2θ range from 5 to 50 was scanned with a step size of 0.02.

2.5. Gas Permeation. For an evaluation and comparison of the neat Matrimid membrane with the MMMs, mixed gas separation was measured in a modified Wicke-Kallenbach apparatus using an equimolar H_2/CO_2 feed with a total flow rate of 60 mL min^{-1} at 0.2–2.2 bar overpressure and 25 °C. N_2 was used as sweep gas with 2 mL min^{-1} .

For the permeation experiment we used a Wicke-Kallenbach apparatus and an equimolar H_2/CO_2 mixture. The ideal permselectivity $\alpha_{ij}^{\text{ideal}}$ can be calculated from the neat component gas permeabilities P_i and P_j :

$$\alpha_{ij}^{\text{ideal}} = \frac{P_i}{P_j} \quad (1)$$

The corresponding binary mixture separation factor $\alpha_{ij}^{\text{real}}$ has been calculated by dividing the molar ratio of the permeate x_i/x_j as determined in gas chromatography by the molar ratio of

the feed gas mixture y_i/y_j , which nearly corresponds to the molar ratio of the retentate since the feed flux \gg permeate flux.⁶⁰

$$\alpha_{ij}^{\text{real}} = \frac{x_i/x_j}{y_i/y_j} \quad (2)$$

3. RESULTS AND DISCUSSION

3.1. Membrane Preparation. The TEM image in scanning transmission electron microscopic (STEM) mode and the SEM

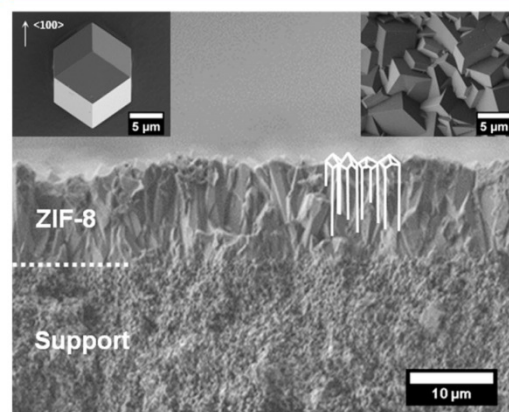


Figure 2. SEM cross section of the neat ZIF-8 membrane under study. The ZIF-8 membrane layer is located on an $\alpha\text{-Al}_2\text{O}_3$ support. The inset on the upper left shows the orientation of the ZIF-8 crystal as it follows from XRD (see Figure 4), and the inset on the upper right shows the top view of the ZIF-8 membrane with the oriented ZIF-8 crystals.

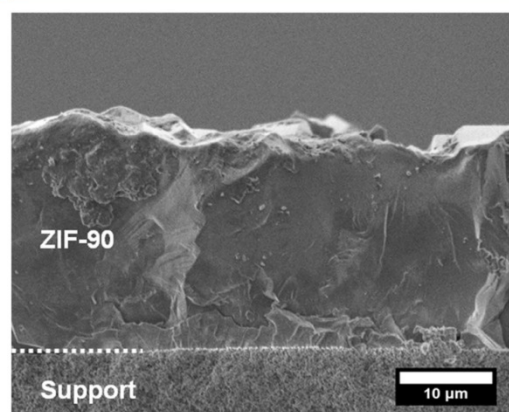


Figure 3. SEM cross section of the neat ZIF-90 membrane under study. The ZIF-90 membrane layer is located on an $\alpha\text{-Al}_2\text{O}_3$ support. From comparing powder and supported layer XRDs, no preferred crystallographic orientation of the ZIF-90 membrane is found (see Figure 5).

image demonstrate a homogeneous distribution and good embedding of the ZIF-8 and ZIF-90 nanoparticles in the

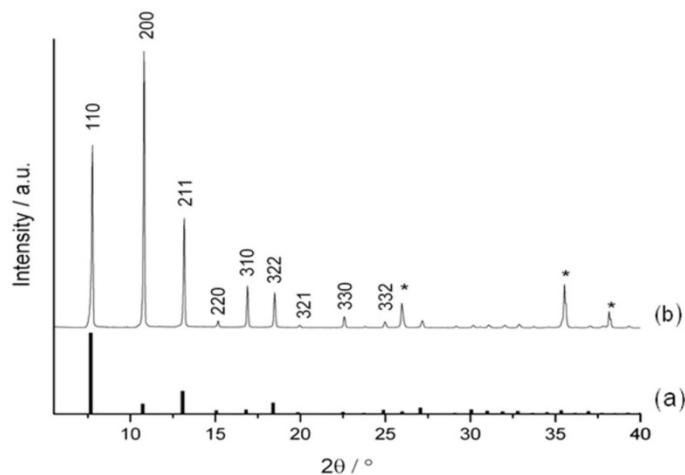


Figure 4. XRDs of (a) a simulated ZIF-8 powder sample with random crystal orientation and of (b) the measured neat supported ZIF-8 membrane (see Figure 3) with a certain crystallographic orientation. The asterisks denote the XRD patterns of the alumina support.

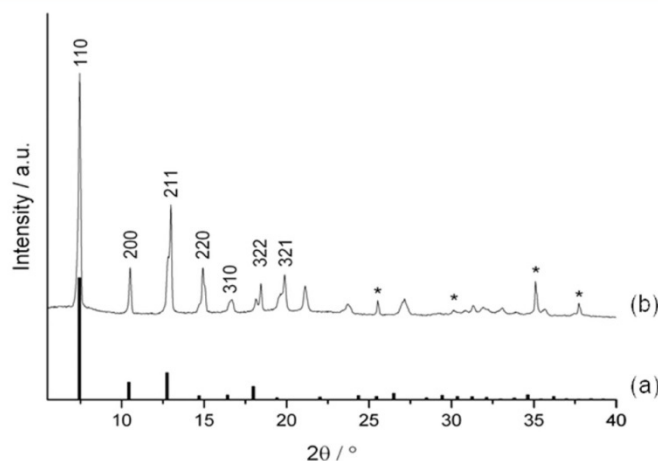


Figure 5. XRDs of (a) the simulated ZIF-90 powder sample with randomly oriented crystals and of (b) the measured neat supported ZIF-90 membrane (see Figure 4) without any crystallographic orientation. The asterisks denote the patterns of the alumina support.

Matrimid matrix (see Figure 1). The neat supported ZIF-8 and ZIF-90 membranes do not show major defects like cracks or pinholes (Figures 2 and 3). However, it seems that there is a certain crystal orientation in the supported ZIF-8 membrane (see Figure 2). In the following, this orientation will be proven by comparing the ZIF-8 powder XRD with the XRD of the supported ZIF-8 layer (see Figure 4).

From comparing the powder XRD of ZIF-8 with the XRD of the supported ZIF-8 membrane, we can conclude that the crystals in the neat supported ZIF-8 membrane layer have an orientation. This orientation can be quantitatively characterized by the so-called crystallographic preferred orientation index $CPO(X)/(Y)$.⁶¹

$$CPO \frac{(X)}{(Y)} = \frac{(I_M^{(X)}/I_M^{(Y)}) - (I_P^{(X)}/I_P^{(Y)})}{I_P^{(X)}/I_P^{(Y)}} \quad (3)$$

where I refers to the intensity of a reflection (X) or (Y) and “M” and “P” refer to the membrane and the nontextured powder. If the CPO index is not equal to 0, then the crystals have a preferred orientation. For the CPO index of the ZIF-8 membrane under study, we compare the intensity of the (200) reflection with the intensities of the (110) and (211) reflections (Figure 4). The CPO indices are $CPO(200/110) = 10$ and $CPO(200/211) = 3$, which demonstrates the organization of the {100} plane of the ZIF-8 crystals parallel to the alumina support. The preferred crystallographic orientation can be explained by the evolutionary crystal growth by van der Drift⁶² which says that the fastest growth of ZIF-8 takes place along the $\langle 100 \rangle$ direction and that all crystallites which have the right orientation will overgrow all the other slowly growing crystals and dominate the crystal orientation in the layer. These results are in complete accordance with the results of Bux et al.⁶³ In

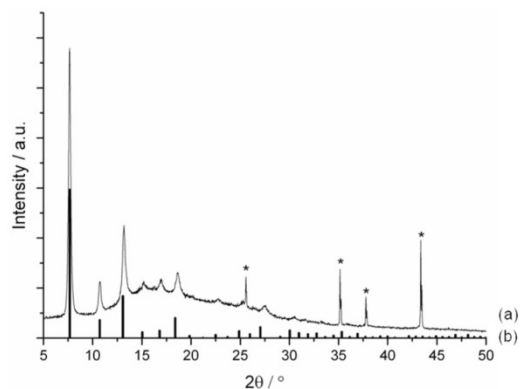


Figure 6. XRDs of (a) the measured ZIF-8/Matrimid MMM (see Figure 1 a) in comparison with (b) the simulated powder XRD of ZIF-8. The asterisks denote the reflections of the alumina support.

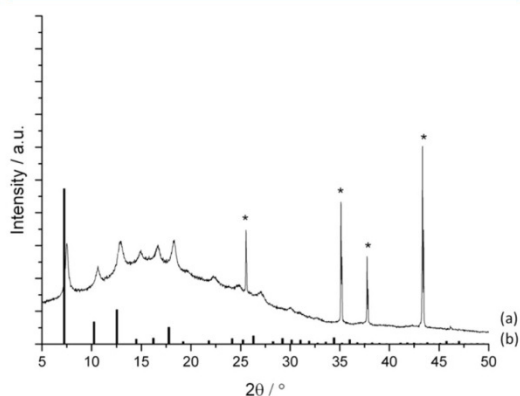


Figure 7. XRDs of (a) the measured ZIF-90/Matrimid MMM (see Figure 1 b) in comparison with (b) the simulated powder XRD of ZIF-90. The asterisks denote the reflections of the alumina support.

contrast, the crystals in the neat supported ZIF-90 membrane show no orientation (Figure 5).

As expected, the ZIF-8 and the ZIF-90 crystals in the corresponding MMM have no preferred orientation, and correspondingly the CPO indices are near 0 (Figures 6 and 7).

3.2. H₂/CO₂ Separation on the “Neat” Membranes Matrimid, ZIF-8, and ZIF-90. Figure 8 shows the results of the gas permeation for an equimolar H₂/CO₂ mixture on the three “neat” membranes under study: supported ZIF-8, ZIF-90, and Matrimid. In complete accordance with previous findings,²⁹ our ZIF-8 membrane shows hydrogen selectivity. For the ZIF-8 membrane we measured mixed gas permeabilities of $P_{H_2} \approx 2600 \pm 87$ barrer and $P_{CO_2} \approx 620 \pm 21$ barrer. This gives a mixed gas separation factor of $\alpha_{H_2/CO_2}^{real} \approx 4.2 \pm 0.3$. The neat ZIF-90 membrane shows a higher hydrogen permeability and also a higher selectivity than the ZIF-8 membrane. Through the neat ZIF-90 membrane we measured mixed gas permeabilities of $P_{H_2} \approx 3600 \pm 120$ barrer and $P_{CO_2} \approx 490 \pm 16$ barrer which give a mixed gas separation factor of $\alpha_{H_2/CO_2}^{real} \approx 7.3 \pm 0.5$ (see

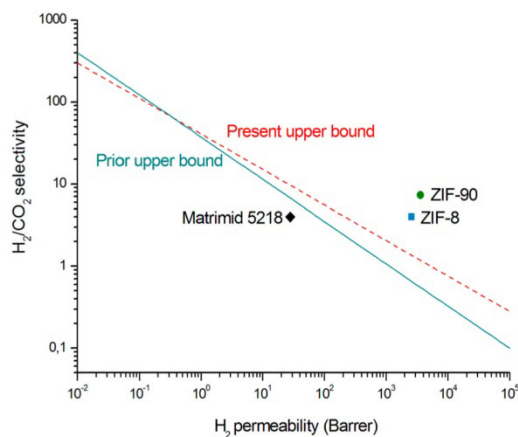


Figure 8. Robeson plot for the separation of the H₂/CO₂ mixture with the three “neat” membranes under study: ZIF-8 (see Figure 3), ZIF-90 (see Figure 4), and Matrimid 5218. The measurements of all three membranes were performed at 25 °C and a pressure difference of $\Delta p = 0.2$ bar between upstream and downstream. Prior and present upper bounds are taken from refs 12 and 13.

Table 1. Measured Mixed Gas Permeabilities (P_{H_2} and P_{CO_2}) and Mixed Gas Separation Factor α_{H_2/CO_2}^{real} for the Neat Matrimid and the MMMs at 25 °C and 0.2 bar Upstream Overpressure

	neat Matrimid 5218	MMM		
		ZIF-8	ZIF-90	ZIF-90 + ethylenediamine
$P_{H_2}/$ barrer	28 ± 0.9	31 ± 1.0	30 ± 1.0	19 ± 0.6
$P_{CO_2}/$ barrer	8 ± 0.3	9 ± 0.3	6 ± 0.2	2 ± 0.1
α_{H_2/CO_2}^{real}	3.5 ± 0.3	3.5 ± 0.3	5.0 ± 0.4	9.5 ± 0.6

Table 2. Calculation of the Effective Predicted Permeabilities $P_{eff,pred}$ through the ZIF-8 and ZIF-90 MMMs by the Maxwell Model According to eq 4 Using the Given Single Component Permeabilities P_C and P_D and ϕ_D Data^a

	ZIF-8 MMM	ZIF-90 MMM
$P_{eff,pred}(H_2)/$ barrer	54 ± 1.8 (31 ± 1.0)	55 ± 1.8 (30 ± 1.0)
$P_{eff,pred}(CO_2)/$ barrer	15 ± 0.5 (9 ± 0.3)	15 ± 0.5 (6 ± 0.2)

^aThe measured permeabilities (from Figure 9) are given in parentheses. Permeabilities of the neat membranes used for the prediction of the MMM (all values in barrer): (i) Matrimid, $P_{C,matr}(H_2) = 28 \pm 0.9$ and $P_{C,matr}(CO_2) = 8 \pm 0.3$; (ii) ZIF-8, $P_{D,ZIF}(H_2) = 2600 \pm 87$ and $P_{D,ZIF}(CO_2) = 620 \pm 21$; (iii) ZIF-90, $P_{D,ZIF}(H_2) = 3600 \pm 120$, $P_{D,ZIF}(CO_2) = 490 \pm 16$. Volume fraction $\phi_D = 0.25$.

Figure 8). Since the pore size of ZIF-90 (3.5 Å) is slightly larger than that of ZIF-8 (3.4 Å) and the structure of ZIF-90 is very similar to that of ZIF-8 in terms of topology, the higher H₂/CO₂ selectivity of the ZIF-90 membrane cannot be explained by any diffusion selectivity. This experimental finding of a higher selectivity for the H₂/CO₂ mixture is explained by the strong interaction of CO₂ with the aldehyde group of the ZIF-

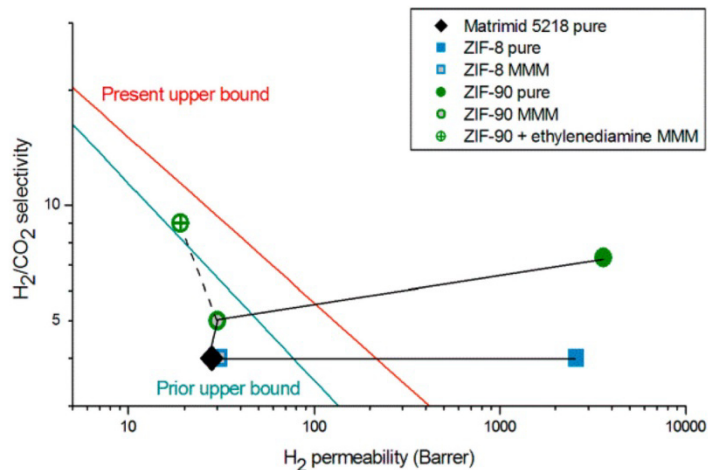


Figure 9. Gas permeation properties of the neat Matrimid 5218 membrane in comparison with the neat ZIF-8 (Figure 3) and its MMM (Figure 1a) as well as the neat ZIF-90 (Figure 4) and its MMM (Figure 1b) (simply added and covalently bound to the Matrimid matrix). The measurements of all membranes have been done at 25 °C and 0.2 bar upstream overpressure with downstream pressure of 1 bar. Prior and present upper bounds are taken from refs 12 and 13.

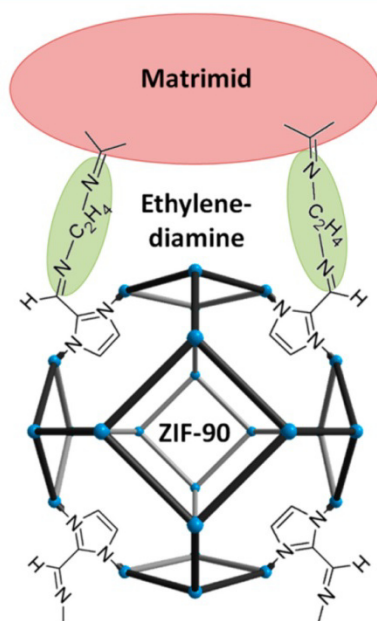


Figure 10. Model of the covalent link of ZIF-90 particles to the Matrimid matrix by ethylenediamine as a bidentate coupling agent. This covalent bonding leads to an increased H₂/CO₂ selectivity.

90 linker 2-carboxyaldehyde imidazolate as found in recent DFT-D studies.^{64,65} It can be expected from Figure 8 that combining Matrimid and ZIF-8 will give an MMM with improved hydrogen permeability while combining Matrimid and ZIF-90 should result in an MMM with an improved hydrogen permeability and an improved H₂/CO₂ selectivity.

3.3. H₂/CO₂ Separation on the MMM ZIF-8 and ZIF-90 in Matrimid.

All MMMs have been sealed with FKM-70 O-rings and polyethyleneimide glue which showed no measurable leakages.

As expected, in comparison with the starting neat Matrimid membrane, the ZIF-8-based MMM shows a higher hydrogen permeability with a constant H₂/CO₂ selectivity. This finding is in complete agreement with previous experimental and theoretical studies. Reference 66 also found that the embedding of 20 wt % ZIF-8 into Matrimid does not alter the H₂/CO₂ selectivity of about 4 but doubles both the H₂ and CO₂ permeabilities. By using molecular simulations, also ref 67 predicted that the incorporation of ZIFs into polyimides for H₂/CO₂ separation will enhance the gas permeability rather than improve the selectivity. Different from the ZIF-8-based MMM, the ZIF-90-based MMM shows a slightly improved H₂/CO₂ selectivity with a higher permeability (see Table 1). The latter finding is different from the results of ref 68, which predict by atomic simulations for increasing the volume fraction of ZIF-90 in polyimide-based MMM from 0 to 0.3 a doubling of the hydrogen permeability without any selectivity improvement.

In the following, we will apply the Maxwell model—which was originally developed for the calculation of the electrical conduction through heterogeneous media⁶⁹—for a quantitative interpretation and correlation of the MMM permeation data since the electrical conduction through such a heterogeneous medium is analogous with the permeation flux through membranes.^{49,50} The Maxwell model can be used to describe the permeability of gases through a polymer membrane with spherical, porous additives. Hence, the permeability of the gas molecules through this membrane depends only on the permeability of the gas through the polymer as continuous phase (P_c), and the molecular sieve as dispersed phase (P_D) as well as on the volume fraction (ϕ_D) of the dispersed phase in the continuous polymer matrix. According to the Maxwell

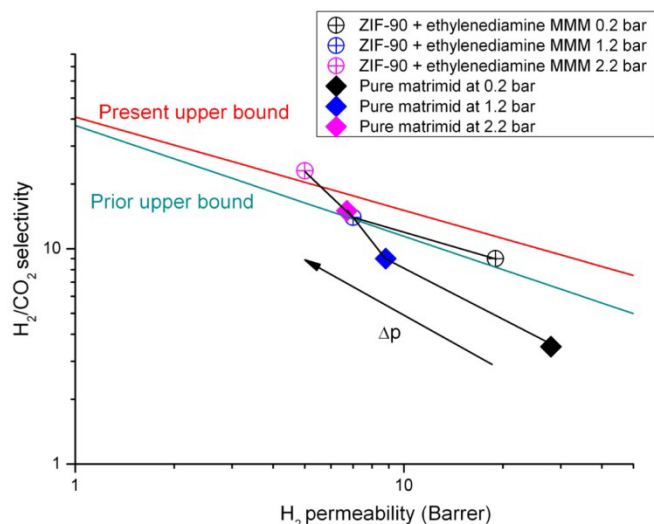


Figure 11. Gas permeation properties of neat Matrimid 5218 membrane and ZIF-90 plus ethylenediamine MMM at different upstream overpressures. The measurements of all membranes have been done at 25 °C, and downstream pressure was 1 bar. Prior and present upper bounds are taken from refs 12 and 13.

model, the effective permeability P_{eff} of a MMM can be described by the following expression:

$$P_{\text{eff}} = P_C \left[\frac{P_D + 2P_C - 2\phi_D(P_C - P_D)}{P_D + 2P_C + \phi_D(P_C - P_D)} \right] \quad (4)$$

Predicting the permeabilities of a binary H_2/CO_2 mixture through ideal ZIF-8- and ZIF-90-based MMMs with the Maxwell model using the neat membrane data (see Table 2), values for the ZIF-8/Matrimid MMM of $P_{\text{eff},\text{H}_2} = 54 \pm 1.8$ barrer and $P_{\text{eff},\text{CO}_2} = 15 \pm 0.5$ barrer and values for the ZIF-90/Matrimid MMM of $P_{\text{eff},\text{H}_2} = 55 \pm 1.8$ barrer and $P_{\text{eff},\text{CO}_2} = 15 \pm 0.5$ barrer result.

It follows from Table 2 that for the ZIF-8/Matrimid MMM the measured mixed gas permeabilities $P_{\text{eff},\text{H}_2} = 31 \pm 1.0$ barrer and $P_{\text{eff},\text{CO}_2} = 9 \pm 0.3$ barrer are much lower than the predicted ones. As the ZIF-8 particles are well embedded in the polymer matrix (see Figure 1a), we can conclude that the Maxwell model overestimates the influence of the ZIF-8 nanoparticles on the total permeability of the gases through the MMM. Since the neat Matrimid and the neat ZIF-8 membranes show the same selectivity of $\alpha_{\text{H}_2/\text{CO}_2}^{\text{real}} \approx 3.5$ in the H_2/CO_2 separation (Figure 8), the ZIF-8/Matrimid MMM exhibits the same mixed gas H_2/CO_2 selectivity. Nevertheless, the ZIF-8/Matrimid MMM represents an improvement in comparison with neat Matrimid because of its slightly higher hydrogen permeability (Figure 9).

In comparison with the ZIF-8/Matrimid MMM, the incorporation of ZIF-90 nanoparticles into Matrimid membrane is expected to increase the selectivity and the hydrogen permeability since the neat ZIF-90 membrane has a higher H_2 permeability and also a higher H_2/CO_2 separation factor than the neat Matrimid (Figure 8). We could indeed improve both parameters with the addition of ZIF-90 particles. The hydrogen

permeability increased slightly to $P_{\text{eff},\text{H}_2} = 30 \pm 1.0$ barrer and $P_{\text{eff},\text{CO}_2} = 6 \pm 0.2$ barrer and the selectivity increased slightly to $\alpha_{\text{H}_2/\text{CO}_2}^{\text{real}} = 5.0 \pm 0.4$. Again, the H_2 and CO_2 permeabilities of the MMM could not be predicted by the Maxwell model (see Table 2). Thus, the Maxwell model overestimated again the influence of the ZIF-90 network on the permeability of the MMM.

The ZIF-90/Matrimid MMM allows a unique coupling of filler and matrix. ZIF-90 contains 2-carboxaldehyde imidazolate as linker molecule with an aldehyde group for covalent coupling. This aldehyde group can be bonded by a diamine as a bidentate coupling agent to the Matrimid matrix which also contains aldehyde groups (see Figure 10). Indeed, better separation results could be obtained by coupling the ZIF-90 particles with ethylenediamine to the Matrimid matrix (see Figure 9, Table 1).^{70,71} The hydrogen permeabilities decrease slightly but the H_2/CO_2 separation factor increases as a result of this covalent coupling. A possible explanation of this experimental finding could be that linker distortion of the carboxyaldehyde imidazolate molecules in the surface of the ZIF-90 crystals—which are in direct contact with the Matrimid matrix—are suppressed.

As the precombustion techniques and hydrogen purification are performed at elevated pressures, we tested the influence of the feed pressure on the MMM separation performance. Figure 11 shows that the hydrogen permeabilities decrease slightly with higher upstream pressure. This behavior is typical for low-sorbing penetrants in glassy polymeric membranes as the transport is more diffusion dependent than sorption controlled. In the case of CO_2 the permeability decreases much more strongly with increasing upstream pressure, thus causing increasing H_2/CO_2 selectivities. This behavior shows the higher solubility of CO_2 in the polymer matrix. Similar behaviors of CO_2 at increasing pressures could also be observed for other glassy polymers.⁷² The CO_2 permeability decreases

until reaching a minimum—at the so-called plasticization pressure—from which the permeability increases again. The decrease of the CO₂ permeability depends herein on the sorption of the gas molecules in the polymer matrix. The polymer sorption sides become saturated with gas molecules until the penetrants plasticize the polymer at the plasticization pressure. At this point the polymeric chain packing is disrupted by the CO₂ molecules due to an increase in the chain mobility so that the diffusion coefficient—and therewith the permeation—increases with increasing upstream pressure.⁷³ The plasticization point of Matrimid by CO₂ is around 12 bar and has not been reached in the present work.⁷⁴

4. CONCLUSIONS

We prepared mixed matrix membranes (MMMs) with bulky ZIF-8 and ZIF-90 additives and studied the permeation behavior of these MMMs for the gas mixture H₂/CO₂. We found that the ZIF-8/Matrimid MMM improved the hydrogen permeability, while the mixed gas separation factor remained constant at $\alpha_{\text{H}_2/\text{CO}_2}^{\text{real}} = 3.5 \pm 0.3$. With the ZIF-90/Matrimid MMM we could observe a slight improvement of the mixed gas separation factor $\alpha_{\text{H}_2/\text{CO}_2}^{\text{real}} = 5.0 \pm 0.4$ and the hydrogen permeability that increased slightly from 28 ± 0.9 to 30 ± 1.0 barrer.

Plotting the H₂/CO₂ selectivity as a function of the H₂ permeability (Robeson plot), we can state an improvement in comparison to the neat Matrimid polymer membrane toward the Robeson line. A decisive improvement of the H₂/CO₂ separation factor could be achieved with the covalently bonded ZIF-90-based MMM. In this membrane, ethylenediamine linkers have been used to improve the interaction between the Matrimid polymer and the ZIF-90 particles. Thus, we could improve the separation factor again to $\alpha_{\text{H}_2/\text{CO}_2}^{\text{real}} = 9.5 \pm 0.6$ while the hydrogen permeability decreased to 19 ± 0.6 barrer, which is most probably due to a densified polymer structure near the filler particles.

AUTHOR INFORMATION

Corresponding Author

*E-mail: lisa.diestel@pci.uni-hannover.de.

Notes

The authors declare no competing financial interest.

ACKNOWLEDGMENTS

This work was financed by DFG in the frame of Priority Program 1362 (Porous Metal–Organic Frameworks), organized by S. Kaskel (Dresden).

REFERENCES

- Berchtold, K.; Young, J.; Dudeck, K. *High Temperature Separation Membranes for Hydrogen Purification and Carbon Capture*; MST: Los Alamos, NM, 2006; pp 1–2.
- Ruthven, D.; Farooq, S.; Knaebel, K. *Pressure Swing Adsorption*; Wiley: Hoboken, NJ, 1993.
- Gary, J.; Handwerk, G.; Dekker, M. *Petroleum Refining Technology and Economics*, 2nd ed.; Marcel Dekker Inc.: New York, 1984; pp 1–488.
- Mersmann, A.; Fill, B.; Hartmann, R.; Maurer, S. The Potential of Energy Saving by Gas-Phase Adsorption Processes. *Chem. Eng. Technol.* **2000**, *23*, 937.
- Aaron, D.; Tsouris, C. Separation of CO₂ from flue gas: A review. *Sep. Sci. Technol.* **2005**, *40*, 321.
- Chung, T.-S.; Jiang, L.; Li, Y.; Kulprathipanja, S. Mixed matrix membranes (MMMs) comprising organic polymers with dispersed inorganic fillers for gas separation. *Prog. Polym. Sci.* **2007**, *32*, 483.
- Koros, W.; Fleming, G. Membrane-based gas separation. *J. Membr. Sci.* **1993**, *83*, 1.
- Koros, W. Gas separation membranes: needs for combined materials science and processing approaches. *Macromol. Symp.* **2002**, *188*, 13.
- Koros, W.; Mahajan, R. Pushing the limits on possibilities for large scale gas separation: which strategies? *J. Membr. Sci.* **2000**, *175*, 181.
- David, O.; Gorri, D.; Ortiz, I.; Urtiaga, A. Dual-sorption model for H₂/CO₂ permeation in glassy polymeric Matrimid membrane. *Desalin. Water Treat.* **2011**, *27*, 31.
- Jiang, L.; Chung, T.; Li, D.; Cao, C.; Kulprathipanja, S. Fabrication of Matrimid/polyethersulfone dual-layer hollow fiber membranes for gas separation. *J. Membr. Sci.* **2004**, *240*, 91.
- Robeson, L. The upper bound revisited. *J. Membr. Sci.* **2008**, *320*, 390.
- Robeson, L. Polymer membranes for gas separation. *Curr. Opin. Solid State Mater. Sci.* **1999**, *4*, 549.
- Cecopieri-Gómez, M.; Palacios-Alquisira, J.; Domínguez, J. On the limits of gas separation in CO₂/CH₄, N₂/CH₄ and CO₂/N₂ binary mixtures using polyimide membranes. *J. Membr. Sci.* **2007**, *293*, 53.
- Powell, C.; Qiao, G. Polymeric CO₂/N₂ gas separation membranes for the capture of carbon dioxide from power plant flue gases. *J. Membr. Sci.* **2006**, *279*, 1.
- Kyo, S.; Ni, Z.; Côté, A.; Choi, J.; Huang, R.; Uribe-Romo, F.; Chae, H.; O'Keeffe, M.; Yaghi, O. Exceptional chemical and thermal stability of zeolitic imidazolate frameworks. *Proc. Natl. Acad. Sci. U.S.A.* **2006**, *103*, 10186.
- Diestel, L.; Bux, H.; Wachsmuth, D.; Caro, J. Pervaporation studies of n-hexane, benzene, mesitylene and their mixtures on zeolitic imidazolate framework-8 membranes. *Microporous Mesoporous Mater.* **2012**, *164*, 288.
- Zhang, K.; Lively, R.; Zhang, C.; Chance, R.; Koros, W.; Sholl, D.; Nair, S. Exploring the Framework Hydrophobicity and Flexibility of ZIF-8: From Biofuel Recovery to Hydrocarbon Separations. *J. Phys. Chem. Lett.* **2013**, *4*, 3618.
- Güçüyener, C.; van den Bergh, J.; Gascon, J.; Kapteijn, F. Ethane/ethene separation turned on its head: selective ethane adsorption on the metal-organic framework ZIF-7 through a gate-opening mechanism. *J. Am. Chem. Soc.* **2010**, *132*, 17704.
- Fairen-Jimenez, D.; Moggach, S.; Wharmby, M.; Wright, P.; Parsons, S.; Düren, T. Opening the gate: framework flexibility in ZIF-8 explored by experiments and simulations. *J. Am. Chem. Soc.* **2011**, *133*, 8900.
- Moggach, S.; Bennett, T.; Cheetham, A. The Effect of Pressure on ZIF-8: Increasing Pore Size with Pressure and the Formation of a High-Pressure Phase at 1.47 GPa. *Angew. Chem.* **2009**, *121*, 7221.
- Chokbunpiam, T.; Chanajaree, R.; Remsungnen, T.; Saengsawang, O.; Fritzsche, S.; Chmelik, C.; Caro, J.; Janke, W.; Hannongbua, S. N₂ in ZIF-8: Sorbate induced structural changes and self-diffusion. *Microporous Mesoporous Mater.* **2014**, *187*, 1.
- Aguado, S.; Bergeret, G.; Titus, M.; Moizan, V.; Nieto-Draghi, C.; Bats, N.; Farrusseng, D. Guest-induced gate-opening of a zeolite imidazolate framework. *New J. Chem.* **2011**, *35*, 546.
- van den Bergh, J.; Güçüyener, C.; Pidko, E.; Hensen, E.; Gascon, J.; Kapteijn, F. Understanding the Anomalous Alkane Selectivity of ZIF-7 in the Separation of Light Alkane/Alkene Mixtures. *Chem.—Eur. J.* **2011**, *17*, 8832.
- Chen, D.; Wang, N.; Wang, F.; Xie, J.; Zhong, Y.; Zhu, W.; Johnson, J.; Krishna, R. Utilizing the Gate-Opening Mechanism in ZIF-7 for Adsorption Discrimination between N₂O and CO₂. *J. Phys. Chem. C* **2014**, *118*, 17831.
- Ania, C.; García-Pérez, E.; Haro, M.; Gutiérrez-Sevillano, J.; Valdés-Solis, T.; Parra, J.; Calero, S. Understanding Gas-Induced Structural Deformation of ZIF-8. *J. Phys. Chem. Lett.* **2012**, *3*, 1159.

- (27) Venna, S.; Carreon, N. Highly Permeable Zeolite Imidazolate Framework-8 Membranes for CO₂/CH₄ Separation. *J. Am. Chem. Soc.* **2010**, *132*, 76.
- (28) Huang, A.; Dou, W.; Caro, J. Steam-Stable Zeolitic Imidazolate Framework ZIF-90 Membrane with Hydrogen Selectivity through Covalent Functionalization. *J. Am. Chem. Soc.* **2010**, *132*, 15562.
- (29) Bux, H.; Liang, F.; Li, Y.; Cravillon, J.; Miebcke, M.; Caro, J. Zeolitic Imidazolate Framework Membrane with Molecular Sieving Properties by Microwave-Assisted Solvothermal Synthesis. *J. Am. Chem. Soc.* **2009**, *131*, 16000.
- (30) Li, Y.; Liang, F.; Bux, H.; Yang, W.; Caro, J. Zeolitic imidazolate framework ZIF-7 based molecular sieve membrane for hydrogen separation. *J. Membr. Sci.* **2010**, *354*, 48.
- (31) Bux, H.; Feldhoff, A.; Cravillon, J.; Wiebcke, M.; Li, Y.; Caro, J. Oriented Zeolitic Imidazolate Framework-8 Membrane with Sharp H₂/C₃H₈ Molecular Sieve Separation. *Chem. Mater.* **2011**, *23*, 2262.
- (32) Li, Y.; Liang, F.; Bux, H.; Feldhoff, A.; Yang, W.; Caro, J. Molecular Sieve Membrane: Supported Metal–Organic Framework with High Hydrogen Selectivity. *Angew. Chem., Int. Ed.* **2010**, *49*, 548.
- (33) Huang, A.; Caro, J. Covalent Post-Functionalization of Zeolitic Imidazolate Framework ZIF-90 Membrane for Enhanced Hydrogen Selectivity. *Angew. Chem., Int. Ed.* **2011**, *50*, 4979.
- (34) Huang, A.; Bux, H.; Steinbach, F.; Caro, J. Molecular-Sieve Membrane with Hydrogen Permselectivity: ZIF-22 in LTA Topology Prepared with 3-Aminopropyltriethoxysilane as Covalent Linker. *Angew. Chem., Int. Ed.* **2010**, *49*, 4958.
- (35) Bux, H.; Chmelik, C.; Krishna, R.; Caro, J. Ethene/ethane separation by the MOF membrane ZIF-8: Molecular correlation of permeation, adsorption, diffusion. *J. Membr. Sci.* **2011**, *369*, 284.
- (36) Thornton, A.; Dubbeldam, D.; Liu, M.; Ladewig, B.; Hill, A.; Hill, M. Feasibility of zeolitic imidazolate framework membranes for clean energy applications. *Energy Environ. Sci.* **2012**, *5*, 7637.
- (37) McCarthy, M.; Varela-Guerrero, V.; Barnett, G.; Jeong, H. Synthesis of Zeolitic Imidazolate Framework Films and Membranes with Controlled Microstructures. *Langmuir* **2010**, *26*, 14636.
- (38) Diestel, L.; Liu, X.; Li, Y.; Yang, W.; Caro, J. Comparative permeation studies on three supported membranes: Neat ZIF-8, neat polymethylphenylsiloxane, and mixed matrix membranes. *Microporous Mesoporous Mater.* **2013**, *189*, 210.
- (39) Sheffel, J.; Tsapatsis, M. A model for the performance of microporous mixed matrix membranes with oriented selective flakes. *J. Membr. Sci.* **2007**, *295*, 50.
- (40) Mahajan, R.; Koros, W. Factors controlling successful formation of mixed-matrix gas separation materials. *Ing. Eng. Chem. Res.* **2000**, *39*, 2692.
- (41) Car, A.; Stropnik, C.; Peinemann, K. Hybrid membrane materials with different metal–organic frameworks (MOFs) for gas separation. *Desalination* **2006**, *200*, 424.
- (42) Zhang, Y.; Musselman, I.; Ferraris, J.; Balkus, K. Gas permeability properties of Matrimid® membranes containing the metal-organic framework Cu–BPY–HFS. *J. Membr. Sci.* **2008**, *313*, 170.
- (43) Josephine, A.; Ordoñez, C.; Balkus, K.; Ferraris, J.; Musselman, I. Molecular sieving realized with ZIF-8/Matrimid® mixed-matrix membranes. *J. Membr. Sci.* **2010**, *361*, 28.
- (44) Bae, T.; Lee, J.; Qiu, W.; Koros, W.; Jones, C.; Nair, S. A high-performance gas-separation membrane containing submicrometer-sized Metal–Organic Framework crystals. *Angew. Chem., Int. Ed.* **2010**, *49*, 9863.
- (45) Mahajan, R.; Burns, R.; Schaeffer, M.; Koros, W. Challenges in forming successful mixed matrix membranes with rigid polymeric materials. *J. Appl. Polym. Sci.* **2002**, *86*, 881.
- (46) Moore, T.; Mahajan, R.; Vu, D.; Koros, W. Hybrid membrane materials comprising organic polymers with rigid dispersed phases. *AIChE J.* **2004**, *50*, 311.
- (47) Bouma, R.; Checchetti, A.; Chidichimo, G.; Drioli, E. Permeation through a heterogeneous membrane: the effect of the dispersed phase. *J. Membr. Sci.* **1997**, *128*, 141.
- (48) Mahajan, R.; Koros, W. Mixed matrix membrane materials with glassy polymers. Part 1. *Polym. Eng. Sci.* **2002**, *42*, 1420.
- (49) Mahajan, R.; Koros, W. Mixed matrix membrane materials with glassy polymers. Part 2. *Polym. Eng. Sci.* **2002**, *42*, 1432.
- (50) Huang, Z.; Li, Y.; Wen, R.; Teoh, M.; Kulprathipanja, S. Enhanced gas separation properties by using nanostructured PES-Zeolite 4A mixed matrix membranes. *J. Appl. Polym. Sci.* **2006**, *101*, 3800.
- (51) Li, Y.; Chung, T.; Cao, C.; Kulprathipanja, S. The effects of polymer chain rigidification, zeolite pore size and pore blockage on polyethersulfone (PES)-zeolite A mixed matrix membranes. *J. Membr. Sci.* **2005**, *260*, 45.
- (52) Hillock, A.; Miller, S.; Koros, W. Crosslinked mixed matrix membranes for the purification of natural gas: Effects of sieve surface modification. *J. Membr. Sci.* **2008**, *314*, 193.
- (53) Gascon, J.; Kapteijn, F.; Zornoza, B.; Sebatian, V.; Casado, C.; Coronas, J. Practical Approach to Zeolitic Membranes and Coatings: State of the Art, Opportunities, Barriers, and Future Perspectives. *Chem. Mater.* **2012**, *24*, 2829.
- (54) Cussler, E.; Hughes, S.; Ward, W., III; Aris, R. Barrier membranes. *J. Membr. Sci.* **1988**, *38*, 161.
- (55) Lape, N.; Nuxoll, E.; Cussler, E. Polydisperse flakes in barrier films. *J. Membr. Sci.* **2004**, *236*, 29.
- (56) Rodenas, T.; Luz, I.; Prieto, G.; Seoane, B.; Miro, H.; Corma, A.; Kapteijn, F.; Llabrés i Xamena, F.; Gascon, J. Metal-organic-framework nanosheets in polymer composite materials for gas separation applications. *Nat. Mater.* **2014**, *14*, 48.
- (57) Jeong, H.; Krych, W.; Ramanan, H.; Nair, S.; Marand, E.; Tsapatsis, M. Fabrication of polymer/selective-flake nanocomposite membranes and their use in gas separation. *Chem. Mater.* **2004**, *16*, 3838.
- (58) Sheffel, J.; Tsapatsis, M. A semi-empirical approach for predicting the performance of mixed matrix membranes containing selective flakes. *J. Membr. Sci.* **2009**, *326*, 595.
- (59) Morris, W.; Doonan, C.; Furukawa, H.; Banerjee, R.; Yaghi, O. Crystals as molecules: Postsynthesis covalent functionalization of Zeolitic Imidazolate Frameworks. *J. Am. Chem. Soc.* **2008**, *130*, 12626.
- (60) Koros, W.; Ma, Y.; Shimidzu, T. Terminology for membranes and membrane processes. *Pure Appl. Chem.* **1996**, *68*, 1479.
- (61) Verduijn, J.; Bons, A.; Anthonis, M.; Czarnetzi, L. Int. Pat. Appl. PCT WO 96/01683, 1996.
- (62) van der Drift, A. Evolutionary Selection, A principle governing growth orientation in vapour-deposited layers. *Philips Res. Rep.* **1967**, *22*, 267.
- (63) Bux, H.; Feldhoff, A.; Cravillon, J.; Wiebcke, M.; Li, Y.; Caro, J. Oriented Zeolitic Imidazolate Framework-8 membrane with sharp H₂/C₃H₈ molecular sieve separation. *Chem. Mater.* **2011**, *23*, 2262.
- (64) Fischer, M.; Bell, R. Interaction of hydrogen and carbon dioxide with sod-type zeolitic imidazolate frameworks: a periodic DFT-D study. *CrystEngComm* **2014**, *16*, 1934.
- (65) Huang, A.; Dou, W.; Caro, J. Steam-Stable Zeolitic Imidazolate Framework ZIF-90 membrane with hydrogen selectivity through covalent functionalization. *J. Am. Chem. Soc.* **2010**, *132*, 15562.
- (66) Song, Q.; Nataraj, S.; Roussanova, M.; Tan, J.; Hughes, D.; Li, W.; Bourgoin, P.; Alam, M.; Cheetham, A.; Al-Muhtaseb, S.; Sivaniah, E. Zeolitic imidazolate framework (ZIF-8) based polymer nanocomposite membranes for gas separation. *Energy Environ. Sci.* **2012**, *5*, 8359.
- (67) Yilmaz, G.; Keskin, S. Predicting the Performance of Zeolite Imidazolate Framework/polymer mixed matrix membranes for CO₂, CH₄, and H₂ separations using molecular simulations. *Ind. Eng. Chem. Res.* **2012**, *51*, 14218.
- (68) Atci, E.; Keskin, S. Atomically detailed models for transport of gas mixtures in ZIF membranes and ZIF/polymer composite membranes. *Ind. Eng. Chem. Res.* **2012**, *51*, 3091.
- (69) Maxwell, J. *A Treatise on Electricity & Magnetism*; Dover Publications: New York, 1954.
- (70) Rodenas, T.; van Dalen, M.; García-Pérez, E.; Serra-Crespo, P.; Zornoza, B.; Kapteijn, F.; Gascon, J. Visualizing MOF Mixed Matrix

Membranes at the Nanoscale: Towards Structure-Performance Relationships in CO₂/CH₄ Separation Over NH₂-MIL-53(Al)@PL. *J. Adv. Funct. Mater.* **2014**, *24*, 249.

(71) Rodenas, T.; van Dalen, M.; Serra-Crespo, P.; Kapteijn, F.; Gascon, J. Mixed matrix membranes based on NH₂-functionalized MIL-type MOFs: Influence of structural and operational parameters on the CO₂/CH₄ separation performance. *Microporous Mesoporous Mater.* **2014**, *192*, 35.

(72) Matteucci, S.; Yampolskii, Y.; Freeman, B.; Pinnau, I. Transport of gases and vapors in glassy and rubbery polymers. In *Materials Science of Membranes for Gas and Vapor Separation*; Yampolskii, Y., Pinnau, I., Freeman, B., Eds.; Wiley: New York, 2006; pp 1–48.

(73) David, O.; Gorri, D.; Urtiaga, A.; Ortiz, I. Mixed gas separation study for the hydrogen recovery from H₂/CO/N₂/CO₂ post combustion mixtures using a Matrimid membrane. *J. Membr. Sci.* **2011**, *378*, 359.

(74) Bos, A.; Pünt, L.; Wessling, M.; Strathmann, H. CO₂-induced plasticization phenomena in glassy polymers. *J. Membr. Sci.* **1999**, *155*, 67.

3.4 MOF based MMMs with enhanced selectivity due to hindered linker distortion

Lisa Diestel, Nanyi Wang, Bärbel Schwiedland, Frank Steinbach, Ulrich Giese, and Jürgen Caro

Journal of Membrane Science 2015, 492, 181-186.

Reprinted (adapted) with permission from Journal of Membrane Science. Copyright (2015) Elsevier.

[doi:10.1016/j.memsci.2015.04.069](https://doi.org/10.1016/j.memsci.2015.04.069)



Contents lists available at ScienceDirect

Journal of Membrane Science

journal homepage: www.elsevier.com/locate/memsci

MOF based MMMs with enhanced selectivity due to hindered linker distortion



Lisa Diestel^{a,*}, Nanyi Wang^a, Bärbel Schwiedland^b, Frank Steinbach^a, Ulrich Giese^b, Jürgen Caro^a

^a Institute for Physical Chemistry and Electrochemistry, Callinstr. 22, 30167 Hannover, Germany

^b German Institute for Rubber Technology (DIK), Eupener Straße 33, 30519 Hannover, Germany

ARTICLE INFO

Article history:

Received 3 March 2015
Received in revised form
28 April 2015
Accepted 29 April 2015
Available online 8 May 2015

Keywords:

Zeolitic imidazolate framework
Mixed Matrix Membrane
Framework flexibility
Gate opening effect
Breathing

ABSTRACT

In this paper the separation of the binary mixture H₂/CH₄ on (i) neat supported ZIF (zeolitic imidazolate framework) membranes of types ZIF-8 and ZIF-90, (ii) a neat supported Matrimid polymer membrane, and (iii) Mixed Matrix Membranes (MMMs) with 10, 20 and 30 vol-% ZIF-8 and ZIF-90 nanocrystals in Matrimid is compared. A high separation performance was found surprisingly for the MMMs and it was concluded that the polymer matrix prevents the framework flexibility of the embedded Metal Organic Framework (MOF) particles, thus increasing the selectivity of MMMs with particle loadings ≤ 20 vol-%. Higher loadings, however, lead to agglomerations and segregations, which result in MMMs with lower selectivities. To approve the idea of the hindered linker distortion caused by the surrounding polymer, we coated the top of neat supported ZIF-8 and neat ZIF-90 membranes with an additional Matrimid polymer layer (dual-layer membrane). Indeed, the polymer coating also caused a suppression of the linker distortion of the ZIF layer in contact with the polymer which results in an enhanced H₂/CH₄ selectivity.

© 2015 Elsevier B.V. All rights reserved.

1. Introduction

As energy-efficient separation technology, membranes play an increasingly important role in industrial gas separation processes [1]. At the moment, the most widely used membranes are polymers. Nevertheless, the usage of polymeric membranes is limited due to the trade-off relationship between the permeability and the selectivity, plastification by feed absorption, and low thermal as well as solvent stability. Therefore, alternatives such as inorganic zeolite, metal or ceramic membranes are proposed in many studies. Metal-organic framework (MOF) membranes can show comparatively high permeabilities and selectivities combined with acceptable chemical and thermal stabilities. But these supported crystalline membranes suffer from a lack of reproducibility and problems in the scale up [2–10]. Due to these limitations, Mixed Matrix Membranes (MMMs) seem to be a future viable pathway [11–18]. MMMs are composed of additives like zeolites or MOFs, which are embedded in a polymer matrix to combine the flexibility and the easy handling of the polymer with the excellent separation performances of the filler materials. In contrast to most inorganic materials like zeolites, many MOFs – especially the subgroup zeolitic imidazolate frameworks (ZIFs) – are not rigid and can undergo structural changes. This means external stimuli like for example changing pressures and temperatures or

adsorptions and desorption of guest molecules inclusive solvents can induce pore openings or phase transformations, which are identifiable by XRD or sorption studies [19–22]. In a recent theoretical paper [23], the Density Functional Theory (DFT) has been used to unravel the vibration patterns of selected ZIFs (4, 7 and 8) on the molecular level. Vibrations in the THz region can explain the cooperative phenomena of the “gate opening” and “breathing”. With other words, these DFT calculations support the assumptions of a flexible pore architecture and support the absence of a clear *cut off* as found in numerous permeation experiments on MOF membranes [7,8,24]. MOF-based MMMs on the contrary, showed surprisingly high selectivities which are higher than those of the neat polymer and the neat MOF membrane [25]. A possible explanation for this finding could be that the continuous Matrimid matrix prevents the framework flexibility of the embedded ZIFs thus increasing the selectivity of the MMMs.

2. Experimental

2.1. Membrane preparation

2.1.1. ZIF-8 membrane synthesis

The ZIF-8 membranes were produced by the secondary growth method. 0.12 g sodium hydrogen carbonate and 1.20 g polyethyleneimine were solved in 30 mL water and mixed with 0.80 g ZIF-8 particles. Then, the clear suspension was used for seeding α -

* Corresponding author.

E-mail address: lisa.diestel@pci.uni-hannover.de (L. Diestel).

3. Mixed matrix membranes

182

L. Diestel et al. / Journal of Membrane Science 492 (2015) 181–186

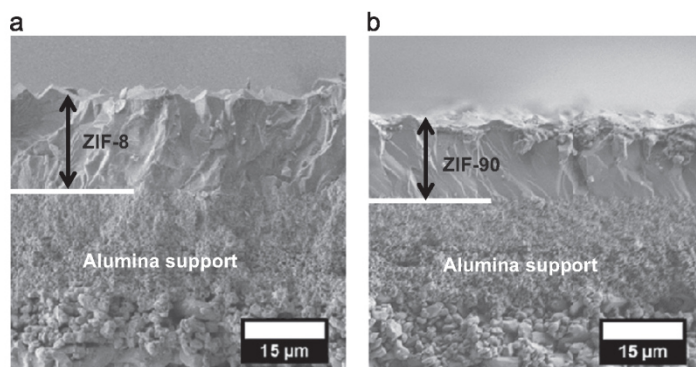


Fig. 1. SEM of the cross-sections of (a) a neat ZIF-8 membrane, and (b) a neat ZIF-90 membrane on a macroporous α -alumina support.

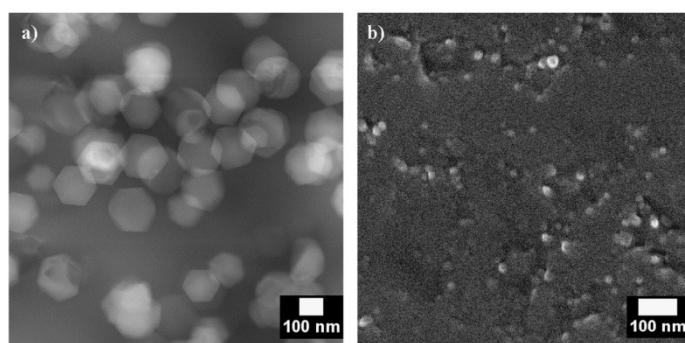


Fig. 2. (a) HRTEM of a 20 vol-% ZIF-8 MMM, and (b) SEM of a 20 vol-% ZIF-90 MMM.

alumina supports (70 nm pore size of the top layer; Fraunhofer IKTS, former Hermsdorfer HITK, Germany). The dipping parameters were: up speed = 200 mm min⁻¹, down speed = 300 mm min⁻¹, lower delay = 10 s, and upper delay = 3 min. The coated supports were dried overnight at room temperature. For the secondary growth process, 0.54 g ZnCl₂ (3.94 mmol, 1 eq.), 0.49 g 2-methylimidazole (5.92 mmol, 1.5 eq.) and 0.27 g sodium formate (3.94 mmol, 1 eq.) (Sigma Aldrich) were solved in 80 mL methanol. The solution was filled in a 200 mL Teflon autoclave and one of the coated supports was put vertically in the solution. The closed autoclave was heated in the microwave oven with a heating rate of 7.5 °C min⁻¹ at 100 °C for 1.5 h. After the autoclave was cooled down to room temperature, the membrane was washed with 20 mL methanol and dried overnight at room temperature. The thickness of the membrane is about 20 μm .

2.1.2. ZIF-90 membrane synthesis

The α -alumina supports (70 nm pore size of the top layer; Fraunhofer IKTS, former Hermsdorfer HITK, Germany) were treated at 110 °C for 2 h with 0.46 g APTES (3-aminopropyltriethoxysilane, Sigma Aldrich) in 10 mL toluene. Afterwards the functionalized disks were washed several times with toluene. Then the disks were placed horizontally in a Teflon autoclave which was filled with a solution out of 0.43 g Zn(NO₃)₂·4 H₂O and

0.23 g imidazole-2-carboxaldehyde (SigmaAldrich) solved in 24 mL N,N-dimethylformamide. The autoclave was heated to 100 °C in a convection oven for 18 h. After the synthesis the membranes were washed with N,N-dimethylformamide and dried at 60 °C overnight. The thickness of the ZIF-90 membrane is about 15 μm .

2.1.3. Matrimid membrane synthesis

The pure Matrimid membranes were produced by solving 0.30 g Matrimid[®]5218 in 3 mL dichloromethane. The solution was spread on an α -alumina support (70 nm pore size of the top layer; Fraunhofer IKTS, former Hermsdorfer HITK, Germany), dried under dichloromethane atmosphere for 24 h and dried finally for 24 h under ambient atmosphere. The neat matrimid membrane has a thickness of about 30 μm .

2.1.4. Dual-layer ZIF-8 and ZIF-90-Matrimid membrane synthesis

For the dual-layer ZIF-8 and ZIF-90-Matrimid membranes neat ZIF-8 and ZIF-90 membranes were coated with the neat Matrimid solution. Afterwards, the dual-layer membranes were dried under dichloromethane atmosphere for 24 h and finally for additional 24 h under ambient atmosphere.

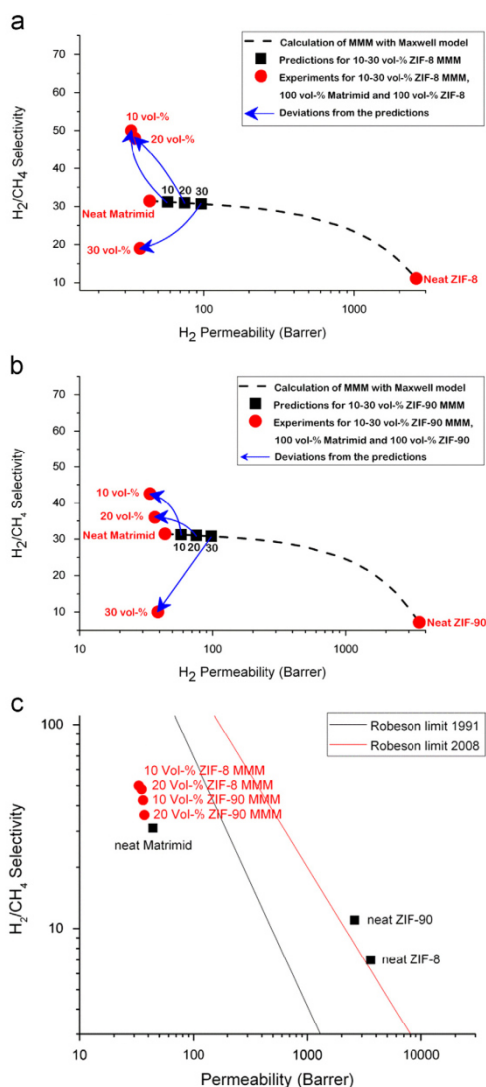


Fig. 3. H_2/CH_4 selectivity versus H_2 permeability plot for (a) the ZIF-8 based membranes, (b) the ZIF-90 based membranes, and (c) the Robeson limits in comparison with the neat membranes and the 10 to 20 vol-% MMMs. Comparison of the neat supported Matrimid and the neat supported ZIF membranes as well as the corresponding MMMs. Red: Measured data, black: Predictions from the Maxwell model for the MMM according to Eq. (2). All permeation measurements at 25 °C and a pressure difference of $\Delta p = 0.2$ bar between upstream (1.2 bar) and downstream (1 bar). (For interpretation of the references to color in this figure legend, the reader is referred to the web version of this article.)

2.1.5. ZIF-8 particle synthesis

The ZIF-8 particles were produced at room temperature by adding 70 mL of a zinc precursor solution (70 mL methanol with 1.03 g $Zn(NO_3)_2 \cdot 6H_2O$) to 70 mL of a stirred 2-methylimidazole solution (70 mL methanol with 2.07 g 2-methylimidazole). After 1 h the particles were collected by centrifugation, washed with methanol.

2.1.6. ZIF-90 particle synthesis

For the ZIF-90 particle synthesis 1.92 g 2-carboxaldehyde imidazole were solved at 70 °C in 50 mL N,N-dimethylformamide. In between this time 1.48 g $Zn(NO_3)_2 \cdot 6H_2O$ was dissolved at room temperature in 50 mL methanol. After the imidazole solution was cooled down to 50 °C, the zinc nitrate solution was mixed under vigorous stirring into the carboxaldehyd imidazole solution. A haze and slowly precipitation can be observed, which is separated after 30 min by centrifugation and washed two times with methanol.

2.1.7. MMM synthesis

For the MMM synthesis 10, 20 and 30 vol-% of ZIF-8 or ZIF-90 particles, respectively, were mixed with 0.30 g Matrimid in 1 mL dichloromethane. The solutions were casted on α -alumina supports (70 nm pore size of the top layer; Fraunhofer IKTS, former Hermsdorfer HITK, Germany) and dried under dichloromethane atmosphere for 24 h and under ambient atmosphere for additional 24 h.

2.2. Membrane characterization

For the characterization of the homogeneity of the MMMs and the crystal size, orientation and intergrowth, all membranes were manually broken, coated with carbon and analyzed by Scanning Electron Microscopy (SEM) or Transmission Electron Microscopy (TEM). The SEM images were taken on a JEOL JSM-6700F instrument (acceleration voltage = 5 kV, current = 5 μ A). The TEM picture, the STEM picture and the SEAD have been prepared with a field-emission JEOL JEM-2100F instrument. Therefore, the membranes were glued with epoxide on a supporting glass plate, cut with a diamond wire saw, polished by a precision polisher and further thinned with an argon beam.

The mixed gas separation experiments were performed in a modified Wicke-Kallenbach apparatus using equimolar gas feeds with a total flow rate of 100 mL min^{-1} at 1.2 bar pressure. The sweep gas had a flow rate of 2 mL min^{-1} at a pressure of 1 bar.

The binary mixture separation factor α_{ij}^{real} has been calculated by dividing the molar ratio of the permeate x_i/x_j as determined in gas chromatography by the molar ratio of the feed gas mixture y_i/y_j which nearly corresponds to the molar ratio of the retentate since the feed flux \gg permeate flux (Eq. (1)) [26].

$$\alpha_{ij}^{real} = \frac{x_i/x_j}{y_i/y_j} \quad (1)$$

3. Results and discussion

The SEM pictures of the neat ZIF-8 and the neat ZIF-90 supported membranes (Fig. 1) show no major defects like cracks or pinholes. Also the supported MMMs with 10, 20 and 30 vol-% ZIF-8 or ZIF-90 particles, respectively (Fig. 2) are free of major defects as it follows from the SEM and TEM pictures. Thus, it seems that all membranes seem to be dense and can be evaluated in the gas permeation.

From the measured permeabilities of the mixed gas permeation on the neat supported ZIF membranes and the neat supported Matrimid membranes, we calculated the expected permeabilities and selectivities for the MMMs by the Maxwell model (Eq. (2), Fig. 3) [27]. The Maxwell model was originally developed for the calculation of the electrical conduction through heterogeneous media [26], but it can also be used for a quantitative calculation of the MMM permeation data since the electrical conduction through heterogeneous media is analog with the permeation flux through a polymer membrane with spherical, porous additives [28]. The

3. Mixed matrix membranes

184

L. Diestel et al. / Journal of Membrane Science 492 (2015) 181–186

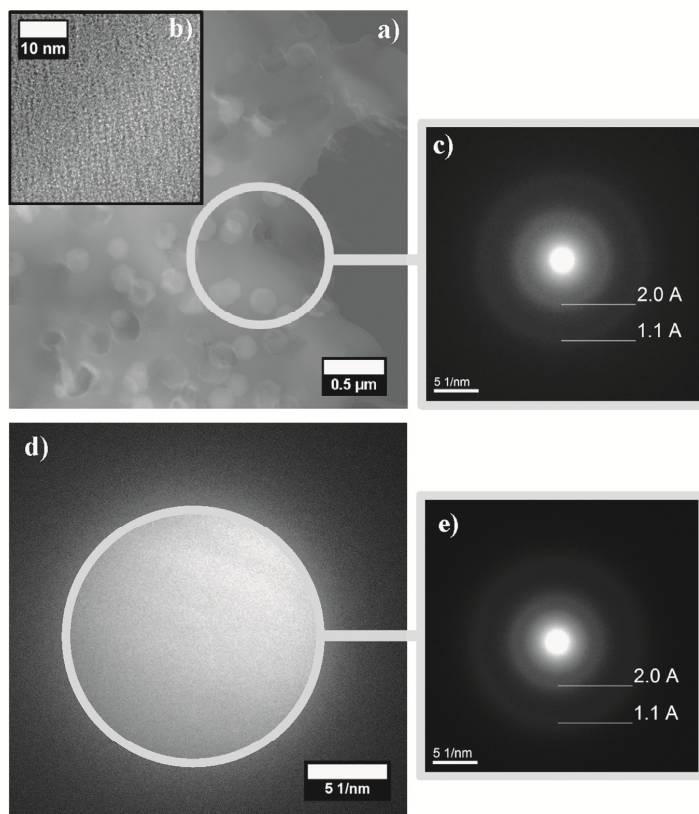


Fig. 4. (a) STEM dark-field picture of the ZIF-8 particles embedded in the Matrimid polymer matrix, (b) STEM bright-field picture of a ZIF-8 nanocrystal with the embedding Matrimid polymer, (c) SAED of the marked areas that reveals spots with d -spacings of 0.2 nm and 0.1 nm for the polymer, the ZIF-8 particles are “invisible” since they have been amorphized in the electron beam, (d) neat matrimid film which has been analyzed by SAED (e) to compare the diffractogram with the one of the ZIF-8 MMM as shown in (c).

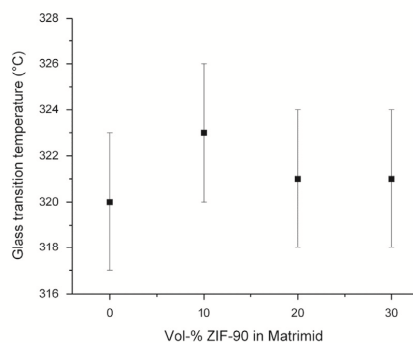


Fig. 5. Glass transition temperature of the pure Matrimid polymer and the MMMs with 10 to 30 vol-% ZIF-90. During the DSC-measurements the polymers have been heated twice with a heating rate of 10 K/min in N_2 atmosphere (Flux 20.0 ml/min) to avoid artefacts and to normalize the thermal history.

permeability of the gas molecules through MMMs depends only on the permeability of the gas through the polymer as continuous phase (P_C), and the molecular sieve additive as dispersed phase (P_D) as well as on the volume fraction (ϕ_D) of the dispersed phase

in the continuous polymer matrix. According to the Maxwell model, the effective permeability P_{eff} of a MMM can be described by the following expression:

$$P_{eff} = P_C \frac{P_D + 2P_C - 2\phi_D(P_C - P_D)}{P_D + 2P_C + \phi_D(P_C - P_D)} \quad (2)$$

Comparing the predicted permeation results for the binary mixture H_2/CH_4 on ZIF-8/Matrimid and ZIF-90/Matrimid MMMs with the measured data for these MMMs, we can state a selectivity enhancement for the MMMs with 10 and 20 vol-% ZIF particles (Fig. 3). But the H_2 permeabilities of the MMMs were lower than the expected values from the Maxwell model. For MMM particle loadings > 20 vol-%, however, we measured for both the ZIF-8 and ZIF-90 based MMM lower mixed gas selectivities and lower hydrogen permeances than predicted (Fig. 3) since in our case the filler particles agglomerate at particle loadings > 20 vol-%, which leads to particle clusters with interfacial voids. Comparing the measured membrane results with the Robeson plot, which illustrates the upper bound limit of the trade-off relationship between the selectivity and permeability for the best polymeric membranes, we can conclude that the MMMs could not exceed the limits. But nevertheless we could gain unexpectedly high gas selectivities in comparison with the neat matrimid (Fig. 3c).

3. Mixed matrix membranes

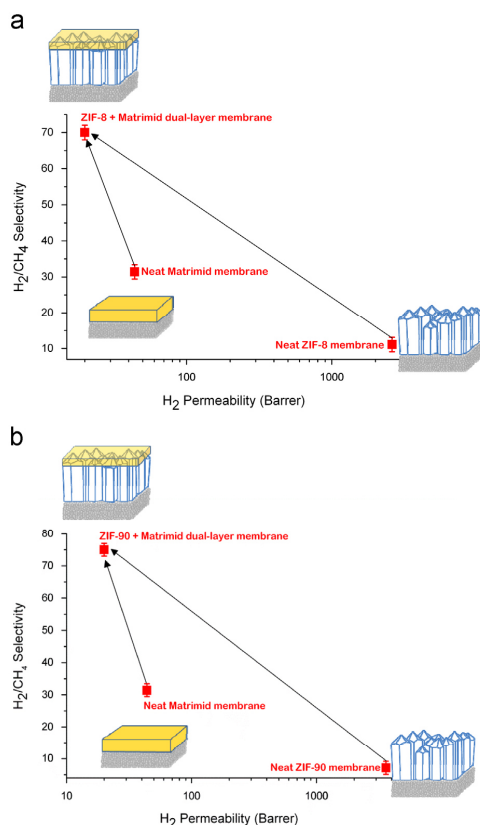


Fig. 6. Selectivity enhancement for coated ZIF-8 and ZIF-90 membranes with a Matrimid polymer layer. H₂/CH₄ selectivity versus H₂ permeability plot for (a) neat ZIF-8 membrane as shown in Fig. 1a, neat Matrimid membrane and the dual-layer ZIF-8 + Matrimid membrane, and (b) neat ZIF-90 membrane as shown in Fig. 1b, neat Matrimid and the dual-layer ZIF-90 + Matrimid membrane. All permeation measurements at 25 °C and a pressure difference of $\Delta p = 0.2$ bar between upstream (1.2 bar) and downstream (1 bar). The error bars mark the deviations of the membrane performances.

The higher H₂/CH₄ selectivity and lower H₂ permeabilities of the measured ZIF based MMMs can be explained by either (i) a rigidified polymer layer around the embedded ZIF particles, or by (ii) a hindered gate-opening effect of the ZIFs caused by the surrounding polymer matrix. Both models can explain our experimental findings of the enhanced selectivity and slightly decreased hydrogen permeability at low particle loadings of 10 and 20 vol-% ZIF in Matrimid. If the particle loading of the MMM is higher, the particles tend to agglomerate and segregate, which leads to defective membranes with unselective pathways for the gas molecules since the ZIF particles are not completely surrounded by the polymer [29].

Rigidified polymer layers could often be found for zeolites and other additives in polymer matrices if the contact between both phases was very attractive. The mobility of the polymer chains in the region directly contacting the particle is inhibited relative to the polymer chains of the bulk polymer [30]. Thus, the higher selectivity of these MMMs was only attributed to an enhanced diffusivity selectivity caused by the increased rigidity of the polymer matrix. But for MOFs, also a hindered linker distortion of the imidazolate linker molecules in the ZIF frameworks can

cause higher selectivity and lower permeability. For ZIF-8, there are some recent reports, that the MOF framework can adsorb bulky molecules such as benzene or xylenes [31], despite of the ZIF-8 pore openings of 3.4 Å. Hence, it is possible that adsorbed molecules can “open the gate” under certain conditions as found in [32]. This behavior leads to declined gas selectivities for certain MOFs an adsorption and permeation like in the case of the neat ZIF membranes. A hindered linker distortion can cancel this effect and generate “molecular sieving”.

To answer the question about the reason for the unexpected separation performance of the ZIF based MMMs, we analyzed the polymer structure of the surrounding Matrimid in the neighborhood of the ZIF-8 particles by STEM and HR-TEM (Fig. 4).

Any change could not be identified in the arrangement of the polymer chains near to the ZIF particles in the STEM picture (Fig. 4a and b) which could explain an increased selectivity. The selected area electron diffraction (SAED) of the ZIF-8 MMM contains two diffuse Debye Scherrer rings (Fig. 4c) which correspond to a maximum in the radial electron intensity distribution at 0.2 nm and 0.1 nm. Aromatic polyimides, like Matrimid, have a relatively disordered chain packing structure and form a rather amorphous structure due to the variation in the conformation around the chain axis. But in the amorphous phase, there can be found some ordered liquid-crystalline-like domains in which the polyimide chains have a preferred layer packing and are packed together both along the in-plane and the out-of-plane direction [33]. Since no polymer structure changes near to the ZIF particle are identifiable, we can conclude, that the polymer seems to be unchanged (Fig. 4c and e). This assumption could be confirmed by DSC measurements of the neat polymer and the 10 to 30 vol-% ZIF-90/Matrimid MMMs, which show no significant differences in their glass transition points (T_g) (Fig. 5). The glass transition point itself is a very sensitive parameter with respect to nearly every aspects of the material microstructure [34,35]. If a particle/polymer interaction is very intense and the polymer gets more rigid around the particle, because of the adsorption of polymer segments, the T_g of the rigid polymer will be higher compared with the T_g of the bulk polymer, because of the reduced chain mobility. Weak interactions instead lead to lower T_g due to less organized polymer chains. An unchanged T_g indicates that the structure of the majority of the bulk polymer is unchanged.

This means that our experimental finding of an improved H₂/CH₄ selectivity for the MMM – much higher than the prediction of the Maxwell model – can be explained most probably by a hindered gate-opening effect of the ZIFs by the surrounding polymer matrix. To confirm this idea we prepared ZIF-8 and ZIF-90 dual-layer ZIF/Matrimid membranes. First, a “normal” supported neat ZIF membrane as shown in Fig. 1 has been prepared, and in a second preparation step, a Matrimid top layer was added to the previously synthesized neat supported ZIF membrane as described under Section 2. For this experiment, we used our best ZIF membranes with H₂/CH₄ selectivities around 11–13 for ZIF-8 (3 membranes) and around 7–9 for ZIF-90 (3 membranes). If the gate-opening effect is really hindered by the presence of Matrimid, we should observe an increased H₂/CH₄ selectivity for so prepared dual-layer ZIF-8 and ZIF-90 membranes after bringing a top layer of Matrimid on the neat supported ZIF membranes. These high H₂/CH₄ selectivities could be found indeed with a very high reproducibility (see the error bar) for the dual-layer membranes, however, with some losses in permeability (Fig. 6).

4. Conclusion

The present study could clearly demonstrate the influence of the framework flexibility on the gas separation selectivity of ZIF-8 and ZIF-90 membranes. When the supported neat ZIF-8 and ZIF-

90 membranes become coated with an additional Matrimid top layer, in the contact zone polymer-ZIF the framework flexibility is frozen, most probably the linker distortion is blocked, and as a result, the H₂/CH₄ selectivity increased dramatically for the coated dual-layer ZIF membranes. The same phenomenon of suppressed linker distortion is responsible for the surprisingly high performance of Mixed Matrix Membranes (MMM) by embedding the ZIF nanoparticles in a Matrimid polymer matrix. The measured H₂/CH₄ selectivities on the MMM were found to be much higher than the predicted data from the so called Maxwell model. It is shown, that the increased selectivity values are not caused by a rigidified polymer layer around the ZIF particles, but by a hindered linker distortion of the imidazolate molecules in the ZIF frameworks. Thus, the presence of a well-fitting polymer layer next to the ZIF particles cancels the negative effect of the imidazolate linker flexibility on the selectivity.

Acknowledgment

This work was financed by DFG in the frame of Priority Program 1362 (Porous Metal–Organic Frameworks), organized by S. Kaskel (Dresden). Prof. Dr. A. Feldhoff (Leibniz University of Hannover) is thanked for stimulating discussions.

References

- [1] M. Freemantle, Membranes for gas separation, *Chem. Eng. News* 83 (2005) 49.
- [2] S. Venna, N. Carreon, Highly permeable zeolite imidazolate framework-8 membranes for CO₂/CH₄ separation, *J. Am. Chem. Soc.* 132 (2010) 76.
- [3] R. Ranjan, M. Tsapatsis, Microporous metal organic framework membrane on porous support using the seeded growth method, *Chem. Mater.* 21 (2009) 4920.
- [4] J. Gascon, F. Kapteijn, Metal–organic framework membranes – high potential, bright future? *Angew. Chem. Int. Ed.* 49 (2010) 1530.
- [5] Y.S. Li, F. Liang, H. Bux, W. Yang, J. Caro, Zeolitic imidazolate framework ZIF-7 based molecular sieve membrane for hydrogen separation, *J. Membr. Sci.* 354 (2010) 48.
- [6] H. Guo, G. Zhu, I.J. Hewitt, S. Qiu, Twin copper source growth of metal–organic framework membrane: Cu₂(BTC)₂ with high permeability and selectivity for recycling H₂, *J. Am. Chem. Soc.* 131 (2009) 1646.
- [7] H. Bux, F. Liang, Y. Li, J. Cravillon, M. Wiebcke, J. Caro, Zeolitic imidazolate framework membrane with molecular sieving properties by microwave-assisted solvothermal synthesis, *J. Am. Chem. Soc.* 131 (2009) 16000.
- [8] A. Huang, W. Dou, J. Caro, Steam-stable zeolitic imidazolate framework ZIF-90 membrane with hydrogen selectivity through covalent functionalization, *J. Am. Chem. Soc.* 132 (2010) 15562.
- [9] M. McCarthy, V. Varela-Guerrero, G. Barnett, H. Jeong, Synthesis of zeolitic imidazolate framework films and membranes with controlled microstructures, *Langmuir* 26 (2010) 14636.
- [10] L. Diestel, X. Liu, Y. Li, W. Yang, J. Caro, Comparative permeation studies on three supported membranes: Pure ZIF-8, pure polymethylphenylsiloxane, and MMMs, *Micropor. Mesopor. Mater.* 189 (2013) 210.
- [11] R. Mahajan, W.J. Koros, Mixed matrix membrane materials with glassy polymers. Part I, *Polym. Eng. Sci.* 42 (2002) 1420.
- [12] T.S. Chung, L.Y. Jiang, Y. Li, S. Kulprathipanja, Mixed matrix membranes (MMMs) comprising organic polymers with dispersed inorganic fillers for gas separation, *Prog. Polym. Sci.* 32 (2007) 483.
- [13] T. Rodenas, I. Luz, G. Prieto, B. Seoane, H. Miro, A. Corma, F. Kapteijn, F.X. Liabrés i Xamena, J. Gascon, Metal–organic framework nanosheets in polymer composite materials for gas separation, *Nat. Mater.* 14 (2015) 48.
- [14] J. Gascon, F. Kapteijn, B. Zornoza, V. Sebastián, C. Casado, J. Coronas, Practical approach to zeolitic membranes and coatings: state of the art, opportunities, barriers, and future perspectives, *Chem. Mater.* 24 (2012) 2829.
- [15] B. Zornoza, C. Téllez, J. Coronas, J. Gascon, F. Kapteijn, Metal organic framework based MMMs: an increasingly important field of research with a large application potential, *Micropor. Mesopor. Mater.* 166 (2013) 67.
- [16] B. Zornoza, B. Seoane, J.M. Zarnaro, C. Téllez, J. Coronas, Combination of MOFs and zeolites for mixed-matrix membranes, *Chem. Phys. Chem.* 12 (2011) 2781.
- [17] T. Rodenas, M. van Dalen, E. García-Pérez, P. Serra-Crespo, B. Zornoza, F. Kapteijn, J. Gascon, Visualizing MOF mixed matrix membranes at the nanoscale: towards structure-performance relationships in CO₂/CH₄ separation over NH₂-MIL-53(Al)/PI, *Adv. Funct. Mater.* 24 (2014) 249.
- [18] X.L. Liu, Y.S. Li, G.Q. Zhu, Y.J. Ban, L.Y. Xu, W.S. Yang, An organophilic pervaporation membrane derived from metal–organic framework nanoparticles for efficient recovery of bio-alcohols, *Angew. Chem. Int. Ed.* 50 (2011) 10636.
- [19] S. Aguado, G. Bergeret, M. Titus, V. Moizan, C. Nieto-Draghi, N. Bats, D. Farrusseng, Guest-induced gate-opening of a zeolite imidazolate framework, *New J. Chem.* 35 (2011) 546.
- [20] C. Ania, E. García-Pérez, M. Hario, J. Gutiérrez-Sevillano, T. Valdés-Solis, J. Parra, S. Calero, Understanding gas-induced structural deformation of ZIF-8, *J. Phys. Chem. Lett.* 3 (2012) 1159.
- [21] J. Bergh, C. Gücüyener, E. Pidko, E. Hensen, J. Gascon, F. Kapteijn, Understanding the anomalous alkane selectivity of ZIF-7 in the separation of light alkane/alkene mixtures, *Chem. Eur. J.* 17 (2011) 8832.
- [22] N. Nijem, H. Wu, P. Canepa, A. Marti, J. Kenneth Jr., T. Thonhauser, J. Li, Y. Chabal, Tuning the gate opening pressure of metal–organic frameworks (MOFs) for the selective separation of hydrocarbons, *J. Am. Chem. Soc.* 134 (2012) 15201.
- [23] M.R. Ryder, B. Civaleri, T.D. Bennett, S. Henke, S. Rudic, G. Cinque, F.F. Alonso, J.C. Tan, Identifying the role of terahertz vibrations in metal–organic frameworks: from gate-opening phenomenon to shear-driven structural destabilization, *Phys. Rev. Lett.* 113 (2014) 215502.
- [24] H. Bux, A. Feldhoff, J. Cravillon, M. Wiebcke, Y. Li, J. Caro, Oriented imidazolate framework-8 membrane with sharp H₂/C₃H₆ molecular sieve separation, *Chem. Mater.* 23 (2011) 2262.
- [25] a) C. Zhang, J. Dai, R. Johnson, O. Karvan, W. Koros, High performance ZIF-8/6FDA-DAM MMM for propylene/propane separations, *J. Membr. Sci.* 389 (2012) 34;
b) T. Bae, J. Lee, W. Qiu, W. Koros, C. Jones, S. Nair, A high-performance gas-separation membrane containing submicrometer-sized metal–organic framework crystals, *Angew. Chem. Int. Ed.* 49 (2010) 9863;
c) Q. Song, S. Nataraj, M. Roussanova, J. Chong, D. Hughes, W. Li, P. Bourgoign, M. Alam, A. Cheetham, S. Al-Muhtaseb, T. Sivaniah, Zeolitic imidazolate framework (ZIF-8) based polymer nanocomposite membranes for gas separation, *Energy Environ. Sci.* 5 (2012) 8359;
d) M. Askari, T.-S. Chung, Natural gas purification and olefin/paraffin separation using thermal cross-linkable co-polyimide/ZIF-8 MMMs, *J. Membr. Sci.* 444 (2013) 173;
e) T. Li, Y. Pan, K.-V. Peinemann, Z. Lai, Carbon dioxide selective mixed matrix composite membrane containing ZIF-7 Nano-fillers, *J. Membr. Sci.* 425 (2013) 235;
f) Y. Dai, J. Johnson, O. Karvan, D. Sholl, W.J. Koros, Ultem®/ZIF-8 mixed matrix hollow fiber membranes for CO₂/N₂ separations, *Membr. Sci.* 401 (2012) 76;
g) S. Basu, A. Cano-Odena, I. Vankelecom, MOF-containing mixed-matrix membranes for CO₂/CH₄ and CO₂/N₂ binary gas mixture separations, *Sep. Purif. Technol.* 81 (2011) 31.
- [26] W. Koros, Y. Ma, T. Shimidzu, Terminologie for membranes and membrane processes, *Pure Appl. Chem.* 68 (1996) 1479.
- [27] J. Maxwell, *A Treatise on Electricity & Magnetism*, third ed., Dover Publications, New York, 1954.
- [28] Z. Huang, Y. Li, R. Wen, M. Teoh, S. Kulprathipanja, Enhanced gas separation properties by using nanostructured PES-zeolite 4A MMMs, *J. Appl. Polym. Sci.* 101 (2006) 3800.
- [29] B. Zornoza, S. Irusta, C. Téllez, J. Coronas, Mesoporous silica sphere-polysulfone MMMs for gas separation, *Langmuir* 25 (2009) 5903.
- [30] M. Moaddeb, W. Koros, Gas transport properties of thin polymeric membranes in presence of silicon dioxide particles, *J. Membr. Sci.* 125 (1997) 143.
- [31] a) L. Diestel, H. Bux, D. Wachsmuth, J. Caro, Pervaporation studies of n-hexane, benzene, mesitylen and their mixtures on zeolitic imidazolate framework ZIF-8 membranes, *Micropor. Mesopor. Mater.* 164 (2012) 288;
b) K. Zhang, R.P. Lively, C. Zhang, R.R. Chance, W.J. Koros, D.S. Sholl, S. Nair, Exploring the framework hydrophobicity and flexibility of ZIF-8: from biofuel recovery to hydrocarbon separations, *J. Phys. Chem. Lett.* 4 (2013) 3618.
- [32] a) C. Gücüyener, J. van den Bergh, J. Gascon, F. Kapteijn, Ethane/ethene separation turned on its head: selective ethane adsorption on the metal organic framework ZIF-7 through a gate-opening mechanism, *J. Am. Chem. Soc.* 132 (2010) 17704;
b) D. Fairen-Jimenez, S.A. Moggach, M.T. Wharmby, P.A. Wright, S. Parsons, T. Düren, Opening the gate: framework flexibility in ZIF-8 explored by experiments and simulations, *J. Am. Chem. Soc.* 133 (2011) 8900;
c) S.A. Moggach, T.D. Bennett, A.K. Cheetham, The effect of pressure on ZIF-8: increasing pore size with pressure and the formation of a high-pressure phase at 1.47 GPa, *Angew. Chem. Int. Ed.* 121 (2009) 7221;
d) T. Chokbunpiam, R. Chanajaree, T. Remsungnen, O. Saengsawang, S. Fritzsche, C. Chmelik, J. Caro, W. Janke, S. Hannongbua, N₂ in ZIF-8: sorbate induced structural changes and self-diffusion, *Micropor. Mesopor. Mater.* 187 (2014) 1;
e) D.L. Chen, N. Wang, F.F. Wang, J. Xie, Y. Zhong, W. Zhu, J.K. Johnson, R. Krishna, Utilizing the gate-opening mechanism in ZIF-7 for adsorption discrimination between N₂O and CO₂, *J. Phys. Chem. C* 118 (2014) 17831.
- [33] J. Wakita, S. Jin, T. Shin, M. Ree, S. Ando, Analysis of molecular aggregation structures of fully aromatic and semialiphatic polyimide films with synchrotron grazing incidence wide-angle X-Ray scattering, *Macromolecules* 43 (2010) 1930.
- [34] G. Spathis, E. Sideridis, P. Theocaris, Adhesion efficiency and volume fraction of the boundary interphase in metal-filled epoxies, *Int. J. Adhes. Adhes.* 1 (1981) 195.
- [35] H. Oh, P. Green, Polymer chain dynamics and glass transition in a thermal polymer/particle mixtures, *Nat. Mater.* 8 (2009) 139.

4 Conclusions

This thesis gives insight into the development of relatively cost-intensive and rarely reproducible supported Metal-Organic Framework (MOF) membranes towards cheaper and more easily reproducible Mixed Matrix Membranes (MMMs).

First, the stable and for the gas permeation already successfully applied (chapter 1.2.6) ZIF-8 membrane was tested in the pervaporation of alkanes and aromatics (chapter 2.2). The gas adsorption studies showed that bulky molecules like n-hexane (critical diameter 4.3 Å) can be adsorbed by ZIF-8 powder (pore size 3.4 Å). In complete accordance with this finding, n-hexane permeated through the ZIF-8 membrane during the pervaporation experiment of the practice-relevant n-hexane/benzene mixture. N-hexane and benzene were separated with a binary mixture separation factor of $\alpha_{nC6,bnz} = 8.4$ at room temperature. This finding means that also benzene (critical diameter 5.8 Å) can be adsorbed by ZIF-8 and passes the ZIF-8 membrane with a low but non-zero permeation rate (chapter 2.2).

To study the molecular motion of benzene in ZIF-8, additional ^2H -NMR studies were carried out. It was concluded that benzene enters the ZIF-8 pore system and does not form any surface layer on the outer surface of the ZIF-8 crystals (chapter 2.3). Further information on benzene dynamics in ZIF-8 was obtained from the analysis of the spin-lattice and the spin-spin relaxation times as a function of the temperature. It was shown that within the ZIF-8 cage, the benzene molecule quickly rotates and performs relatively slow isotropic reorientations when colliding with the ZIF-8 wall. Benzene undergoes a translational jump diffusion between the neighboring cages and has a self-diffusion coefficient of $4 \cdot 10^{-16} \text{ m}^2 \text{ s}^{-1}$ at 50 °C. This self-diffusivity of benzene in ZIF-8 from NMR was found to be in agreement with diffusion coefficients derived from pervaporation studies.

Since the handling and scale-up of synthesized ZIF membranes in the geometry of thin films on porous ceramic supports caused problems, mechanically more stable, easier and cheaper to produce membranes with excellent separation characteristics were looked for. MMMs attracted attention as a possibility to combine the excellent separation performance of MOFs - or in this case ZIFs - with the flexibility and good handling of polymers. Thus, established polymer processing

4. Closing remarks

technologies can be used to produce MMMs in the form of hollow fibers or spiral wound modules.

MMMs can be made of rubbery and glassy polymers which have different influences on the separation ability of the resulting membrane. For zeolite MMMs it is known that rubbery polymers often form the better matrix as they are still flexible at room temperature and can fit the zeolite crystals (chapter 1.3.2.1). Thus, a 9 vol-% MMM out of ZIF-8 nanoparticles and rubbery polymethylphenylsiloxane (PMPS) was examined. The resulting MMM displayed gas selectivities identical with those of the PMPS membrane but with higher gas fluxes which can be explained by a higher free volume of the PMPS due to the incorporation of ZIF nanoparticles (chapter 3.2).

Completely different results were obtained by mixing ZIF nanoparticles with the glassy Matrimid[®] 5218 (Matrimid) polymer (chapter 3.3 and 3.4). The evaporation of the solvent in ambient air during the MMM synthesis can lead to huge tensile stresses in the glassy polymer matrix which can cause void-forming in the interface between the polymer and the additive. Hence, we dried our MMMs under solvent atmosphere. In chapter 3.3, 25 vol-% ZIF-90/Matrimid and 25 vol-% ZIF-8/Matrimid MMMs have been prepared and tested for the H₂/CO₂ mixed gas separation in comparison with the neat ZIF and the neat Matrimid membranes. It was found that the ZIF-8/Matrimid MMM had only a slightly improved hydrogen permeability in comparison to the neat Matrimid membrane while the mixed gas separation factor remains constant at $\alpha_{H_2/CO_2} = 3.5$. The ZIF-90/Matrimid MMM had a slightly improved mixed gas separation of $\alpha_{H_2/CO_2} = 5.0$ and the hydrogen permeability increased slightly from 28 Barrer to 30 Barrer. Plotting the H₂/CO₂ selectivity as a function of the H₂ permeability in the so-called Robeson plot, an improvement compared with the neat Matrimid polymer membrane towards the Robson line was stated. A decisive improvement of the H₂/CO₂ separation factor was achieved with the covalently bonded ZIF-90-based MMM. In this membrane, ethylenediamine linkers have been used to improve the interaction between the matrimid polymer and the ZIF-90 particles. Thus, the separation factor was further improved to $\alpha_{H_2/CO_2} = 9.5$, while the hydrogen permeability decreased. The selectivity improvement was also caused

by the attractive interaction between CO₂ and the amine groups. To describe the gas permeability in MMMs with homogeneously distributed, spherical and porous additives, the Maxwell model can be applied. It is noticeable that the predictions of permeabilities based on the Maxwell model always showed higher results for the 25 vol-% ZIF-8 and ZIF-90/Matrimid MMMs than the measured permeabilities.

This phenomenon could also be observed for the H₂/CH₄ separation by ZIF-90 and ZIF-8/Matrimid MMMs (chapter 3.4). In this case we also obtained lower permeabilities than expected. Additionally, higher separation factors for the 10 and 20 vol-% MMMs were found compared to the neat Matrimid and ZIF membranes. The findings can be explained by either a rigidified polymer layer around the ZIF nanoparticles or by a changed filler separation due to a hindered ZIF framework flexibility. Thus, additional STEM, SAED and DSC measurements have been done. All these measurements showed no changes of the polymer structure around the ZIF particles. Thus, we concluded, that the enhanced selectivity results from a hindered linker distortion on the ZIF surface. This effect was reproducible by using another glassy polymer: 2,2'-bis(3,4-carboxyphenyl) hexafluoropropane dianhydride-diamino-mesitylene (6-FDA-DAM).

This thesis could show that ZIF membranes have excellent separation performances in comparison to the Robeson plot in spite of the markedly framework flexibility which even allows benzene to become adsorbed. However, the handling and scale-up of ZIF membranes caused problems. Thus, MMMs attracted attention as a possibility to combine the excellent separation performance of ZIFs with the flexibility and good handling of polymers. Indeed, enhanced gas separation results or gas permeabilities, respectively, could be found for the MMMs in comparison to those of the neat polymer membranes. For the rubbery PMPS membrane enhanced gas permeabilities were observed after introducing ZIF-8 nanoparticles, while the separation results remained constant. For the glassy Matrimid membranes, instead, unexpected high separations were found after introducing ZIF-8 and ZIF-90 nanoparticles, while the gas permeabilities often decreased. The finding was explained by a hindered framework flexibility caused by the surrounding polymer layer.

5 Appendix

Publications included in the thesis

1. L. Diestel, H. Bux, D. Wachsmuth, J. Caro*, Pervaporation studies of n-hexane, benzene, mesitylene and their mixtures on zeolitic imidazolate framework-8 membranes, *Micropor. Mesopor. Mater.* 2012, 164, 288.
2. D. I. Kolokolov*, L. Diestel, J. Caro, D. Freude, A. G. Stepanov, Rotational and translational motion of benzene in ZIF-8 studied by ^2H NMR: Estimation of microscopic self-diffusivity and its comparison with macroscopic measurements, *J. Phys. Chem. C* 2014, 118, 12873.
3. L. Diestel*, X. L. Liu, Y. S. Li, W. S. Yang, J. Caro, Comparative permeation studies on three supported membranes: Pure ZIF-8, pure polymethylphenylsiloxane, and mixed matrix membranes, *Micropor. Mesopor. Mater.* 2014, 189, 210.
4. L. Diestel*, N. Wang, A. Schulz, F. Steinbach, J. Caro, Matrimid-based mixed matrix membranes: Interpretation and Correlation of experimental findings for zeolitic imidazolate frameworks as filler in H_2/CO_2 separation, *Ind. Eng. Chem. Res.* 2015, 54, 1103.
5. L. Diestel*, N. Wang, B. Schwiedland, F. Steinbach, U. Giese, J. Caro, MOF based MMMs with enhanced selectivity due to hindered linker distortion, *J. Membr. Sci.* 2015, 492, 181.

Publications not included in the thesis

1. L. Diestel, B. Seoane, J. Gascon, F. Kapteijn, J. Caro*, De-mystification of mixed matrix membranes – interpretation of their surprisingly high gas separation performance, Submission in preparation.
2. Y. Liu*, N. Wang, L. Diestel, F. Steinbach, J. Caro, MOF membrane synthesis in the confined space of a vertically aligned LDH network, Chem. Commun. 2014, 50, 4225.
3. N. Wang*, Y. Liu Z. Qiao, L. Diestel, J. Zhou, A. Huang*, J. Caro, Polydopamine-based synthesis of a zeolite imidazolate framework ZIF-100 membrane with high H₂/CO₂ selectivity, J. Mater. Chem. A 2015, 3, 4722.
4. S. Friebe, N. Wang, L. Diestel, A. Schulz, A. Mundstock, J. Caro*, Deuterium/-Hydrogen permeation through different molecular sieve membranes: ZIF, LDH, Zeolite, accepted for Micropor. Mesopor. Mater..

Contributions to Conferences

1. L. Diestel*, H. Bux, F. Liang, J. Caro, Pervaporation: Separation of C₆-hydrocarbons, 12th International Conference on Inorganic Membranes ICIM-12, 09.07. – 13.07.2012, **oral presentation.**
2. L. Diestel*, M. Schweinefuß*, Development of ZIF membranes for separation by pervaporation, MOF Status Report Meeting 2012, 28.11.2012, **oral presentation.**

3. L. Diestel*, X. L. Liu, Y. S. Li, F. Steinbach, J. Caro, ZIF-8 mixed matrix membranes for natural gas and exhaust gas purification, 17th International Zeolite Conference 17th IZC, 07.07. – 12.07.2013, **poster presentation.**

4. L. Diestel*, A. Schulz, F. Steinbach, J. Caro, Mixed matrix membranes: Experimental results for the hydrogen purification, 113th General Assembly of the German Bunsen Society for Physical Chemistry Bunsentagung 2014, 29.05. – 31.05.2014, **oral presentation.**

5. L. Diestel*, A. Schulz, J. Caro, Mixed Matrix Membranes using nanographite, ZIF-8 and non-porous particles: Experimental results for hydrogen purification, 6th International Federation of European Zeolite Associations Conference FEZA 2014, 08.09. – 11.09.2014, **poster presentation.**

6. Y. Liu*, N. Wang, L. Diestel, F. Steinbach, J. Caro, MOFs married to LDHs with enhanced gas selectivity, 6th International Federation of European Zeolite Associations Conference FEZA 2014, 08.09. – 11.09.2014, **poster presentation.**

7. L. Diestel*, S. Friebe*, Energy efficient MOF-based mixed-matrix membranes for CO₂ capture, 3rd Consortium meeting M₄CO₂, 15.12. – 16.12.2014, **oral presentation.**

Curriculum Vitae



Personal details

Born on 11 April 1987 in Fürstentfeldbruck, German national

Education

- | | |
|-------------------|--|
| 11/2011 – present | PhD student and scientific co-worker
Working group of Prof. Dr. J. Caro
Institute for physical chemistry and electrochemistry (PCI)
Gottfried Wilhelm Leibniz University of Hannover |
| 10/2009 – 10/2011 | MASTER OF SCIENCE,
Material- and Nanochemistry
Gottfried Wilhelm Leibniz University of Hannover |
| 10/2006 – 11/2009 | BACHELOR OF SCIENCE,
General Chemistry
Gottfried Wilhelm Leibniz University of Hannover |
| 06/2006 | ABITUR,
Chemistry and Mathematics
Graf-Adolf-Gymnasium, Tecklenburg |
-